NTNU

Norwegian University of
Science and Technology

Upscaling polymer flooding using MRST

Anna Danilova

Abstract

Reservoir simulation models are widely used as a decision making tool in oil and gas industry. Modern technologies allow creating very detailed high-resolution models to represent the properties of a reservoir system as accurately as possible. However, such models become computationally heavy, which complicates field development studies, history matching and other procedures that require testing a large number of possible scenarios.

Upscaling is the common solution that aims to find a balance between the simplification of the model and keeping the accuracy of the simulation results. Extensive research has been devoted to this topic, and a number of methods for single-phase and two-phase flow upscaling have been developed. However, much less attention has been paid to the upscaling of the Enhanced Oil Recovery (EOR) methods. The goal of this thesis was to investigate various upscaling methods of polymer flooding.

In this study, polymer flooding is upscaled with the assumption of steady-state flow. For simplicity, we assume that reduction factor, residual resistance factor and inaccessible pore volume are constant. Then the only polymer related parameter to be upscaled is polymer adsorption, which is in the focus of this thesis. In order to test polymer flooding upscaling in a highly heterogeneous medium, the SPE10 comparative model has been chosen as the fine-scale model. Several polymer adsorption upscaling methods, including a newly developed method based on the fraction of fluid flow in different grid cells, were investigated. Results of polymer flooding simulation with upscaled parameters in coarse models were compared to results in the original fine-scale model. Areal and vertical sweep, zones of intensive adsorption, polymer adsorption behavior through time and production data on coarse and fine scales were analyzed to evaluate the most efficient and accurate methods. Polymer adsorption analysis has been performed for models of different dimensions and complexity to identify the main factors influencing the coarse-scale solution.

Simple volumetric averaging was found the most accurate method in case when all grid cells have the same polymer concentration, but if some areas of reservoir are bypassed, this method overestimates coarse-scale polymer adsorption due to the influence of low-permeability zones. The use of polymer adsorption function on coarse scale accounts for fine-scale flow patterns better and gives more accurate polymer adsorption estimation than volumetric averaging in case when not all zones of reservoir are involved in the fluids flow. The newly developed flow fraction coefficient formula was found to give the most precise estimation of coarse-scale polymer adsorption in synthetic models, but it needs further improvements to take into account the full flow through a coarse cell in the realistic models.

Acknowledgements

Foremost, I would like to express my gratitude to my advisor Prof. Jon Kleppe for the continuous support and guidance during my thesis work, for his advice and the immense knowledge he shared with me and other students through his excellent courses.

My sincere thanks must also go to my co-advisor, Carl Fredrik Berg (Statoil). I am deeply grateful to him for encouraging me to step out of my comfort zone and to work on this topic. I am also thankful to him for the discussions that helped me sort out the theoretical and technical details of my work and for reading and commenting during numerous revisions of this thesis.

I would like to express my great appreciation to Sindre Tonning Hilden who kindly permitted me to use his MATLAB code for the two-phase steady-state upscaling as the base of my work and provided some help with coding in MRST Simulator. I am also thankful to Prof. Knut-Andreas Lie for answering my questions about MRST.

Table of Contents

List of Figures

List of Tables

Chapter 1. Introduction

1.1. Enhanced Oil Recovery methods

Recovery rates differ from field to field, but the average oil recovery rate for oil fields on the Norwegian shelf is currently about 47% (Resource Management in Mature Areas, 2016), and the goal is to increase this number further. Half of the oil that will be left in the reservoirs under current plans is mobile oil, while another half is immobile oil that requires advanced flooding techniques to be recovered. The scope of measures undertaken to boost oil recovery in relation to a reference point (usually, the Plan for Development and Operation or PDO) is defined as Improved Oil Recovery (IOR) and Enhanced Oil Recovery (EOR) (Norwegian Petroleum Directorate, 2016). These two terms are often used interchangeably; however, IOR is a general term which comprises improving oil recovery by any means (e.g. operational strategies, improving vertical and areal sweep, drilling of additional and more advanced wells), while EOR is a subset of IOR that aims to increase oil recovery by injecting materials not typically present in the reservoir (Lake, 1989). According to this definition, EOR can appear as any mode of oil recovery process (e.g. drive, well treatment etc.) during any phase in the producing life of a reservoir (e.g. primary, secondary etc.), comprises the use of many injection fluids; however, waterflooding and pressure maintenance processes are not a part of EOR (Lake, 1989). Different classifications of the EOR methods exist, and one of them is presented in **Fig. 1.1**.
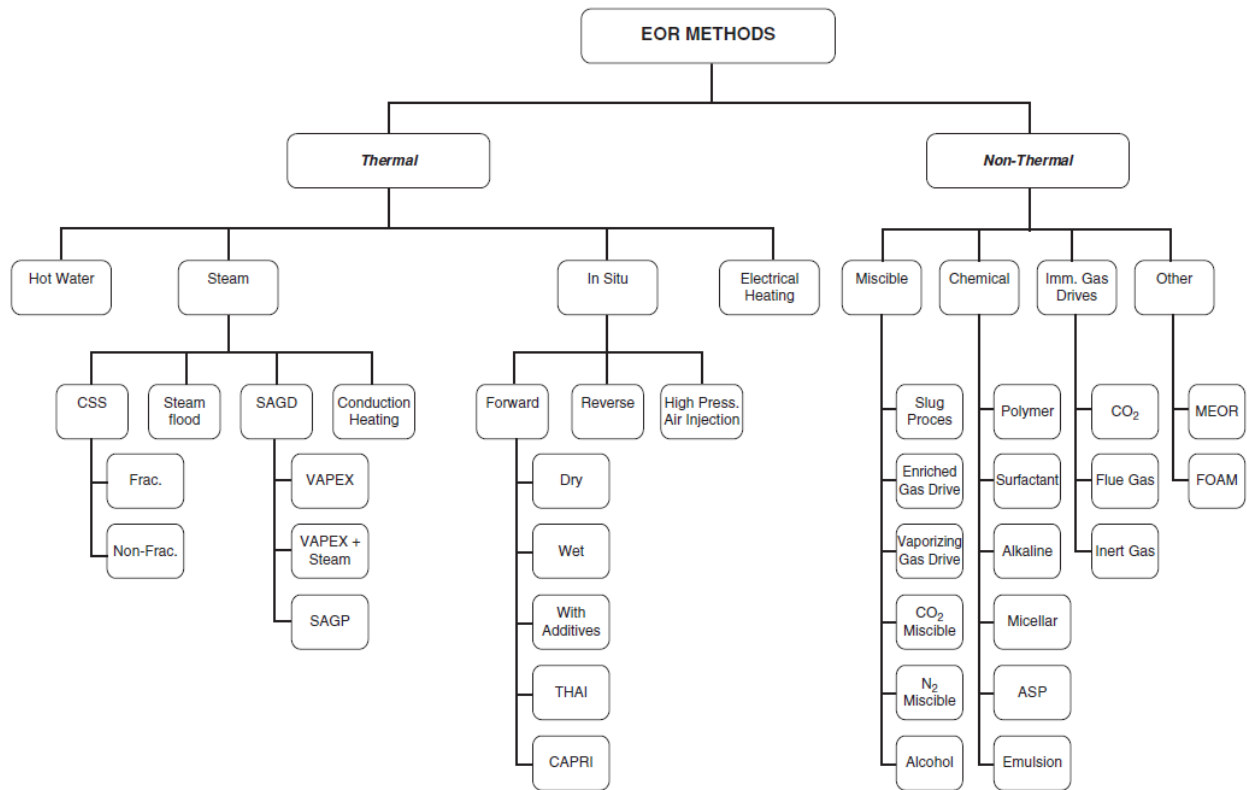
Fig. 1.1 – Classification of EOR methods (taken from Thomas, 2008)

1.2. Polymer flooding

Depending on the EOR methods classification, polymer flooding belongs either to chemical or mobility-control EOR techniques (Green & Willhite, 1998; Thomas, 2008). In order to have a better understanding of the polymer flooding mechanism, it is necessary to introduce the mobility ratio, M, defined as:

$$M = \frac{\lambda_w}{\lambda_o} = \frac{k_{rw}}{\mu_w} \Big/ \frac{k_{ro}}{\mu_o} \qquad \qquad (1.1)$$

where λ, μ and k_r are mobility, viscosity and relative permeability respectively and the subscripts o and w refer to oil and water (Sorbie, 1991). The influence of mobility ratio on water flooding efficiency was widely studied (Aronofsky, 1952; Dyes et al., 1953; Cheek & Menzie, 1955; Bradley et al., 1960), and it was proven that lower mobility ratios are more favorable (Craig, 1971).

During the normal waterflooding some oil is not recovered either because it remains as isolated droplets trapped by the capillary forces (Sorbie, 1991; Green & Willhite, 1998) or because it is bypassed due to the unfavorable mobility ratio in the flood or due to the presence of large-scale heterogeneities in the reservoir, such as stratification or channeling (Sorbie, 1991).

The primary purpose of adding a high-molecular-weight water-soluble polymer to the injected water is to reduce the mobility of displacing fluid; however, other potential ways in which polymer can make oil recovery process more efficient are through the effects of polymers on fractional flow and by diverting injected water from zones that have been swept (Needham & Doe, 1987).

Expression for the fractional flow of water can be derived from Darcy's equations for water and oil phase and appears as follows in case of horizontal flow, with negligible capillary pressure (Kleppe, 2015):

$$f_w = \frac{1}{1 + \dfrac{k_{ro}}{\mu_o}\dfrac{\mu_w}{k_{rw}}} \quad\text{..(1.2)}$$

The effect of adding polymer on flow characteristics is the increase of water viscosity and thereby a reduction of water mobility in the polymer-flooded zones, which results in a smaller percentage of water in the total flow. The fractional flow concept is interconnected with mobility ratio idea (Eq. 1.1) introduced earlier. Reduced mobility ratio during polymer flooding results in a more stable displacement front and improved areal sweep efficiency as illustrated in **Fig. 1.2**.
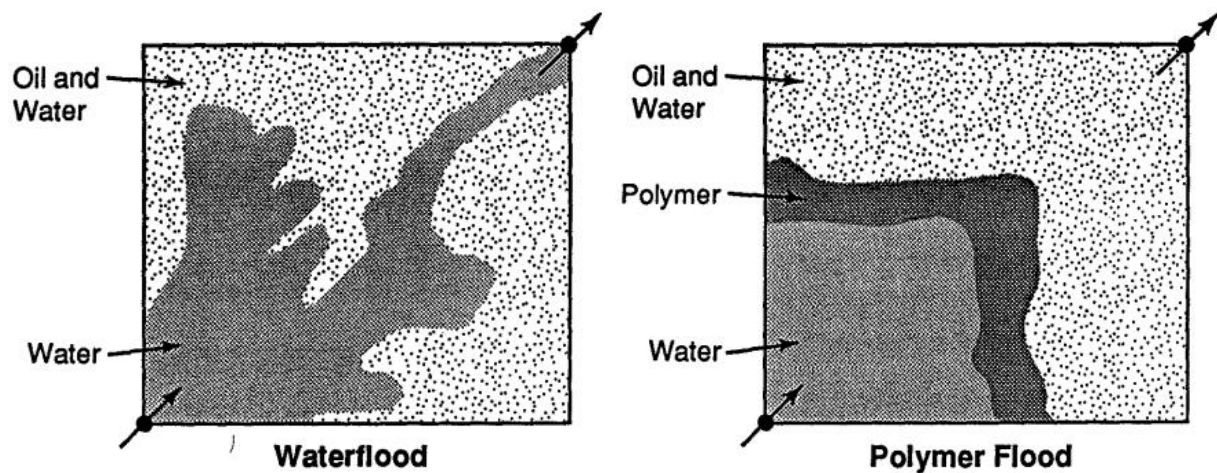
Fig. 1.2 – Schematic of macroscopic displacement efficiency improvement with polymer-augmented waterflooding (quarter of a five-spot pattern)(taken from Green & Willhite, 1998)

The impact of adding polymer to the floodwater on fluid diversion effects becomes more important when significant vertical heterogeneities are present in the reservoir. Presence of high-permeability channels in the reservoir leads to preferential water entry in these zones, while less permeable areas of the reservoir are bypassed. If water-polymer solution is injected into a heterogeneous reservoir, an additional flow resistance is created through permeability reduction and viscosity increase discussed earlier, which will force subsequently injected water to flow into the untouched or poorly swept zones of the reservoir as shown in **Fig. 1.3** (Needham & Doe, 1987).
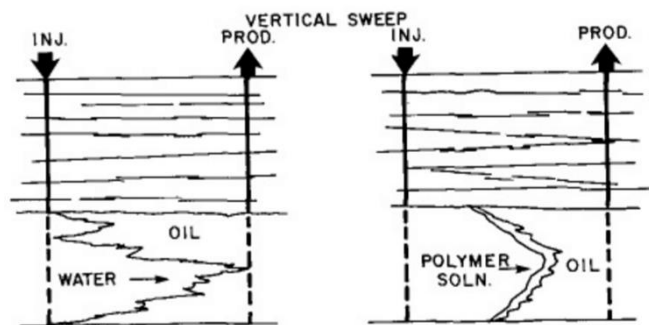
Fig. 1.3 – Vertical sweep schematic diagram (taken from Donaldson et al., 1989)

Chapter 2. Polymer properties and flow through porous media

2.1. Polymer types

Generally, a polymer is a single macromolecule with at least several hundred atoms held together by covalent bonds with a total molecular weight typically from 1 million to 10 million (Dr. Wamser, 2000; Willhite & Seright, 2011). Molecular weights of polymers that are most used in petroleum industry can be even greater.

Two main types of polymers are widely used in the industry: synthetic polymer (polyacrylamide or partially hydrolyzed polyacrylamide) and biopolymer (xanthan gum) (Chang, 1978), and their primary structure is presented in **Fig. 2.1**.

(a)   (b)
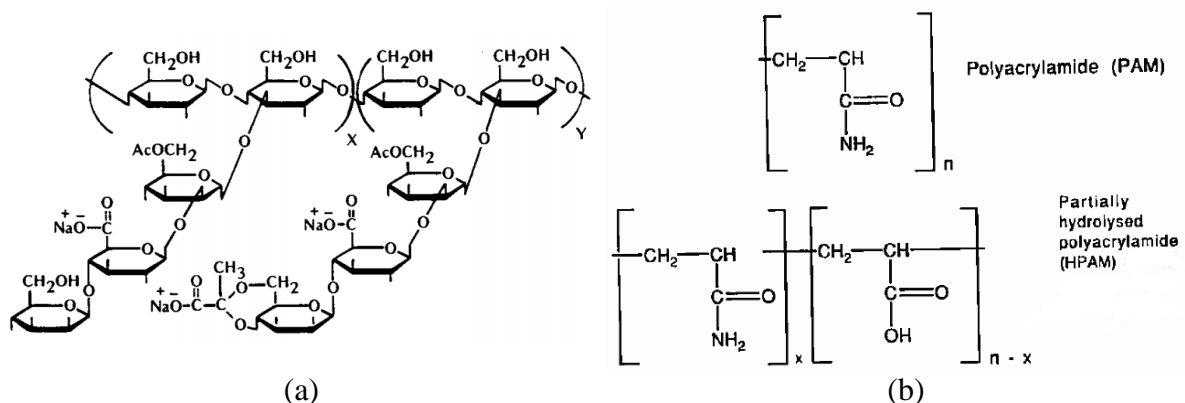
Fig. 2.1 – Xanthan primary structure (a), polyacrylamide and partially hydrolyzed polyacrylamide primary structures (b) (taken from Philips et al., 1985 and Sorbie, 1991)

Each polymer type has its own strengths and weaknesses. Those of polyacrylamide and xanthan biopolymer are described by Needham & Doe (1987) and can be summarized as follows:

Polyacrylamides:
- + relatively cheap
- + good viscosifiers of fresh waters
- + long-lasting permeability reduction
- − shear degradation at high flow rates
- − impaired performance in presence of high salt concentration

Biopolymers:
+ more efficient in high-salinity waters
+ resistant to shear degradation
− less viscosifying power in fresh waters

2.2. Polymer viscosity and influence of shear rate

Viscosity of polymer solution is an important factor influencing sweep efficiency and flow characteristics during polymer flooding, and is therefore considered one of the main properties of polymer solutions. Sorbie (1991) interprets viscosification of aqueous fluids by polymer as the result of an increased number of interactions between solvent molecules and molecules constituting the entire polymer chain. It should be noted that this interaction between solvent molecules and polymer chains emerges from the frictional effects that occur in sedimentation and diffusion (Flory, 1953).

Xanthan biopolymer or polyacrylamide diluted with water are non-Newtonian fluids unlike, for example, pure water, which is a Newtonian fluid. This implies that the linear relationship between shear stress and shear rate given in the Eq. 2.1 below, where viscosity is a constant proportionality factor, is not valid for xanthan or polyacrylamide solutions.

$$\tau = \mu \dot{\gamma} \quad \text{..(2.1)}$$

where
τ − shear stress
μ − solution viscosity
$\dot{\gamma}$ − shear rate

Such fluids as polymers are described using a so-called "viscosity function", which depends on the shear rate (Bird et al., 1987), instead of a constant coefficient in the relationship between shear stress and shear rate:

$$\tau = -\eta \left(\frac{dV}{dr} \right) = \eta \left(\dot{\gamma} \right) \dot{\gamma} \quad \text{..(2.2)}$$

Relationship between shear rate and viscosity may vary for different types of non-Newtonian fluids. **Fig. 2.2** presents typical viscosity-shear rate behavior for different fluid types.
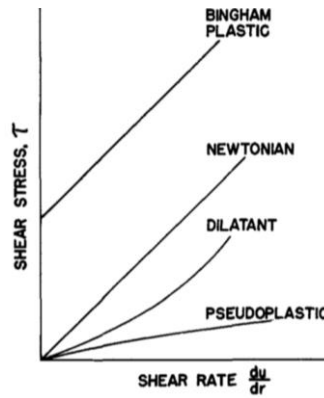
Fig. 2.2 – Fluids viscosity behavior with shear rate (taken from Metzner & Otto, 1957)

Several authors have developed empirical models describing the viscosity function that appears in Eq. 2.2 (Kincaid et al., 1941; Bird et al., 1960; Bingham, 1962; Carreau, 1972).

Power-law model (De Waele, 1923; Ostwald, 1925) is the simplest expression that describes non-Newtonian fluids viscosity:

$$\eta = K\dot{\gamma}^{n-1}$$ ....(2.3)

where

K − constant, which is equivalent to Newtonian viscosity at $n=1$

n − dimensionless constant, typically in range of $0.4 \leq n \leq 1.0$ for pseudoplastic fluids

The advantage of power-law fluid expression is its simplicity, but it does not capture well the viscosity behavior at very high and very low shear rates. Carreau (1972) proposed another model that provided a better fit for the whole range of shear rates:

$$\eta\left(\dot{\gamma}\right) = \eta_{\infty} + \left(\eta_0 - \eta_{\infty}\right)\left[1 + \left(\lambda\dot{\gamma}\right)^2\right]^{(n-1)/2}$$ ....(2.4)

where

η_0 − zero shear rate viscosity

η_{∞} − infinite shear rate viscosity

λ − time constant

This model aims to describe pseudoplastic flow with asymptotic viscosities at zero- and infinite shear rates (Hackley & Ferraris, 2001), so that a Newtonian behavior with constant viscosity will be observed at low shear rates, and at high shear rates the fluid will behave as a power-law fluid.

Viscosity of the polymer solutions is also influenced by other factors, such as polymer concentration, polymer molecular weight, temperature, salt concentration in the solvent.

Several authors (Evans & Young, 1942; Jennings et al., 1971; Chang, 1978; Sheng, 2010) reported that viscosity tends to increase with increase in polymer concentration or molecular weight. The impact of salinity may vary depending on polymer type; however, polyacrylamide viscosity is more affected by presence of salt (Green & Willhite, 1998). The main effect of salinity is a considerable decrease of viscosities in polyacrylamide solutions with

higher salinity (Mungan, 1969; Martin & Sherwood, 1975; Chang, 1978; Sheng, 2010). Temperature influence on polymer viscosity results in viscosity decrease when temperature increases (Wang et al., 1970; Al-Shammari et al., 2011).

2.3. Polymer retention

When polymer solution is flowing through porous media, significant interactions between porous media and molecules in polymer chain may occur, which may result in retention of polymer molecules by the porous media. As a part of injected polymer is retained, the polymer concentration is reduced, which results in viscosity decrease, and thus, reduced efficiency of the polymer flood (Sorbie, 1991).

Pye (1964) first observed differences in viscosities of water-soluble polymers measured using a viscometer and those determined by applying Darcy's law to a formation rock. The observed effect occurring in tortuous passages far from the core inlet was determined as *polymer resistance factor* and was described by the following formula (Pye, 1964):

$$R = \left(\frac{k_w}{\mu_w}\right) \Big/ \left(\frac{k_p}{\mu_p}\right) = \frac{\lambda_w}{\lambda_p} \quad \text{...(2.5)}$$

where μ_p – apparent viscosity of the polymer solution in the core.

Burcik (1965) reported brine mobility reduction in a core that was previously flushed by polyacrylamide. He conducted an experiment when brine, polymer solution and a considerable volume of brine again, respectively, were flooding a Berea sandstone disk, and observed that brine mobility reduction persisted independently of the amount of brine injected after the polymer solution. Only when the core had been flushed with ethyl alcohol solution that collapsed polymer particles, one could again observe mobility identical to the initial brine mobility. That led to the conclusion that there were polymer molecules retained in the pore openings due to mechanical entrapment or adsorption that were hindering brine flow through the core.

Other investigators (Sandiford, 1964; Chain, 1965; Mungan et al., 1966; Gogarty, 1967) have also reported similar phenomena. Gogarty (1967) described results of his broad experimental study of HPAM solutions flow through porous media and drew a conclusion that mechanical entrapment and adsorption mechanisms play the biggest role in polymer retention in the porous media, which causes flow residual resistance effect.

The quantitative assessment of this residual resistance effect is usually given as a ratio of brine mobility before the polymer comes into contact with the porous media, λ_w, to the brine mobility after the polymer has flowed through the porous media, λ_{wp}, which is called *residual resistance factor* (Green & Willhite, 1998):

$$RRF = \lambda_w \Big/ \lambda_{wp} \quad \text{...(2.6)}$$

Dawson & Lantz (1972) compared experimental breakout curves for polymer and salt that were injected simultaneously and demonstrated that polymer concentration peak at the

outlet occurs earlier than salt concentration peak. This implied that the two types of injected particles travelled with different velocities through the same porous media, which was concluded to be a result of the fact that some fraction of connected pore space was not accessible for polymer particles to flow through. The fraction of the pore space, which is inaccessible for the polymer molecules due to a small pore size compared to the size of polymer molecules or due to presence of retained polymer is called *inaccessible pore volume* (IPV).

Many experiments were conducted to study polymer retention using different approaches (Marker, 1973; Chaveteau & Kohler, 1974; Szabo, 1975; Dominguez & Willhite, 1977), and it was concluded that the main mechanisms of polymer retention in porous media are:

- Polymer adsorption
- Mechanical entrapment
- Hydrodynamic retention

Fig. 2.3 illustrates different polymer retention mechanisms listed above. It can be seen that when adsorption takes place due to interaction between polymer molecules and porous media, polymer molecules stay retained by the surface of rock grains. The greater rock surface area, the more polymer molecules are adsorbed. When the flow path goes through a narrow pore throat, mechanical entrapment of polymer molecules can occur if polymer molecules are too large to pass through. Polymer molecules can also be temporarily trapped in stagnant zones, and this mechanism is called hydrodynamic retention.
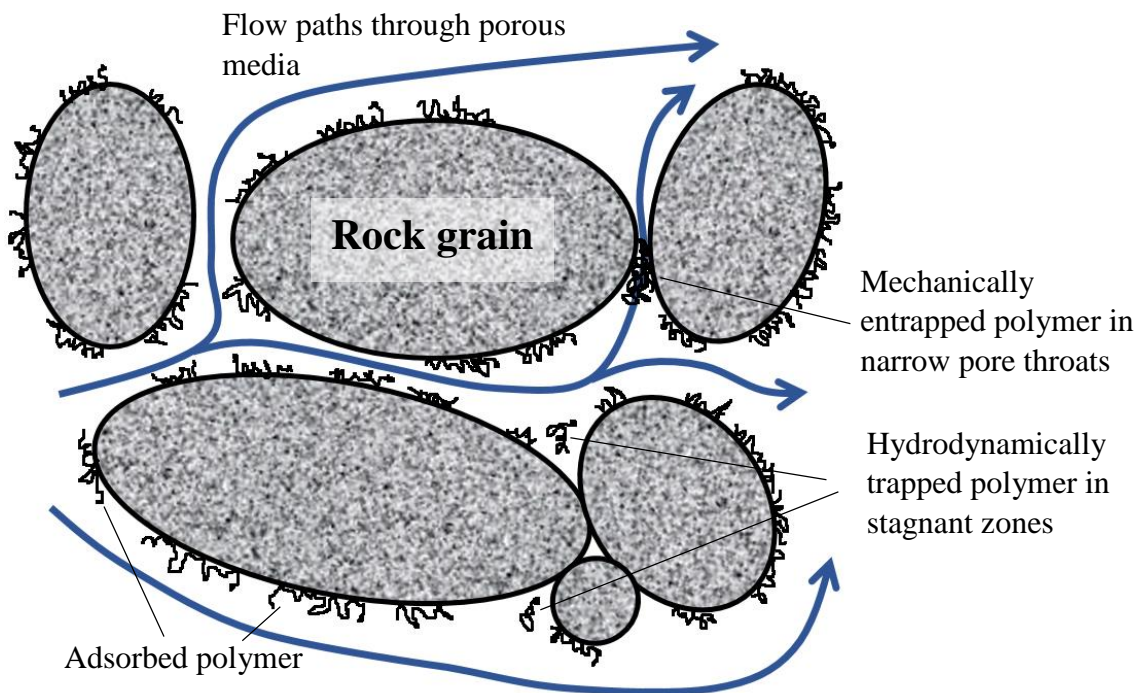
Fig. 2.3 – Schematic representation of different polymer retention mechanisms
(adapted from Sorbie, 1991)

Polymer adsorption, however, is considered the most important mechanism of polymer retention and a "fundamental property of polymer-rock surface-solvent system" (Sorbie, 1991).

2.4. Polymer flow governing equations

2.4.1. Polymer flow model

When standard black-oil model is used to describe multidimensional non-horizontal flow of oil and water phases in porous media, flow equations for oil and water phase respectively are

$$\nabla \cdot \left(\frac{k_{ro}}{\mu_o B_o} K(\nabla p_o - \rho_o g \nabla z) \right) - q_o' = \frac{\partial}{\partial t} \left(\frac{\varphi S_o}{B_o} \right) \dots\dots\dots\dots\dots\dots\dots(2.7a)$$

$$\nabla \cdot \left(\frac{k_{rw}}{\mu_w B_w} K(\nabla p_w - \rho_w g \nabla z) \right) - q_w' = \frac{\partial}{\partial t} \left(\frac{\varphi S_w}{B_w} \right) \dots\dots\dots\dots\dots\dots(2.7b)$$

with closing equation $S_w + S_o = 1$, and where

φ – porosity

S_o and S_w – oil and water saturations

B_o and B_w – oil and water formation volume factors

q_o' and q_w' – oil and water source/sink terms

ρ_o and ρ_w – oil and water densities

g – gravity

z – height above a given datum

p_o and p_w – oil and water densities

K – absolute permeability

k_{ro} and k_{rw} – oil and water relative permeabilities

μ_o and μ_w – oil and water viscosities

When polymer flood model is considered, the system of Eqs. 2.7a – 2.7b above changes. It is assumed that polymer solution flowing through porous media does not influence the flow of the oil phase, so the oil flow equation remains the same. The modifications needed to transform standard black-oil model into polymer flood model are related to the effect of polymer on water viscosity and the need to describe the flow of polymer using an additional equation. Thus, flow equations for water and water with polymer are

$$\nabla \cdot \left(\frac{k_{rw}}{\mu_{w,eff} B_w R_k} K(\nabla p_w - \rho_w g \nabla z) \right) - q_w' = \frac{\partial}{\partial t} \left(\frac{\varphi S_w}{B_w} \right) \dots\dots\dots\dots\dots(2.8a)$$

$$\nabla \cdot \left(\frac{c_p k_{rw}}{\mu_{p,eff} B_w R_k} K(\nabla p_w - \rho_w g \nabla z) \right) + \frac{\partial}{\partial t} \left(\rho_r c_p^a (1-\varphi) \right) - q_w' c_p = \frac{\partial}{\partial t} \left(\frac{\varphi (1 - S_{dpv}) S_w c_p}{B_w} \right) \dots\dots\dots(2.8b)$$

with closing equation $S_w + S_o = 1$, and where

R_k – permeability reduction factor

S_{dvp} – dead pore space

c_p – polymer concentration

c_p^a – amount of polymer adsorbed on the rock surface

$\mu_{w,eff}$ and $\mu_{p,eff}$ – effective viscosities of water and polymer

Another assumption in the model is that the density and formation volume factor of water do not depend on polymer concentration. Polymer flooding effect is modelled by introducing local polymer concentration that affects fluid viscosities and permeability reduction factor that represents the impact of polymer retention on aqueous phase relative permeability. Since polymer solution and water are miscible, the effective viscosities representing the degree of mixing are used in the flow equations; these terms will be discussed in more details below. An additional term on the left-hand side of Eq. 2.8b represents polymer adsorption.

2.4.2. Treatment of fluid viscosities

In polymer flooding polymer solution is considered soluble in water; thus, a miscible flow in porous media occurs. Miscible flow, especially at unfavorable mobility ratios, is characterized by such phenomena as viscous fingering or gravity tongues, which are forms of unstable frontal advance (Todd & Longstaff, 1972). The factors influencing these instabilities have been studied experimentally (Blackwell et al., 1959; Habermann, 1960), and some methods have been developed to predict the behavior of unstable miscible displacement (Koval, 1963; Dougherty, 1963; Todd & Longstaff, 1972).

However, the most widely used model was the one developed by Todd & Longstaff (1972), as it allowed modelling miscible flow in porous media and representing physical dispersion and fingering effects phenomena without the need to reproduce the fine structure of the flow or handle physical dispersion distortion by numerical dispersion in the solution. The main idea behind Todd & Longstaff model is to capture the effects occurring due to the heterogeneous nature of miscible flow by varying phases' viscosities and densities with the degree of mixing of the phases.

To do so, Todd & Longstaff (1972) introduced a *mixing parameter ω*. The value of mixing parameter should fall between 0 and 1, where 0 corresponds to a complete segregation of polymer from water, 1 corresponds to the full mixing of polymer and water, and any value in between determines some degree of partial mixing. In polymer flooding modelling, only viscosities are treated using the mixing parameter, while densities are kept independent of the degree of mixing.

The viscosity terms used in the Eqs. 2.8a – 2.8b are defined using Todd & Longstaff model discussed above, so that the effective polymer viscosity is

$$\mu_{p,eff} = \mu_m \left(c_p \right)^{\omega} \mu_m \left(c_{p,\max} \right)^{1-\omega} \quad \text{...(2.9)}$$

where
$\mu_m(c_p)$ – viscosity of a fully mixed water-polymer solution
$c_{p,max}$ – maximum polymer concentration

Analogically, the viscosity of a partially mixed water is

$$\mu_{w,e} = \mu_m \left(c_p \right)^{\omega} \mu_w^{1-\omega} \quad \text{...(2.10)}$$

Expression for the effective water viscosity takes into account the contribution from polymer solution and from pure water and appears as follows:

$$\frac{1}{\mu_{w,eff}} = \frac{1-\bar{c}}{\mu_{w,e}} + \frac{\bar{c}}{\mu_{p,eff}} \quad\text{...}(2.11)$$

where $\bar{c} = \dfrac{c_p}{c_{p,\max}}$ – effective concentration of the polymer within the total aqueous phase.

2.4.3. Treatment of polymer retention effects

The process of polymer adsorption is included as an additional term in Eq. 2.8b, which represents a mass accumulation of polymer at the rock surface. A reverse process, or desorption, can be introduced in the model, so that adsorbed polymer concentration may decrease with time.

Permeability reduction as one of consequences of polymer retention is modelled using resistance factor R_k

$$R_k = 1 + (RRF - 1)\frac{c_p^a}{c_p^{a,\max}} \quad\text{...}(2.12)$$

where
$RRF \geq 1$ – residual resistance factor
$c_p^{a,max}$ – maximum polymer adsorbed

The inaccessible pore volume effect is considered in Eq. 2.8b, so that the polymer solution travels with a greater speed compared to tracers in the water phase.

Chapter 3. Upscaling

Nowadays, incorporating core petrophysical properties measurement, well logs and seismic reservoir characterization enables creation of large high-resolution 3D geological models. For instance, 900-million cell geological model of the Greater Burgan field in Kuwait, which is considered the biggest geological model, represents the complex structure of this giant field and its heterogeneities (Filak et al., 2012). Present reservoir simulators cannot handle more than on the order of 10^6 simulation cells efficiently; flow simulations for large models become computationally heavy and require special treatment such as parallel simulation, which was implemented for an older version of Burgan full-field model that consisted of 1.6 million cells (Su et al., 2011). However, this approach may be inefficient if the number of simulation cases rises due to use of several geological models that aim to treat subsurface uncertainties differently, or due to needs in history matching of the model.

Upscaling is a common solution for such problems, as it aims to replace a high-resolution fine-scale model with a lower-resolution coarse model. The upscaling process should assign effective properties to each cell of the coarse grid to represent the flow behavior occurring in the part of the fine-scale model represented by the associated coarse cell. This concept is illustrated in **Fig. 3.1**. A number of neighboring fine grid cells (black edges) is extracted from the original fine-scale model with a large number of grid cells and some vertical and lateral heterogeneities. These fine scale cells will then be aggregated into a bigger coarse cell (red edges), which properties are homogenized by implementing one of the averaging techniques and which can finally be put back into the model together with other coarse cells created using the same procedure. The resulting model consists of a smaller number of cells, which makes simulations faster. However, fine scale details and heterogeneities are lost due to a lower resolution, which may have a significant impact on the coarse-scale simulation results.

Fine model

Coarse model

Upscaling

Sampling

Upscaling region
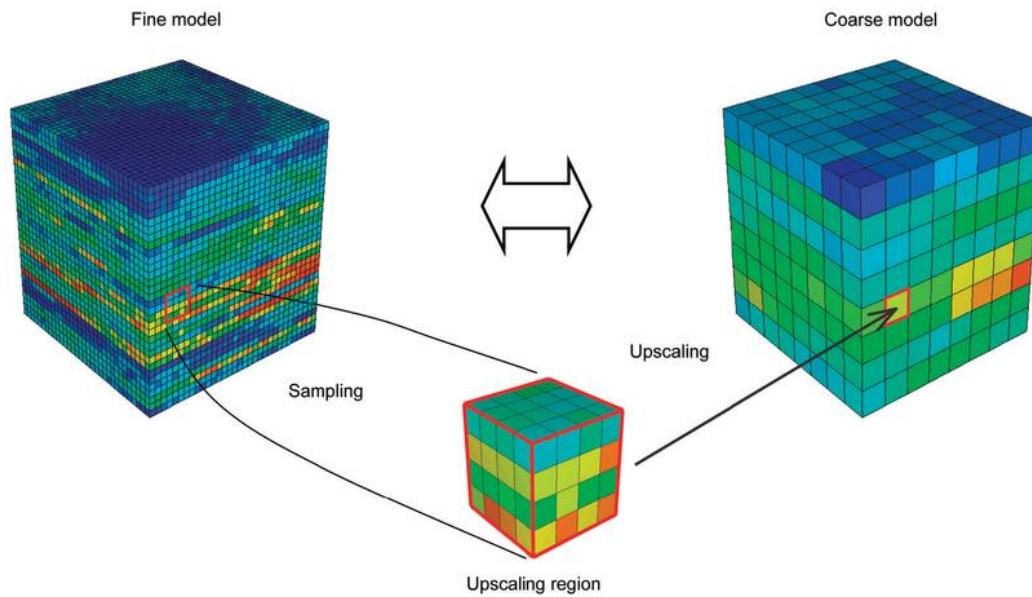
Fig. 3.1 – Representation of the upscaling concept (taken from SPE International, 2015)

When upscaling is being performed, the solution obtained with the fine-scale model is referred to as the truth, and the main goal of upscaling becomes to fit fine-scale simulation results as close as possible. To find upscaling techniques that are not computationally demanding and that allow generating coarse models, which would reproduce fine models results, is the main objective of study in the field of models upscaling.

3.1. Upscaling methods classification

Various upscaling techniques have been developed, and different classifications of the upscaling techniques exist. Mansoori (1994) divided upscaling methods into numerical, analytical, and tensor. Another classification approach was described by Farmer (2002) who considered upscaling methods as two-stage procedures where the first stage was to solve a fine grid problem in one or more dimensions, and the second stage was to use the results obtained at the first stage to determine coarse scale properties. If a stage is performed locally, within a region corresponding to a single coarse cell or a region that includes a coarse cell and some fine cells around it, it is named local, otherwise it is said to be global. Since there are two stages, the methods are therefore classified into local-local, global-local, local-global and global-global (Farmer, 2002). The main difference between global and local methods performance is that the global methods can give very accurate results for a particular set of boundary conditions and wells (Durlofsky, 2005); however, if a model upscaled using a global method is used for a different flow scenario (e.g. a different well placing), huge discrepancies may occur. This problem is avoided in local methods, but these methods are sensitive to the choice of boundary conditions at the stage of solving fine-scale problem, so that the results may be affected severely.

Christie (1996) uses another type of classification in his review, which takes into account the types of parameters that are upscaled. Thus, the upscaling methods can be divided into single-phase methods (e.g. power-law averaging, harmonic-/arithmetic-mean techniques,

pressure-solver methods, renormalization techniques, flow-based methods) that determine "effective permeability" that transfers the main flow behavior trends from fine scale to coarse scale, and two-phase methods that can capture more features of the flow by determining effective relative permeabilities besides effective absolute permeability. This last classification approach or its combination with the one described by Farmer (2002) are the most commonly used in the literature.

3.2. Single-phase upscaling

Single-phase upscaling is the simplest form of upscaling and, therefore, is the best understood and most widely used one (Christie, 1996). A broad overview of different single-phase upscaling techniques can be seen in the review of Durlofsky (2005).

In case of single-phase flow, only bulk parameters, such as porosity and absolute permeability, need to be upscaled. If a three-dimensional domain Ω represents the coarse-scale grid cell to be upscaled (see **Fig. 3.2**), then porosity can be upscaled by using volumetric averaging:

$$\varphi^* = \frac{1}{V_\Omega} \int_\Omega \varphi(x)dx \quad \dots\dots\dots\dots\dots\dots\dots\dots\dots\dots\dots\dots\dots\dots\dots\dots\dots\dots\dots\dots\dots\dots\dots\dots\dots\dots\dots\dots(3.1)$$

where V_Ω is the total volume of the domain, and the asterisk denotes an upscaled parameter.
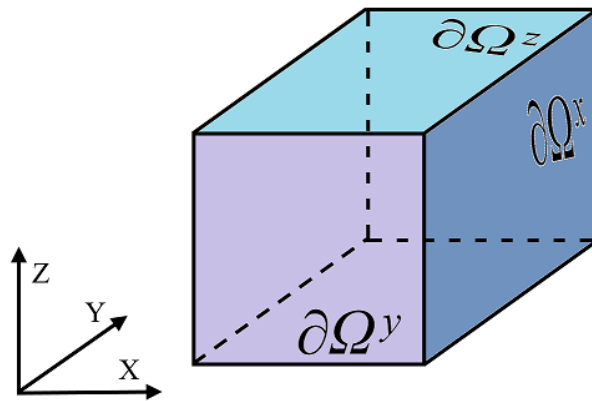
Fig. 3.2 – Representation of the three dimensional domain Ω. Here $\partial\Omega^x$, $\partial\Omega^y$, $\partial\Omega^z$ denote boundaries of the domain at the low pressure side in directions *X*, *Y* and *Z*, respectively

One method to upscale the absolute permeability *K* is using a flow-based upscaling method. Assume that fixed boundary conditions are applied for the domain Ω:

$$p\left(\partial\Omega_{inlet}^{d_1}\right) - p\left(\partial\Omega_{outlet}^{d_2}\right) = \begin{cases} \Delta p_d & \text{if } d_1 = d_2 \\ 0 & \text{if } d_1 \neq d_2 \end{cases} \quad \dots\dots\dots\dots\dots\dots\dots\dots\dots\dots\dots\dots\dots\dots(3.2)$$

where d_1 and d_2 denote direction and Δp_d is the pressure drop in this direction.

To find the effective absolute permeability, the pressure equation

$$\nabla \cdot (K\nabla p) = 0 \dotfill (3.3)$$

should be solved for each direction *X*, *Y* and *Z* by applying a pressure drop across the domain *Ω* in order to define total flow rates in all directions. By equating the total flow rate in each direction *d* defined on the fine scale with total flow rate that should pass through the coarse scale cell, the upscaled absolute permeability can be determined as follows:

$$K_d^* = \frac{q_d L_d}{A_d \Delta p_d} \dotfill (3.4)$$

where q_d, L_d and A_d are total flow rate, domain length and domain face area, respectively, in direction *d*. The obtained effective absolute permeability tensor K^* will consist of diagonal elements K_x^*, K_y^*, K_z^*. The full tensor of absolute permeability can be obtained when periodic boundary conditions are applied. The equations and analysis for this procedure can be found in the articles of Durlofsky (1991), Bøe (1994) and Pickup et al. (1994).

3.3. Two-phase upscaling

Two-phase upscaling procedure is more complex than single-phase upscaling, since it involves calculations of other effective parameters besides absolute permeability (i.e. relative permeabilities, capillary pressure, saturation), and it is less understood compared to simpler upscaling techniques (Christie, 1996). As it can be seen in the flow Eqs. 2.7a - 2.7b, saturations are time-dependent, and capillary pressure and relative permeability are functions of saturation. Thus, to upscale relative permeabilities and capillary pressure, numerous saturation values should be considered to obtain the full curves of upscaled two-phase parameters.

Two main approaches in two-phase upscaling exist: the dynamic approach and the steady-state approach. Dynamic methods imply computation of the flow on the fine scale using appropriate boundary conditions to determine pseudorelative permeabilities that relate flow rate to the pressure gradient, which depend on saturation distribution within gridblocks that is changing with time (Barker & Thibeau, 1997). The review of different dynamic methods can be found in articles of Barker & Thibeau (1997) and Barker & Dupouy (1999). Steady-state methods are based on the assumption that the fluid flow has reached steady state, which gives advantages in terms of computational efficiency compared to the dynamic methods (Ekrann & Aasen, 2000). However, the applicability of these methods can be questioned, since the flow of fluids through porous media during oil recovery is a transient process by its nature (Ekrann & Aasen, 2000). Herein, however, the steady-state methods stay in the main focus of the study.

Two-phase flow upscaling is rate dependent (Ekrann et al., 1996; Kumar et al., 1997), and some methods to evaluate the force balance and perform upscaling when neither capillary nor viscous forces can be neglected were developed (Virnovsky et al., 2004; Odsæter et al., 2015; Hilden & Berg, 2016). Herein the extreme cases of capillary and viscous limits will be considered.

3.3.1. Capillary limit

The capillary limit (CL) method assumes that the fluids in the area of interest are in capillary equilibrium. This is only valid in the case of a small viscous pressure gradient, which is, however, a reasonable assumption for regions where the flow rate is low (Pickup et al., 2000). In the CL method, the problem of determining saturation on fine scale is solved by declaring a constant capillary pressure. The CL method procedure description can be found in the works of Pickup et al. (2000) or Hilden et al. (2014), the schematic representation of its algorithm is shown in **Fig. 3.3**.
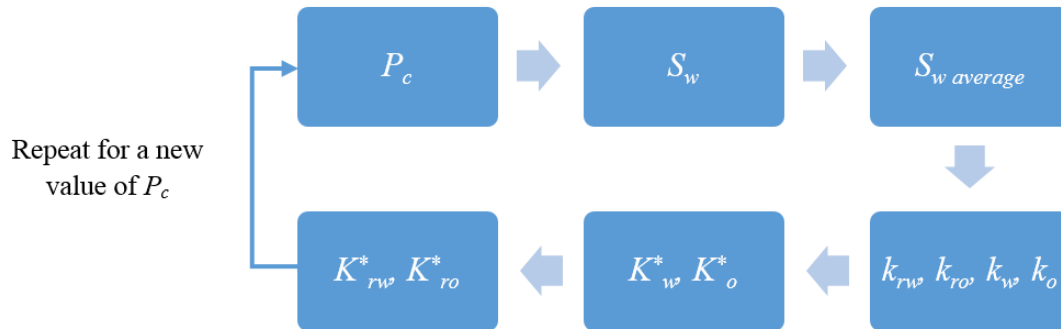
Fig. 3.3 – CL method algorithm scheme

As presented in Fig. 3.3, a value of the capillary pressure P_c is first selected. The capillary pressure is then used to obtain the saturation distribution S_w by calculating the fine-scale values from the capillary pressure curve. The volumetric average of water saturation $S_{w\ average}$ can thus be calculated for the region of interest. Then the values of water and oil relative permeabilities k_{rw} and k_{ro} should be obtained for all cells in the fine grid. These values should be used to define phase permeabilities k_w and k_o by multiplying by the cell permeabilities. Two separate single-phase upscaling runs, one for each phase, need to be performed after that to determine effective phase permeabilities K^*_w and K^*_o. These will be used to find effective relative permeabilities K^*_{rw} and K^*_{ro} when divided by effective absolute permeability. The whole procedure should be repeated for other values of capillary pressure in order to obtain full curves of relative permeabilities.

3.3.2. Viscous limit

Viscous limit (VL) is based on the assumption that viscous forces in the region dominate, and the capillary forces can be neglected. This may be a valid assumption in case of high flow velocities in the region. The saturation equation for steady-state flow in case when capillary forces are neglectable can be described as follows (Ekrann & Aasen, 2000, see the derivation details in Appendix 1):

$$\nabla f_w \cdot u_t = 0 \quad \text{...}(3.5)$$

where
f_w – fractional flow
u_t – total velocity

It can be seen that in case of viscous limit assumption, fractional flow at the inlet face determines the solution, and it does not change along the streamlines (Ekrann & Aasen, 2000). The VL method procedure description can be found in the works of Pickup et al. (2000) or Hilden et al. (2014), the schematic representation of its algorithm is shown in **Fig. 3.4**.
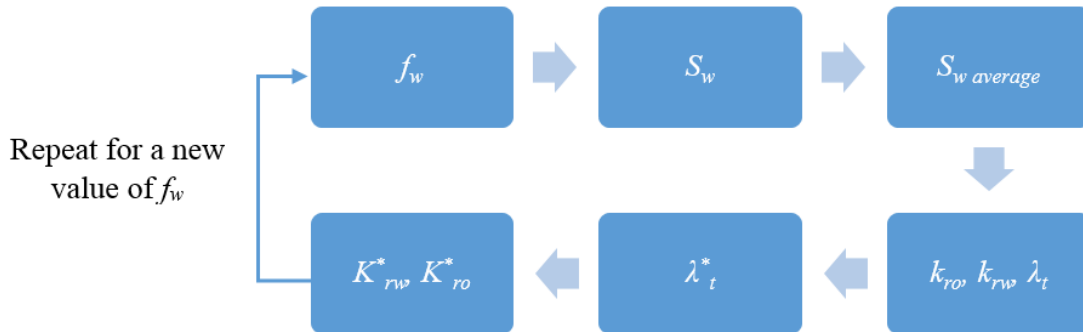
Fig. 3.4 – VL method algorithm scheme

As it is presented in Fig. 3.4, first a value of fractional flow f_w is selected; it is then used to obtain a saturation distribution S_w from the fractional flow curves for each fine grid cell, and the volumetric average of water saturation $S_{w\ average}$ can thus be calculated for the region of interest. Then the values of water and oil relative permeabilities k_{rw} and k_{ro} should be obtained at average water saturation in the region, these values should be used to define total mobility λ_t. Single-phase upscaling should be then performed to determine the effective total mobility λ^*_t, which will be used to find effective relative permeabilities K^*_{rw} and K^*_{ro} when divided by effective absolute permeability. The whole procedure should be repeated for other values of fractional flow in order to obtain full curves of relative permeabilities.

3.3.3. End-point scaling

The idea behind end-point scaling (EPS) method is that the relative permeabilities and capillary pressure curves in the coarse blocks are scaled analogues of the original fine-scale curves with changes in end-points, maximum water relative permeability and maximum capillary pressure values (Hilden & Berg, 2016). The description of the procedure can be found in the article of Hilden & Berg (2016), and it is summarized below.

First, the pore-volume average values of S^*_{wir}, 1-S^*_{or} and $p^*_{cow,max}$ are determined for each coarse block, taking that any pore-volume average property x in a coarse gridblock is obtained as:

$$x_{average} = \frac{\sum_{i=1}^{N} x_i \varphi_i V_i}{\sum_{i=1}^{N} \varphi_i V_i} \quad\text{...(3.6)}$$

Maximum point of the water relative permeability curve $k^*_{rw,max}$=$k^*_{rw}(1$-$S^*_{or})$ should be computed, and the pore-volume average of relative permeabilities and capillary pressure curves need to be obtained. These curves are afterwards scaled using the following relationships:

$$k_{ro}^{*}\left(S_{w}^{*}\right)=k_{ro}^{average}\left(S_{w}^{scaled}\right)$$

$$k_{rw}^{*}\left(S_{w}^{*}\right)=k_{rw}^{average}\left(S_{w}^{scaled}\right)\frac{k_{rw,\max}^{*}}{\max(k_{rw}^{average})}$$ ....(3.7)

$$p_{cow}^{*}\left(S_{w}^{*}\right)=p_{cow}^{average}\left(S_{w}^{scaled}\right)\frac{p_{cow,\max}^{*}}{\max(p_{cow}^{average})}$$

where S_{w}^{scaled} is given by

$$S_{w}^{scaled}=\frac{S_{w}^{*}-S_{wir}^{*}}{1-S_{wir}^{*}-S_{or}^{*}}$$

3.4. Polymer flow upscaling

Upscaling of the EOR processes is a relatively new field of study, and there is not much literature available. Polymer flooding upscaling has been investigated in several studies (Larssen, 2013; Hilden et al., 2014). Polymer flow parameters upscaling methods presented in those works will be summarized herein. In addition, the focus of current study will be presented.

3.4.1. Upscaling of different polymer flow parameters

It can be shown that at steady state polymer concentration is constant in space (Larssen, 2013), and, therefore, effective viscosities of water and water with polymer can be eliminated from the steady-state equations. Thereby, effective viscosities $\mu_{w,eff}$, $\mu_{p,eff}$ and mixing parameter ω are not usually upscaled (Hilden et al., 2014). Then, the polymer flooding parameters to be upscaled are reduction factor R_k, polymer adsorption c_p^a and residual resistance factor RRF.

Larssen (2013) upscaled permeability reduction factor using expression for the upscaled water flux in polymer flooding determined for pressure drop in each direction. Larssen (2013) observed that upscaled reduction factor was dependent on water saturation aside from polymer concentration; however, it was not possible to define the trend of $R_k - S_w$ relationship.

The algorithm of upscaling reduction factor suggested by Hilden et al. (2014) comprises performing a two-phase upscaling of fine-scale relative permeability curves that take permeability reduction into account initially so that

$$k_{rw}^{fine}=\frac{k_{rw}}{R_{k}\left(c_{p}\right)}$$ ....(3.8)

Having upscaled relative permeability curves, the upscaled reduction factor appears as the ratio of upscaled water relative permeability that does not consider R_k to upscaled relative permeability accounting for permeability reduction. Saturation dependence of reduction factor was also reported (Hilden et al., 2014), and the tendency of upscaled reduction factor to decrease with increase in water saturation was observed.

To upscale polymer adsorption, both Larssen (2013) and Hilden et al. (2014) use simple volume averaging procedure:

$$c_a^*\left(c_p^*\right) = \frac{\int_\Omega \rho_{rock}\left(1-\varphi\right)c_a\left(c_p\right)dV}{\int_\Omega \rho_{rock}\left(1-\varphi\right)dV} \quad \text{..(3.9)}$$

Residual resistance factor upscaling proposed in Larssen (2013) is based on the relation between *RRF*, R_k and $c_p{}^a$ (Eq. 2.12). As it can be seen, plotting reduction factor versus adsorbed polymer should produce a straight line, where the slope is defined by *RRF* and $c_p{}^{a,max}$. Assuming that the same relation is valid for the upscaled version of Eq. 2.12, residual resistance factor can be found using the slope of the straight line mentioned above:

$$RRF^* = \frac{\left(R_k^*-1\right)}{c_p^{a*}} c_p^{a,max\,*} + 1 \quad \text{..(3.10)}$$

However, this approach results in an upscaled residual resistance factor varying in space and with saturation, which complicates the model. Therefore, other methods should be considered, for instance, Larssen (2013) suggests using single upscaled RRF value defined as a mean value of saturation-dependent upscaled residual resistance factors.

3.4.2. Upscaling procedure considered in current study

The present thesis is focused on polymer adsorption upscaling for a realistic full-field model, while upscaling of other polymer flow parameters, such as permeability reduction and residual resistance factor, is omitted. Several researchers (Larssen, 2013; Hilden et al., 2014) applied simple averaging techniques to upscale polymer adsorption. In this study, the aim is to go a little beyond this methodology and check the following: if a functional dependence between adsorption and another parameter being upscaled (e.g. permeability) exists, is the averaging of fine-scale adsorption values capturing polymer flooding effects more precisely compared to finding coarse scale adsorption values as function of upscaled permeability?

In other words, accuracy of polymer adsorption upscaling according to the following formulae is being compared:

- Upscaled values of polymer adsorption are calculated using upscaled values of the independent parameter as input

$$x_{upscaled} = x\left(y_{upscaled}\right) \text{..(3.11)}$$

- Upscaled values of polymer adsorption are calculated as simple volumetric average of fine-scale values of polymer adsorption

$$x_{upscaled} = \frac{\sum V_i x\left(y_{fine-scale}\right)}{\sum V_i} \quad \text{..(3.12)}$$

Chapter 4. Numerical model

All simulations were performed using black oil reservoir simulator ECLIPSE (Schlumberger, 2015); therefore, all input data were adapted to the format required by ECLIPSE. Preliminary calculations were performed using MATLAB (The MathWorks, Inc., 2014), which was acting as a computational tool with flexible output format. Upscaled models were created using the MATLAB Reservoir Simulation Toolbox (MRST), an open source code developed by SINTEF ICT (SINTEF ICT, 2015), and the extensions to MRST created by Hilden (2016). In the following chapter, the numerical model used in the study will be presented, and the procedure to obtain input data into the model to perform polymer flooding run will be discussed.

4.1. Model description

In this study, the second data set in the 10th SPE Comparative Solution Project (Christie & Blunt, 2000) is used to investigate different upscaling techniques efficiency. The data set is a three-dimensional computationally heavy model representing a part of a Brent sequence described on a regular Cartesian grid with 1122000 cells. The main parameters of the model are described in **Table 4.1**.

The upper layers of the reservoir model represent a shallow-marine Tarbert formation, and the bottom layers represent a fluvial Upper-Ness formation. Both formations are very heterogeneous with large variations in permeability and porosity (see **Fig. 4.1**). Among 1122000 cells 27630 cells (2.46% of the cells) have zero porosity and are considered to be inactive.

As it can be seen in Fig. 4.1, there are four producing wells in each corner of the model, and one injector in the middle of the model. Well INJE1 injects water in the reservoir at a constant rate of 795 m^3 at reservoir conditions, and production wells PROD1, PROD2, PROD3 and PROD4 operate with a target bottomhole pressure of 275 bar. The model is very heterogeneous, and the presence of capillary pressure data increases computation time significantly. For example, a 2000 day waterflooding experiment was simulated in 109 hours when there were no capillary pressure data; the same simulation but with 10 different capillary pressure curves included took 124.8 hours.

Numerous lateral and vertical heterogeneities, presence of geological features such as tortuous fluvial channels, different saturation functions used and presence of capillary forces make this modified SPE10 model a perfect candidate for testing different upscaling techniques.
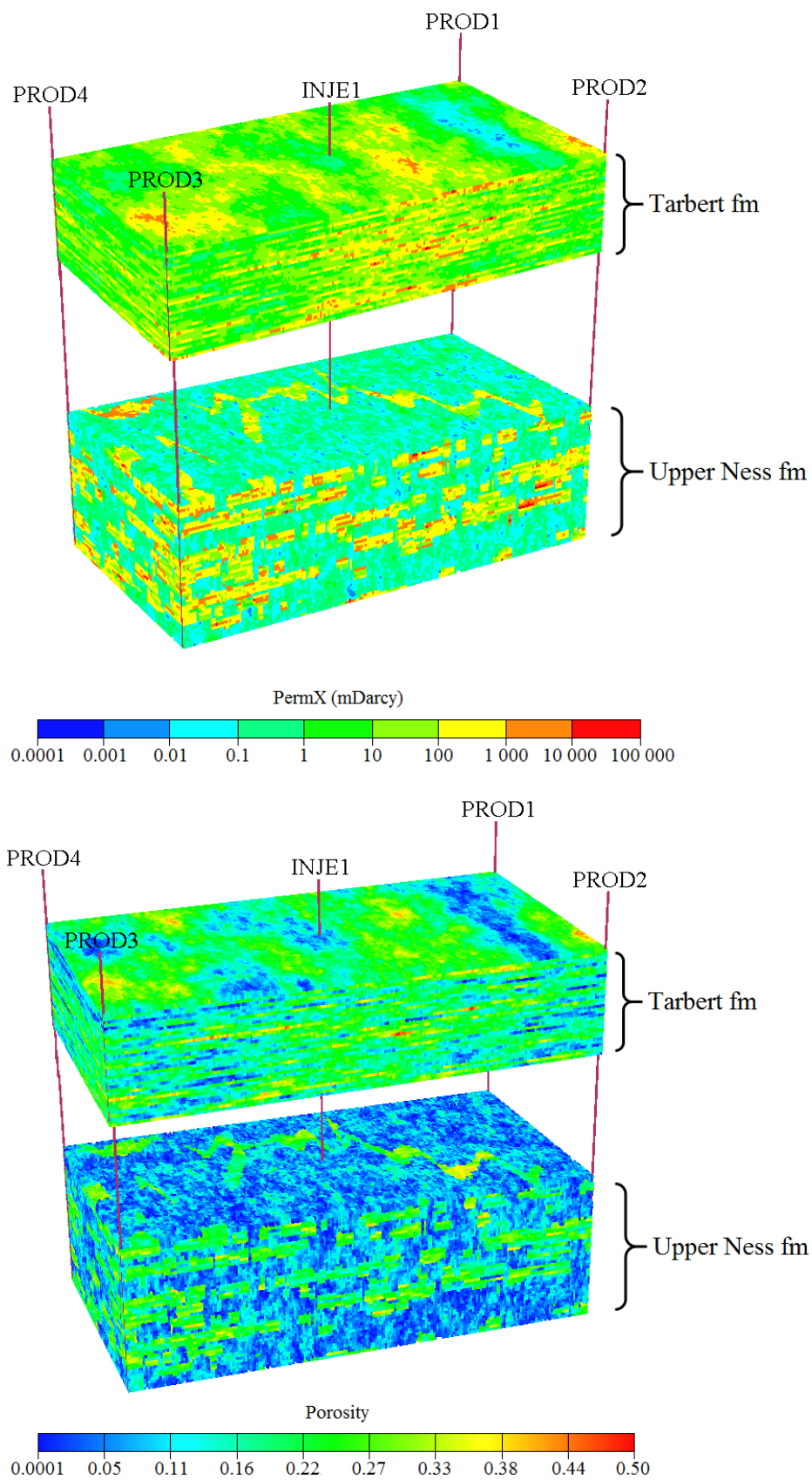
Fig. 4.1 – Porosity and permeability in X-direction distribution of the SPE10 model. The two formations are separated from each other to show lateral distribution of the parameters in the bottommost formation

Table 4.1. Fine grid model properties.

Parameter	Value	Units
Model dimensions (NXxNYxNZ)	60x220x85	–
Number of cells / active cells	1122000 /	–
Gridblock dimensions (DXxDYxDZ)	6.096x3.048x0.6096	m
Depth of the reservoir	3650	m
Thickness of the reservoir	51.816	m
Oil-water contact depth Gas-oil contact depth	3800	m
Density of oil at surface conditions, ρ_o	849	kg/m^3
Density of water at surface conditions, ρ_w	1025	kg/m^3
Density of gas at surface conditions, ρ_g	0.82	kg/m^3
Reference pressure, P_{ref}	275	bar
Water formation volume factor, B_w @ P_{ref}	1.01	m^3/m^3
Water compressibility, c_w @ P_{ref}	4.5e-5	1/bar
Water viscosity, μ_w @ P_{ref}	0.3	cP
Rock compressibility, c_r @ P_{ref}	1.45e-5	1/bar
Initial water saturation, $S_{watinit}$	0.1	–
Initial pressure, P_i	280	bar
Number of production wells	4	–
Number of injection wells	1	–
Injection well control mode	Reservoir volume rate target RESV=795	rm^3/day
Production well control mode	Bottomhole pressure limit BHP=275	bar
Simulation period	2000	days

4.2. Input into the model

4.2.1. Water saturation functions

Basic model properties, such as permeability and porosity distribution, PVT data for each flowing phase, number and placing of wells, their production controls were taken from the original data set. The water saturation functions, however, were changed.

Originally, the SPE10 model does not comprise capillary pressure data (Christie & Blunt, 2000). However, the features of the upscaling methods considered in this study and presented earlier in Chapter 3 imply that capillary pressure curves should be introduced. Thus, a modification of the saturation-dependent functions introduced by Hilden & Berg (2016) was used.

Hilden & Berg (2016) used Leverett J-function and assumed values of surface tension and contact angle to compute capillary pressures for 10 rock types within the model, predefined based on the rock properties. The procedure and formulae used can be seen in the article of Hilden & Berg (2016).

The tabulated results of capillary pressure values calculations were used as input in this study and are presented in **Fig. 4.2** together with relative permeabilities in each region.
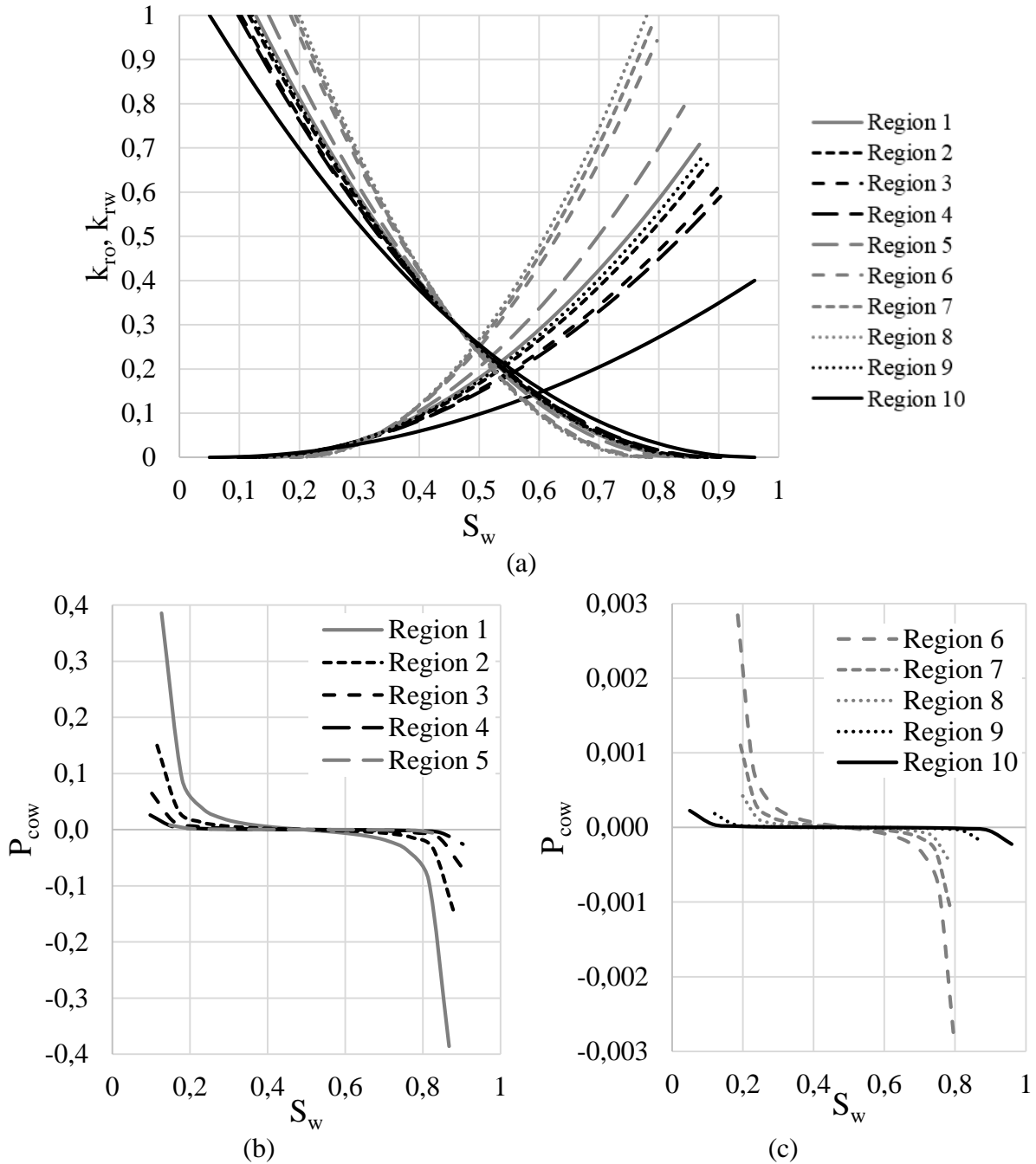
Fig. 4.2 – Relative permeability curves (a) and capillary pressure curves (b, c) in different regions of SPE10 model

4.2.2. Adsorption data for polymer flooding simulation cases

Adsorption of the polymer on the rock face is an important effect influencing the efficiency of polymer flooding, as it was discussed in Chapter 2, and it is in the focus of the present study.

First step was to find experimental data relating adsorption with one of the parameters that are being upscaled. Obviously, such parameter should be rock permeability. However, as

it was discussed in Chapter 2, adsorption is one of the mechanisms of polymer retention, and it cannot be easily separated from mechanical entrapment or hydrodynamic entrapment. Thus, the most experimental data indicate relationship between retention in general and permeability of the core used in experiments. There were not many retention-permeability experimental results available in the literature; however, two of them are considered in this Chapter.

The first data set used was a strongly permeability-dependent retention values obtained by Vela et al. (1976) during polymer flow tests (see **Fig. 4.3**).
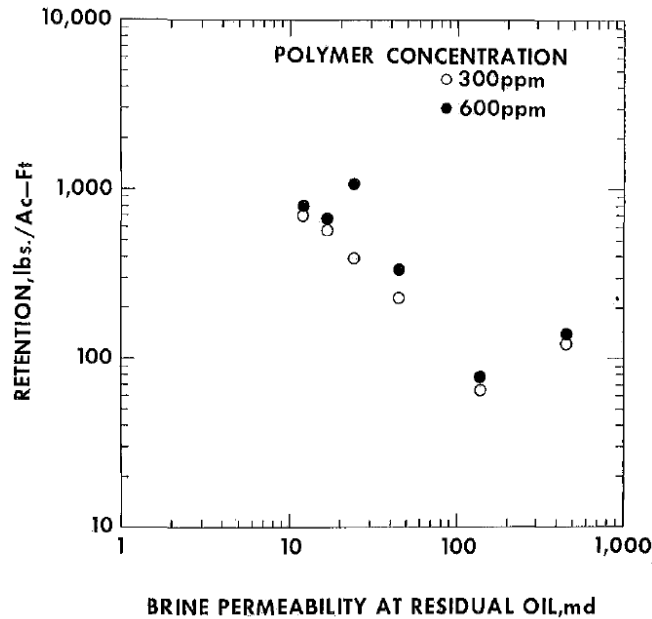
Fig. 4.3 – Variation of polymer retention with permeability (taken from Vela et al., 1976)

Polymer flow tests conducted by Vela et al. (1976) comprised sequential injection of polymer solutions with different concentrations (from smaller to greater) and brine and retention measurement of polymer retention using material balance equation. Results are reported for two different polymer concentrations; however, the differences are not drastic, so it was decided to treat all data points as one data set with some outlying points.

Original data acquired by Vela et al. (1976) is shown in **Table 4.2**, where red color indicates outliers that were taken out to obtain a more accurate straight-line behavior while plotting the data on log-log scale (see **Fig. 4.4**).

Table 4.2. Tabulated retention data from Vela et al. (1976).

k @ S_{or}, mD	Retention, lbm/acre-ft	
	300ppm	600ppm
12	700	772
17	580	668
30	561	818
45	224	332
137	64	75
453	125	130
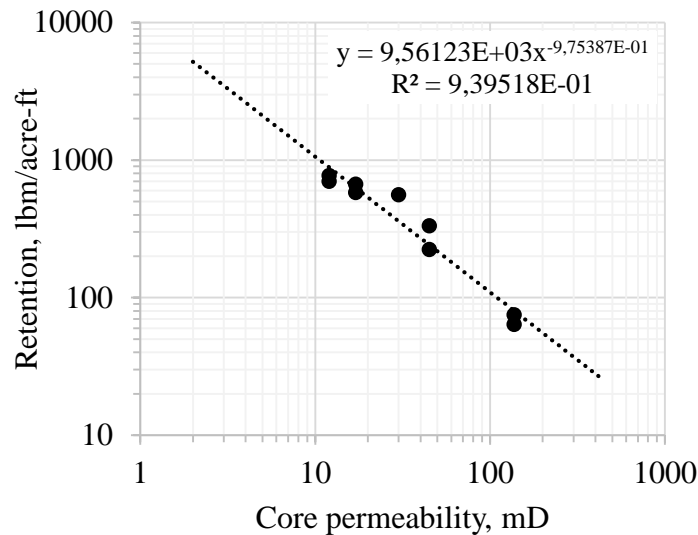
Fig. 4.4 – Plotted retention data without outlier points (based on Vela et al., 1976)

This data set and the trend line equation relating polymer retention and core permeability will be further referred as data set A and function A, respectively.

Second experimental data set was taken from the article of Sorbie et al. (1982), who collected published data and "scaled it into appropriate experimental range for synthetic polymers" (Sorbie et al., 1982). The results obtained by Sorbie et al. (1982) are presented in **Fig. 4.5**.
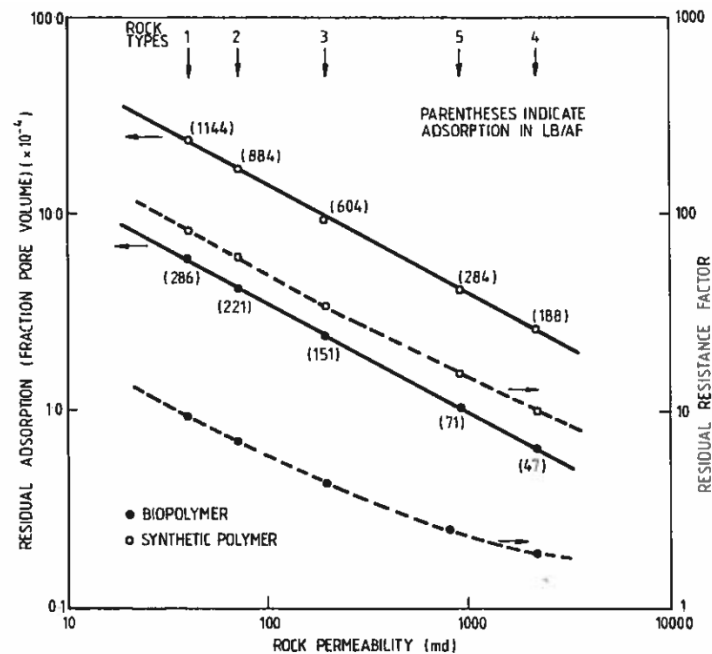
Fig. 4.5 – Correlation of polymer retention and residual resistance factors with rock permeability (taken from Sorbie et al., 1982)

Fig. 4.5 shows residual resistance factor curves (dashed lines) and adsorption curves (bold lines) for biopolymers and synthetic polymers that are marked with black and white markers, respectively. As we will be concentrating on synthetic polymers, only one curve will be used in this thesis: the upper line corresponding to the residual adsorption of synthetic

polymer. Adsorption values corresponding to each rock type are presented in **Table 4.3** and plotted on log-log scale in **Fig. 4.6** to obtain the trend line equation.

Table 4.3. Tabulated retention data from Sorbie et al. (1982).

k, mD	Retention, lbm/acre-ft
40	1144
70	884
187	604
886	284
2113	188
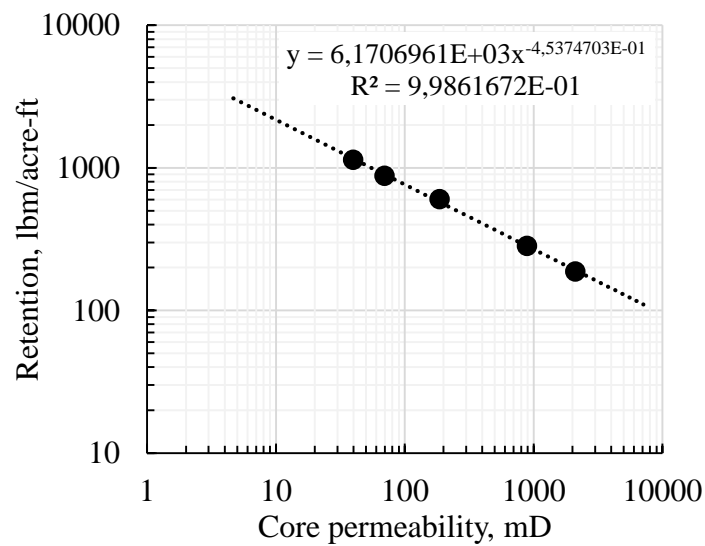
Fig. 4.6 – Plotted retention data (based on Sorbie et al., 1982)

This data set and the trend line equation relating polymer retention and core permeability will be further referred as data set D and function D.

As it can be seen in **Fig. 4.7**, a large part of the model has permeability below 100 mD, which means that functions A and D need to be extrapolated to obtain retention values corresponding to these low permeabilities. When comparing Fig. 4.4 and Fig. 4.6, one might notice that function A, extrapolated towards smaller permeabilities, will give much higher retention values than function D. For instance, if the permeability of the core is 1 mD, retentions estimated with functions A and D will be 9561 and 6170 lbm/acre-ft respectively. The difference increases drastically when permeability becomes one order smaller, so that at 0.1 mD retentions obtained using functions A and D become 90344 and 17542 lbm/acre-ft, respectively.
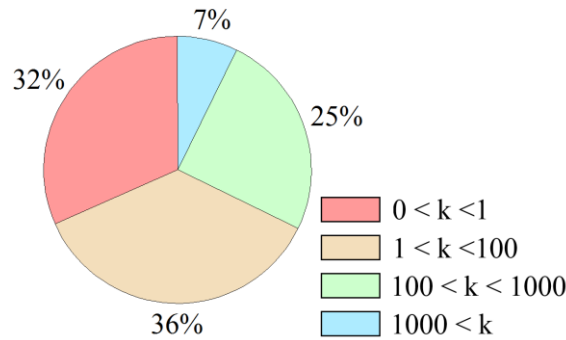
Fig. 4.7 – Fraction of SPE10 model cells with different permeability values k, mD

4.2.3. Converting retention to adsorption

The experimental data presented earlier relate retention of polymer and rock permeability. However, the objective is to define adsorption behavior with permeability. Conversion formula from retention in lbm/acre-ft to adsorption in µg/g is as follows:

$$\left[\frac{\mu g}{g} \right] = \frac{\left[\frac{lbm}{(acre \cdot ft)} \right]}{2.717 \cdot (1 - \varphi) \cdot \rho_{grain}} \quad \text{..(4.1)}$$

To consider adsorption during polymer flooding run in ECLIPSE 100, adsorption values should be entered within PLYADS keyword as a set of tables containing concentration of polymer adsorbed by the rock corresponding to different polymer concentrations in the solution for each type of rock. It is assumed that different rock types are distinguished according to their saturation functions: $k_{ro}(S)$, $k_{rw}(S)$, $P_{cow}(S)$. As it was mentioned before, the model was modified to have 10 different rock types, so a total of 10 PLYADS tables need to be generated.

To define adsorption values on the fine scale, adsorption values need to be grouped as the software will only accept 10 PLYADS tables. This means that instead of calculating adsorption for each cell, it will be calculated one for each rock type using the mean rock properties for each of these rock types. A script in MATLAB was developed to determine the mean rock properties for each rock type (which is called SATNUM region in ECLIPSE 100) and to define corresponding adsorption value that has to be assigned to the cells within the rock type region (see Appendix 2). The script's algorithm is shown in **Fig. 4.8**.
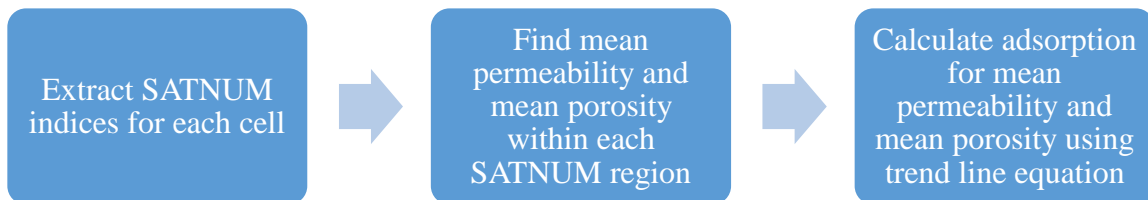
Fig. 4.8 – Algorithm of a MATLAB script to determine fine-scale adsorption values

Fig. 4.9 shows how the cells are distributed between rock types, and the corresponding mean rock properties for each rock type. These mean values were obtained using the MATLAB script described above.

(a)   (b)
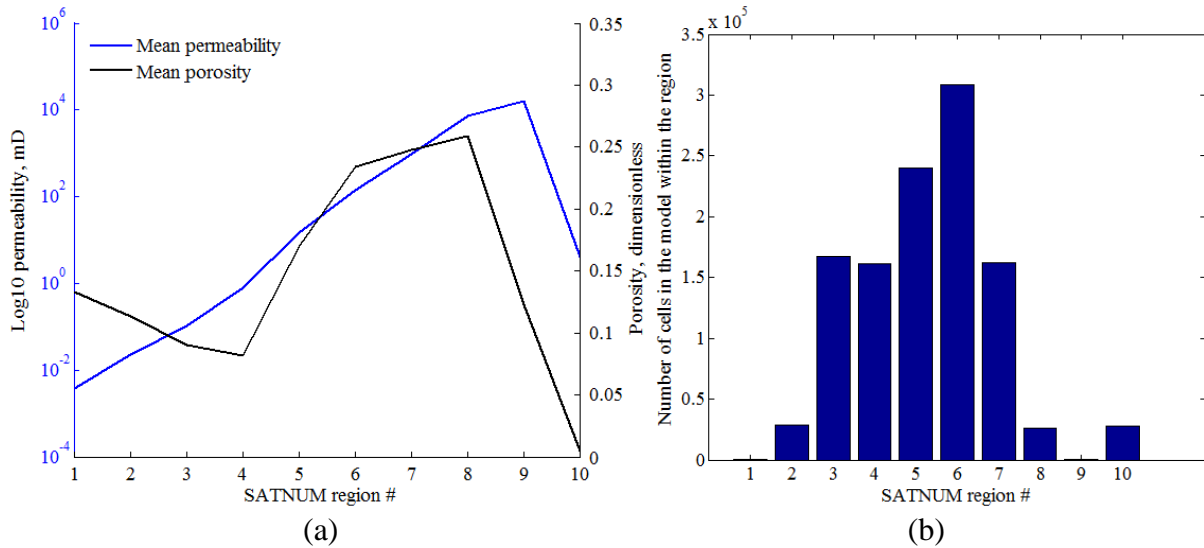
Fig. 4.9 – Mean rock properties (a) and number of cells within each rock type (b)

Using these mean properties and the retention functions A and D defined earlier, adsorption for each rock type can be calculated. The results of using different functions are shown in **Table 4.4** and are visualized in **Fig. 4.10**.

Table 4.4. Adsorption values for each rock type.

Rock type	Mean porosity	Mean permeability, mD	Retention A, lbm/acre-ft	Retention D, lbm/acre-ft	Adsorption A, kg/kg	Adsorption D, kg/kg
1	0.13	0.003	2224947	77869	3.563E-01	1.247E-02
2	0.11	0.02	389350	34611	6.099E-02	5.421E-03
3	0.09	0.1	87385	17272	1.334E-02	2.636E-03
4	0.08	0.8	12032	6867	1.821E-03	1.039E-03
5	0.17	14.8	688	1814	1.151E-04	3.036E-04
6	0.23	141.8	76	651	1.381E-05	1.181E-04
7	0.25	972.9	11	272	2.148E-06	5.019E-05
8	0.26	7125.1	1.7	110	3.129E-07	2.065E-05
9	0.12	15970.5	0.8	76	1.202E-07	1.209E-05
10	0.005	4.0	2469	3287	3.446E-04	4.588E-04
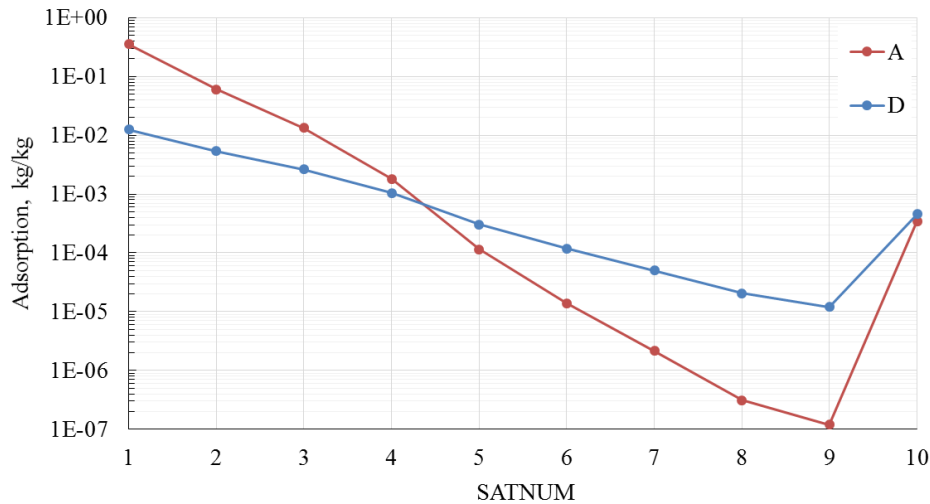
Fig. 4.10 – Adsorption values for each rock type obtained using different functions

As it can be seen in Fig. 4.10, the slope of function A is higher than that of function D; therefore, polymer adsorption values estimated by function A for low-permeability regions 1-3 are greater. Polymer adsorption estimated for rock type 1 is close to 1E+00, which is an unrealistically high number. Function D seems to give more appropriate (smaller) values in the low-permeability zone compared to function A; thus, function D will be in focus in the following discussion.

4.2.4. Cutoff adsorption functions with Carreau fluid model

Even though adsorption values in the low-permeability areas estimated with Function D are lower compared to those estimated with Function A, all the data corresponding to low-permeability areas are extrapolated. Thus, one cannot fully rely on these values, and it was decided to apply some additional modification to the adsorption curve appearing in Fig. 4.10 to limit the growth of adsorption value at low permeabilities.

To do so, a cutoff rule should be applied to the retention function to make retention (and, hence, adsorption) values flatten around some critical level corresponding to the low-permeability regions.

To assure a cutoff of an excessive growth of retention value in case of low permeability of a region, an analogue of the Carreau fluid model mentioned in Chapter 2 was used. An additional fitting parameter α was used in this model in place of the power index equal 2 as used in Chapter 2. This makes the fitting more flexible, and in line with the work of Yasuda et al. (1981).

The main idea behind Carreau fluid model can be applied to modify retention vs permeability dependency to merge all low-permeability regions in one in terms of retention value. To do this, retention and permeability should be used instead of viscosity and shear rate in Eq. 2.4, respectively (see **Table 4.5**).

Table 4.5. Transformation of Carreau model parameters.

Parameter from the original Carreau model	Parameter in the Carreau model analogue	Meaning
η_{inf}	RET_{inf}	Retention @ Maximum *PERMx*
η_0	RET_0	Retention @ Minimum *PERMx*
λ	$\lambda*$	Material coefficient*
γ	*PERMx*	Mean *PERMx* value in the region
2 (power index)	α	Power index*
n	$n*$	Power index*

tuning parameters

There is a high uncertainty in estimating polymer retention at maximum and minimum rock permeability; in the present study, the values of RET_{inf} and RET_0 were chosen based on the experimental data from Sorbie et al. (1982) presented earlier in Fig. 4.6 and on the maximum and minimum permeability values in the model.

The parameters marked with an asterisk in Table 4.5 were tuned by iterative calculations using the Solver option in MS Excel. The reference data for the fitting included rock permeability obtained during experiments by Sorbie et al. (1982), and so-called *Carreau-modified retention* values were calculated using Eq. 2.4 with the modifications described above and some initial guesses for each tuning parameter. Excel Solver was set to minimize the total error between experimental data and Carreau-modified values by changing the tuning parameters. Tuning quality evaluation was based on the value of total error, Carreau-modified curve shape and visual inspection of how well modified data fit experimental data in the region with medium permeability values.

Best match and expected S-shape of the Carreau-modified curve were obtained using values of tuning parameters presented in **Fig. 4.11**. The value of critical rock permeability below which retention values are stabilizing around RET_0 value was approximated as an intersection of the lines extrapolated from the left-hand side and right-hand side regions (analogues of the Newtonian and the power-law regions of the Carreau fluid model, respectively). Critical permeability value was estimated as 20 mD (see **Fig. 4.12**), which is higher than mean permeability value in SATNUM regions 1, 2, 3, 4, 5 and 10 where the greatest polymer retention will be observed.

$$y = 6{,}1706961E{+}03x^{-4{,}5374703E{-}01}$$
$$R^2 = 9{,}9861672E{-}01$$

η_{inf}	50
η_0	1500
λ	0.04469
α	24.2778
n	0.9603
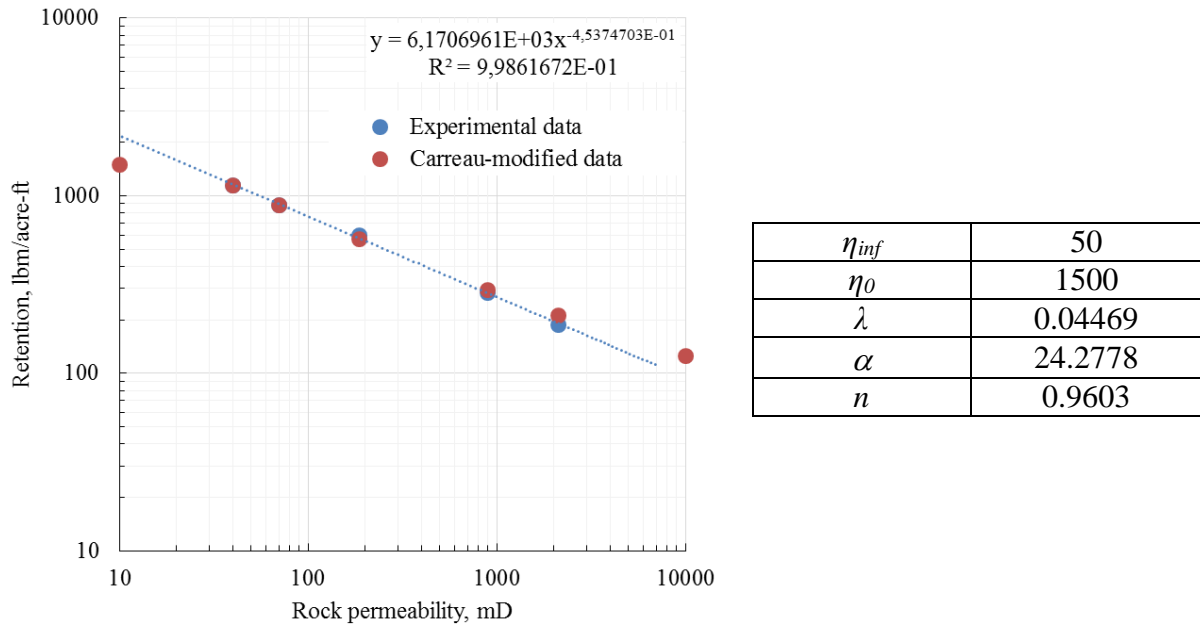
Fig. 4.11 – Optimal values of tuning parameters in the Carreau-modified function (right-hand side) and Carreau-modified retention data plotted together with the experimental data (left-hand side)
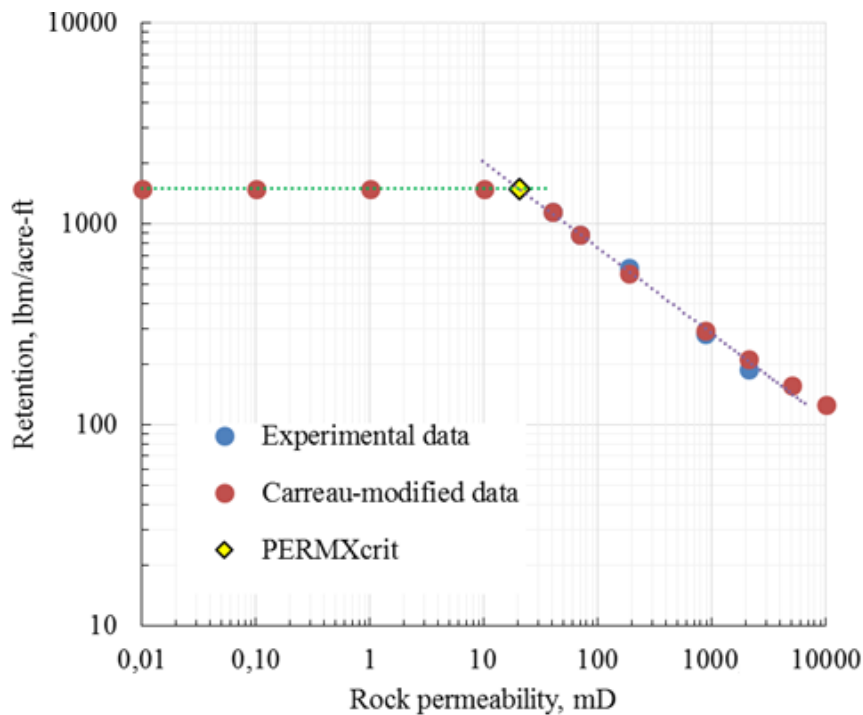
Fig. 4.12 – Critical rock permeability value

Having recalculated retention values using Carreau modification, new adsorption values were obtained for each region and plotted together with the values obtained using non-modified retentions (see **Fig. 4.13**). The values of adsorption in each SATNUM region of the model are listed in **Table 4.6** below.
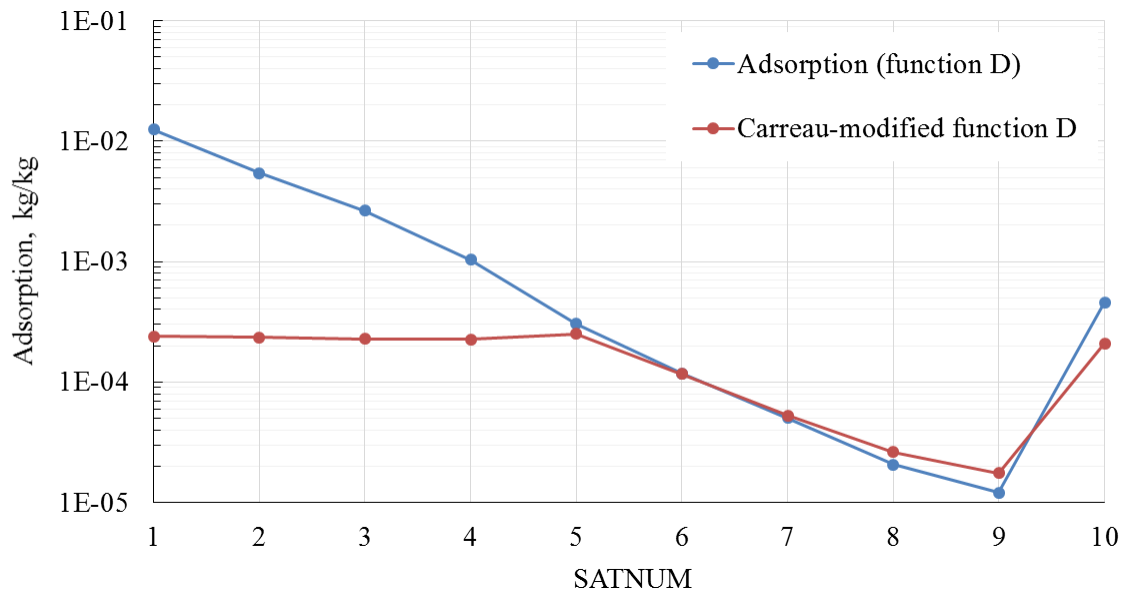
Fig. 4.13 – Original adsorption values and values after Carreau modification (function D)

Table 4.6. Adsorption values assigned to each region of fine-scale model

Rock type	Mean porosity	Mean permeability, mD	Adsorption D modified, kg/kg
1	0.13	0.003	2.402E-04
2	0.11	0.02	2.350E-04
3	0.09	0.1	2.289E-04
4	0.08	0.8	2.270E-04
5	0.17	14.8	2.510E-04
6	0.23	141.8	1.170E-04
7	0.25	972.9	5.262E-05
8	0.26	7125.1	2.624E-05
9	0.12	15970.5	1.757E-05
10	0.005	4.0	2.093E-04

Chapter 5. Upscaled models

SPE10 fine scale model presented in Chapter 4 served as the base to create computationally easier upscaled models. As it was denoted in Chapter 3, different parameters of a simulation model can be upscaled in a variety of ways depending on the type of the parameter and validity of the assumptions made in one or another method. In the present thesis, the upscaling of bulk parameters and absolute permeability were not in the main focus; however, the upscaling of relative permeabilities, capillary pressure and polymer adsorption was performed using the methods described in Chapter 3.

5.1. Properties of the upscaled models

5.1.1. Models dimensions

The original model was coarsened by factor of 4x4x5 in X, Y and Z directions, respectively. That means that each coarse model consists of 15x55x17 cells, making 14025 cells in total, which is 4x4x5=80 times smaller than the number of cells in SPE10 model initially. Thus, the new cells' dimensions became 24.4x12.2x3.05 m (DXxDYxDZ). As the coarsening influences cells dimensions, well placing becomes less flexible, and it should be noted that wells' positions might slightly change after upscaling. **Fig. 5.1** shows how injector and producer positions change after fine cells (black edges) were aggregated into a coarse cell (red edges).

● Well position in fine-scale model
● Well position in coarse model
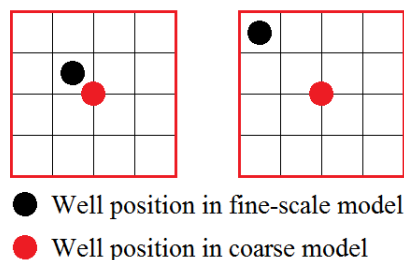
Fig. 5.1 – Well position changes due to upscaling (coarsening factor 4x4x5)

Changes in the injection well position are shown in the left-hand side of Fig. 5.1, production well position changes – on the right-hand side. For the current coarsening factor of 4x4x5, the changes in injection well position are estimated as 3.4 m, while for production wells the change is three times higher – 10.2 m. As the shifts in well position due to the coarsening is significantly shorter than the overall length between the wells, these well position changes will be considered negligible.

5.1.2. Porosity and permeability

Porosity and permeability in all upscaled models were obtained using the same procedure: pore-volume averaging for porosity and flow-based single-phase upscaling for permeability, which was presented in Chapter 3. **Fig. 5.2** represents porosity and permeability of the upscaled model.
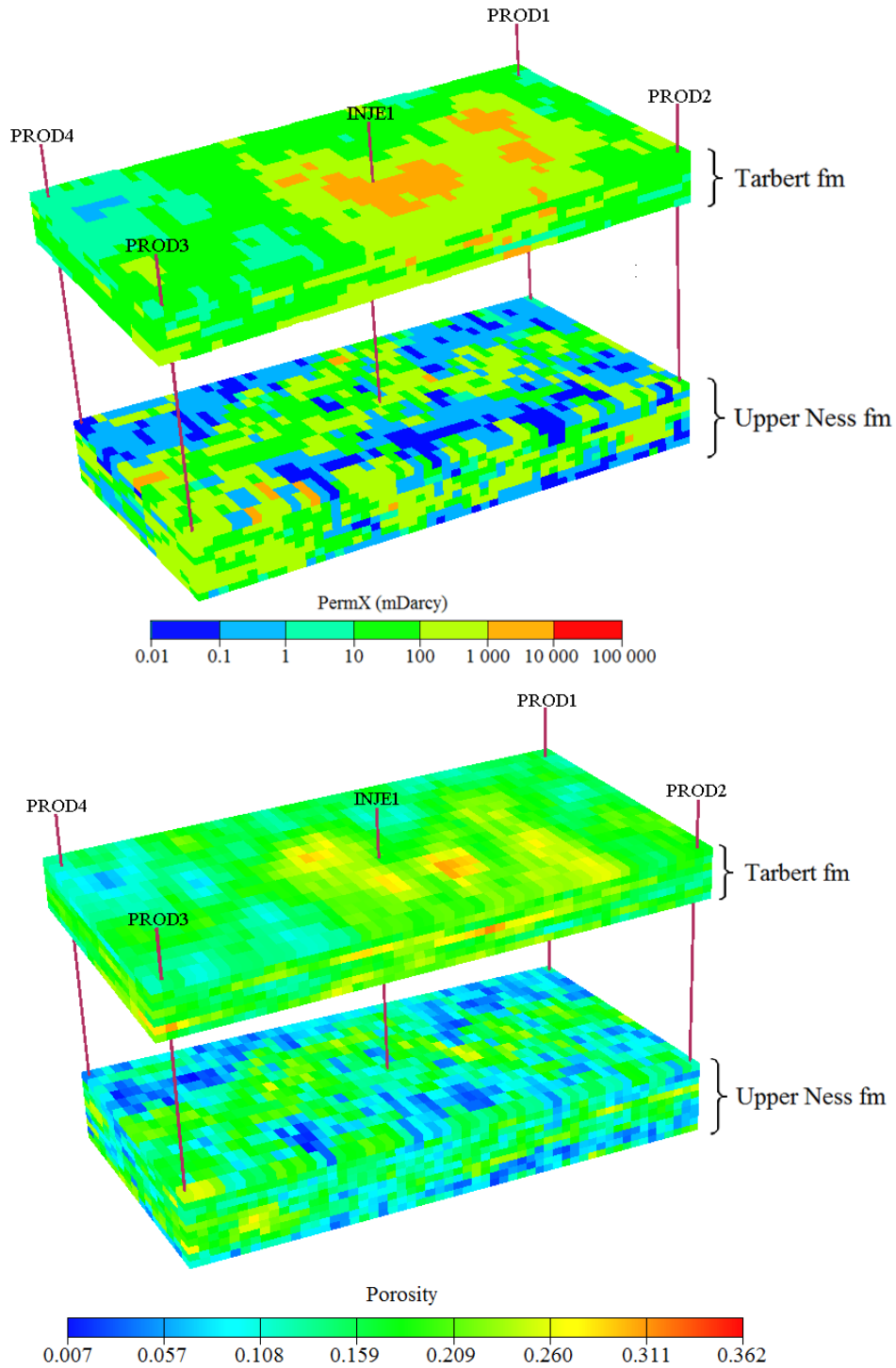
Fig. 5.2 – Porosity and permeability in X-direction distribution in the upscaled models. The two formations are separated from each other to show lateral distribution of the parameters in the bottommost formation

When comparing the distribution of porosity and permeability of the upscaled models and original model (see Fig. 4.1), one may notice that upper and lower scale limits have changed, and that many detailed geological features are no longer distinguishable, as expected. However, the visual similarity is a qualitative indicator of how good is the upscaled model, but not a quantitative one.

5.1.3. Relative permeability and capillary pressure

Relative permeabilities and capillary pressure curves were obtained using the three different methods described in Chapter 3: capillary limit (CL), viscous limit (VL) and end-point scaling (EPS). **Fig. 5.3** shows the upscaled relative permeabilities and capillary pressures for the models upscaled using CL and EPS methods. Water saturation functions for the model upscaled using the VL method were not plotted since they look similar to the curves of the CL model.
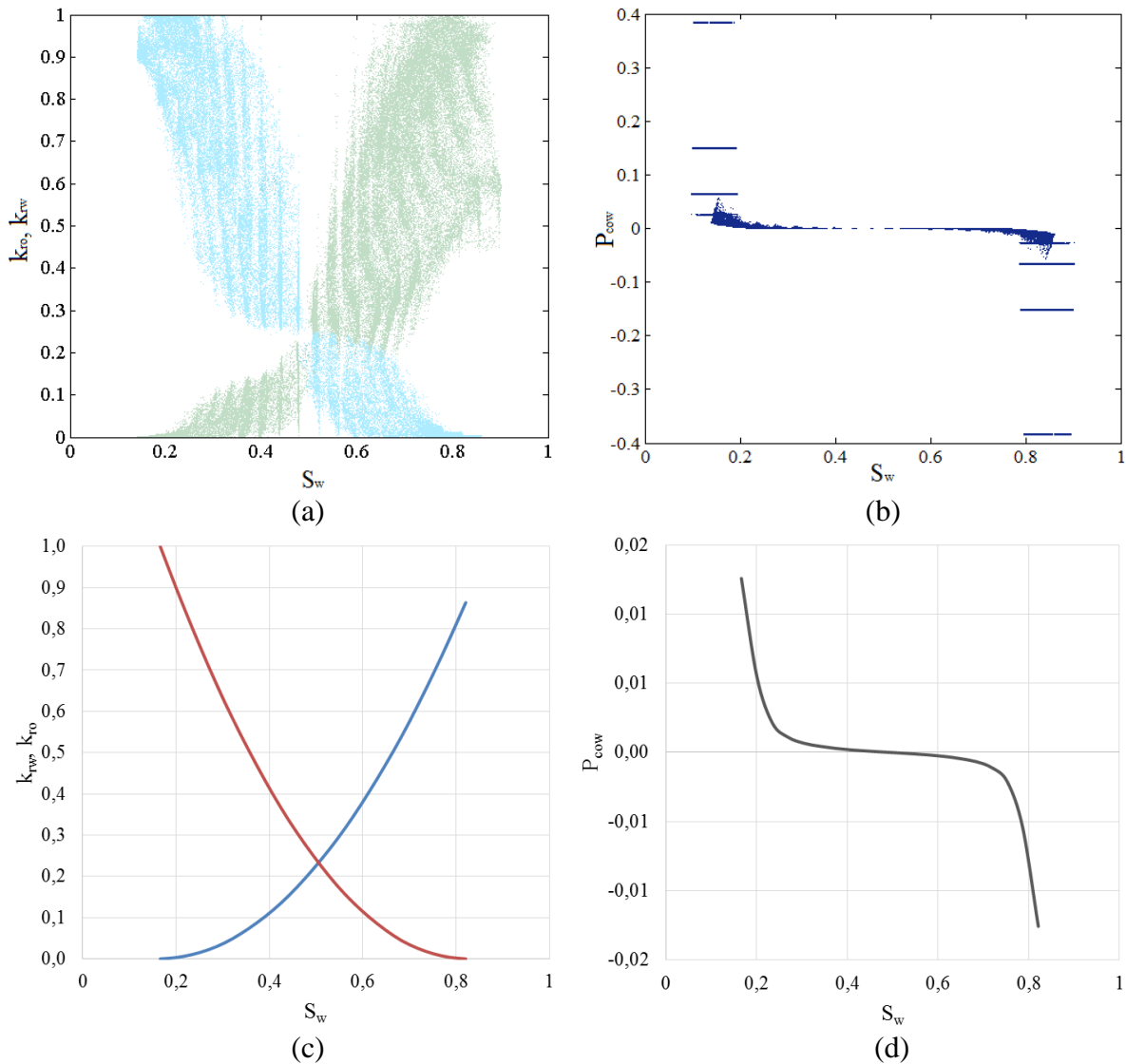
Fig. 5.3 – Relative permeabilites and capillary pressures for the upscaled models. Multiple curves plotted as scatter clouds (a) and (b) for the model upscaled using CL method; single curves (c) and (d) for the model upscaled using EPS method

As it can be observed in Fig. 5.3, CL method produces the number of water saturation functions sets equal to the number of cells in the coarse model; that is why parts (a) and (b) of Fig. 5.3 appear as clouds of semitransparent points. Opacity of the cloud corresponds to the frequency of occurrence of a water saturation function point in the model. Capillary pressure scatter cloud looks less uniformly filled with points due to the great jumps in capillary pressure values close to the endpoint saturations.

Unlike CL method water saturation functions, relative permeabilities and capillary pressure obtained using the EPS method are single curves used for the whole model as the base that is modified, or scaled, for each coarse cell using the keywords SWL, SWU, KRW and PCW during a simulation in ECLIPSE 100. Within each grid cell of the model, the keyword SWL defines scaled connate water saturation, SWU – maximum water saturation, KRW – scaled end-point water relative permeability, and PCW denotes the scaled maximum capillary pressure.

5.2. Upscaled polymer adsorption data

As it was presented in Chapter 3, two options were considered to perform upscaling of polymer adsorption: volumetric average and the use of a permeability-dependent function introduced in Chapter 4, where the upscaled permeability is an input. To illustrate how these different methods of polymer adsorption upscaling work, they were first tested on simple one-dimensional and two-dimensional models that highlight different flow scenarios that may occur during a simulation. Then, the study was extended to investigate the results in 3D realistic models.

5.2.1. Simplified models

5.2.1.1. 1D model test

First, a synthetic 1D model comprising 100 cells in one row of around 1 km length was created (see **Fig. 5.4**). All cells have the same dimensions, pore volume, water saturation functions, but permeability distribution is not homogeneous: every fifth cell was assigned a permeability of 10 mD while the rest of cells – a permeability of 1000 mD. Different permeabilities mean that polymer adsorption values on the fine scale, which were computed using the procedure described in Chapter 4, will vary for each fifth cell. The main properties of the model are listed in the **Table 5.1**.
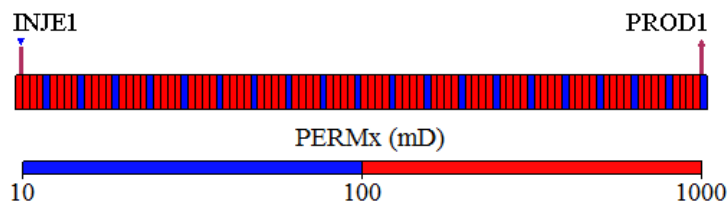
Fig. 5.4 – 1D model for testing different methods of adsorption upscaling

Table 5.1. 1D fine scale test model properties.

Parameter	Value	Units
Model dimensions (NXxNYxNZ)	1x100x1	–
Gridblock dimensions (DXxDYxDZ)	24.384x12.192x3.048	m
Porosity	0.25	–
Permeability	10 / 1000	mD
Inaccessible pore volume	0	–
Polymer adsorption	5.223E-05 / 2.778E-04	kg/kg

Two wells are present in the model: injection well INJE1 and production well PROD1; INJE1 injects successively water, polymer and again water at a constant rate of 10 Sm^3/day, and the polymer injection period is long enough to see polymer breakthrough in well PROD1 that operates with a minimum bottomhole pressure limit of 275 bar.

The fine scale model is to be upscaled to a 1x20x1 model using two methods. In fact, the only parameters to be upscaled in the 1D model are permeability and polymer adsorption, because other properties are distributed homogeneously. Permeability upscaling was performed using harmonic-average formula:

$$k_{avg} = \frac{\sum_{i=1}^{n} l_i}{\sum_{i=1}^{n} (l_i / k_i)} \quad \dots\dots\dots\dots\dots\dots\dots\dots\dots\dots\dots\dots\dots\dots\dots\dots\dots\dots\dots(5.1)$$

where l_i and k_i are length and permeability of ith out of n fine cells within a coarse cell.

Using Eq. 5.1, the upscaled permeability becomes 48.077 mD. This value was used in both upscaled 1D models so that the results emphasize differences in adsorption upscaling. The latter was performed using a volumetric average formula (Eq. 3.12) and the adsorption function used in the fine scale model with the input of upscaled permeability (Eq. 3.11). Upscaled models properties are presented in **Table 5.2**.

Table 5.2. Properties of the upscaled 1D models.

Parameter	Value	Units
Model dimensions (NXxNYxNZ)	1x20x1	–
Gridblock dimensions (DXxDYxDZ)	24.384x60.96x3.048	m
Porosity	0.25	–
Permeability	48.077	mD
Inaccessible pore volume	0	–
Polymer adsorption - volumetric average approach - function of k_{upsc} approach	9.733E-05 1.949E-04	kg/kg

Having injected water and polymer in the same sequence as it was done for the fine scale model, the plots of adsorbed polymer mass and polymer production rate were obtained (see **Fig. 5.5** and **Fig. 5.6**).

Fig. 5.5 – Comparison of polymer adsorption upscaled using different methods and adsorption on fine scale (1D model)

Fig. 5.5 shows that at the moment of polymer breakthrough in PROD1, when the polymer has saturated the whole model, adsorption estimated using the volume average overlaps with the adsorption in fine scale model, while upscaled adsorption as a function of upscaled permeability lies far above the target fine scale curve. It can be observed in Table 5.2 that volumetric averaged adsorption value is half the value obtained using the function of permeability. The low-permeability cells influence on the upscaled adsorption value calculated as a function of upscaled permeability dominates the influence of other cells and leads to an overestimation of polymer adsorption.

Fig. 5.6 – Comparison of polymer adsorption rates in coarse models with adsorption upscaled using different methods and polymer adsorption rate on fine scale (1D model)

In fact, this overestimation is so huge that no polymer is produced in the model with adsorption as a function of upscaled permeability (see Fig. 5.6). However, even though the

adsorption calculated as a function of permeability does not give a good match in this case, we will see later that it gives reasonable results for other models.

When analyzing ultimate adsorption values in the 1D model, a slight discrepancy between the amount of polymer adsorbed in situ and the amount of polymer injected was observed in case when adsorption was upscaled as a function of upscaled permeability. In fact, the ultimate value of the adsorbed polymer was around 3 kg higher than what had been injected to the reservoir in total. The most likely explanation of this is the numerical error effect, which led to a deviation from physically consistent results.

5.2.1.2. 2D model test

To model a different situation when the fluid can choose a more favorable path, a 2D model was developed (see **Fig. 5.7**). The properties in the model were kept the same as in the one-dimensional case; however, the permeability distribution was changed so that the upper layer was assigned lower permeability of 10 mD, and the bottom layer permeability was 1000 mD. It is evident that the bottom layer represents a preferential flow path for the injected fluids, which will change the fluid flow picture significantly.
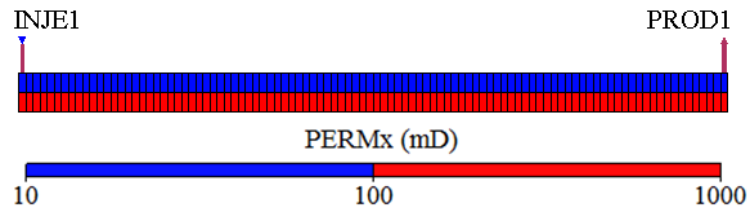
Fig. 5.7 – 2D model for testing different methods of adsorption upscaling

Table 5.3 contains the main properties of the 2D model; it can be observed that the total pore volume of the model is the same as the pore volume of one-dimensional model; therefore, the well INJE1 rate will be kept the same as for the 1D case. The production and injection schedule in 2D model were also kept equal to the 1D model.

Table 5.3. 2D fine scale test model properties.

Parameter	Value	Units
Model dimensions (NXxNYxNZ)	1x100x2	–
Gridblock dimensions (DXxDYxDZ)	24.384x12.192x1.524	m
Porosity	0.25	–
Permeability (upper / lower layer)	10 / 1000	mD
Inaccessible pore volume	0	–
Polymer adsorption (upper / lower layer)	5.223E-05 / 2.778E-04	kg/kg

The 2D fine-scale model was then upscaled to a 1x50x1 model. As in the 1D case, the only upscaling parameters were permeability and polymer adsorption since the rest of the properties were identical in all of the cells. As the current model is represented by two homogeneous layers with different permeabilities, the upscaled value of permeability was calculated as a weighted-average:

$$k_{avg} = \frac{\sum_{i=1}^{n} k_i h_i}{h_t} \quad \text{..(5.2)}$$

where h_i and k_i are thickness and permeability of ith out of n layers with the total thickness h_t.

The use of Eq. 5.2 above gives the upscaled permeability of 505 mD, which was used in all upscaled models. Polymer adsorption was upscaled using the following methods: a volumetric average formula (Eq. 3.12), the adsorption function with the input of upscaled permeability (Eq. 3.11) and, in addition, a volumetric average formula modified with a flow fraction coefficient. The third method aims to improve simple average formula so that it takes into account the fine-scale flow pattern within each coarse cell. Thus, the *modified volumetric-average* formula appears as follows:

$$ADS_{avg} = \frac{\sum_{i=1}^{n} ADS_i RV_i F_i}{RV_t} \cdot N_{cs} \quad \text{................................(5.3)}$$

where
ADS_i – adsorption in each cell
RV_i – rock volume in each of the cells that make up total volume RV_t
N_{cs} – number of cross-sections in the main flow direction in one coarse cell
F_i – flow fraction coefficient given by

$$F_i = \frac{PV_i k_i}{\sum_{i=1}^{n} PV_i} \cdot \frac{1}{k_{av}} = \frac{PV_i k_i}{\sum_{i=1}^{n} PV_i} \cdot \frac{\sum_{i=1}^{n} PV_i}{\sum_{i=1}^{n} PV_i k_i} = \frac{PV_i k_i}{\sum_{i=1}^{n} PV_i k_i} \quad \text{..................................(5.4)}$$

where k_{av} – average permeability in a coarse cell.

The properties of the upscaled models are presented in **Table 5.4**. It can be observed that the two approaches that take into account the influence of permeability (function of upscaled permeability and modified volumetric average approach) give very close estimates of upscaled adsorption: the difference is less than one order of magnitude. Adsorption estimated using a simple volumetric average is one order greater, even though this estimate worked perfectly in the one-dimensional model (see Fig. 5.5).

Table 5.4. Properties of the upscaled 2D models.

Parameter	Value	Units
Model dimensions (NXxNYxNZ)	1x50x1	–
Gridblock dimensions (DXxDYxDZ)	24.384x24.384x3.048	m
Porosity	0.25	–
Permeability	505	mD
Inaccessible pore volume	0	–
Polymer adsorption - volumetric average approach - modified volumetric average approach - function of k_{upsc} approach	1.650E-04 2.723E-05 6.899E-05	kg/kg

Having replicated a polymer slug injection scenario that was first tested on 1D model, the mass of adsorbed and produced polymer was plotted (see **Figs. 5.8 – 5.9**).
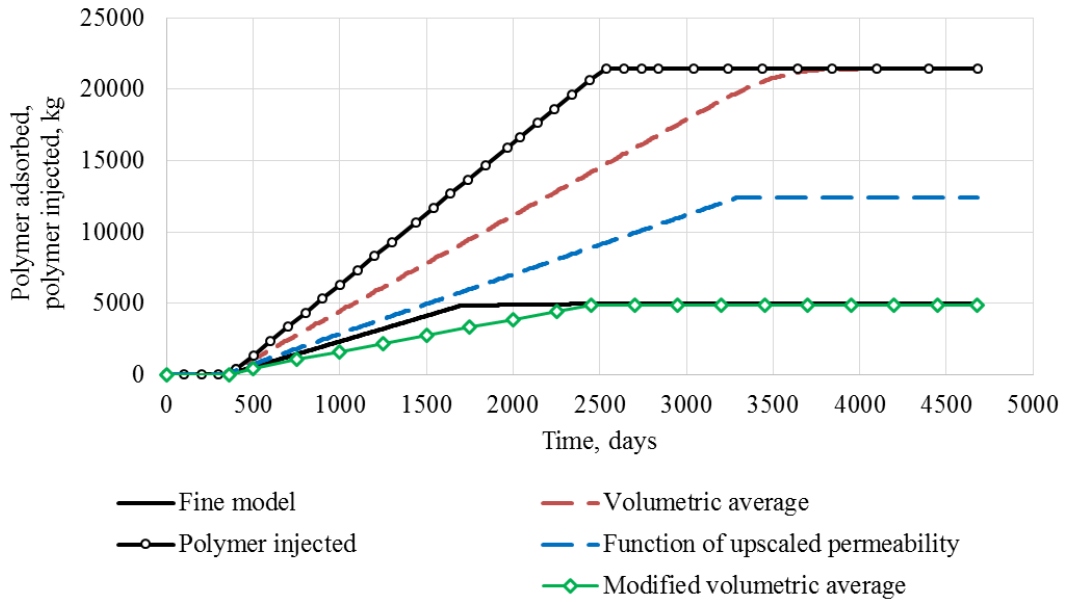
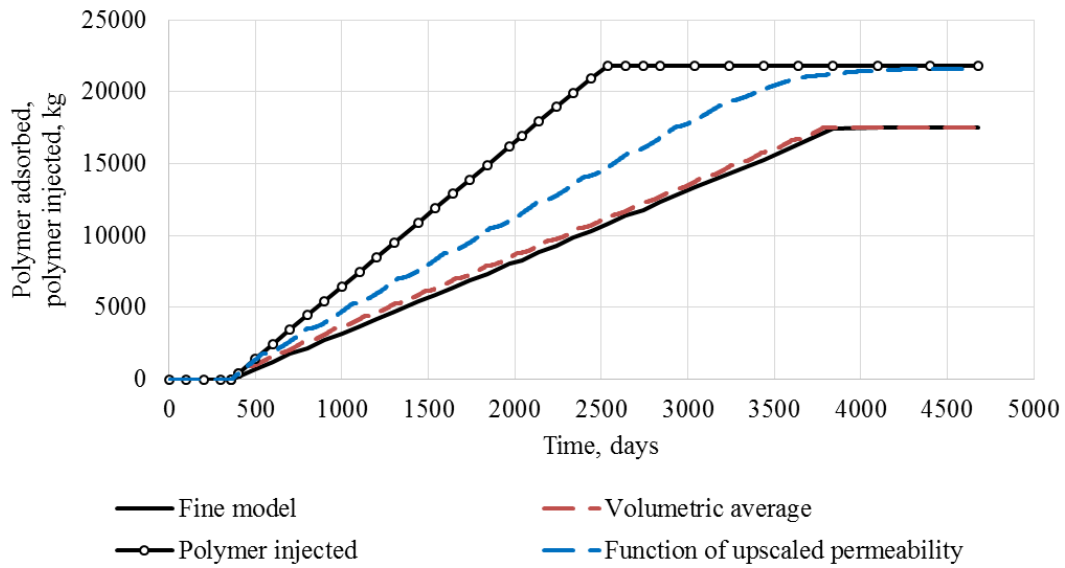**Fig. 5.8 –** Comparison of polymer adsorption upscaled using different methods and adsorption on fine scale (2D model)

Fig. 5.9 shows that in the layered model with high permeability contrast between the layers polymer breakthrough occurred only if upscaled polymer adsorption was estimated in connection with the upscaled permeability (adsorption function and modified volumetric averaging methods). That is, the model with volumetric-averaged polymer adsorption has not seen any polymer production. As it can be seen in Fig. 5.8, polymer adsorption upscaling as a volume average modified with a flow fraction coefficient has given the best results, and the use of permeability function to upscale polymer adsorption has resulted in an overestimation of total amount of adsorbed polymer. Although, the latter method performs better than simple volumetric average in current situation.
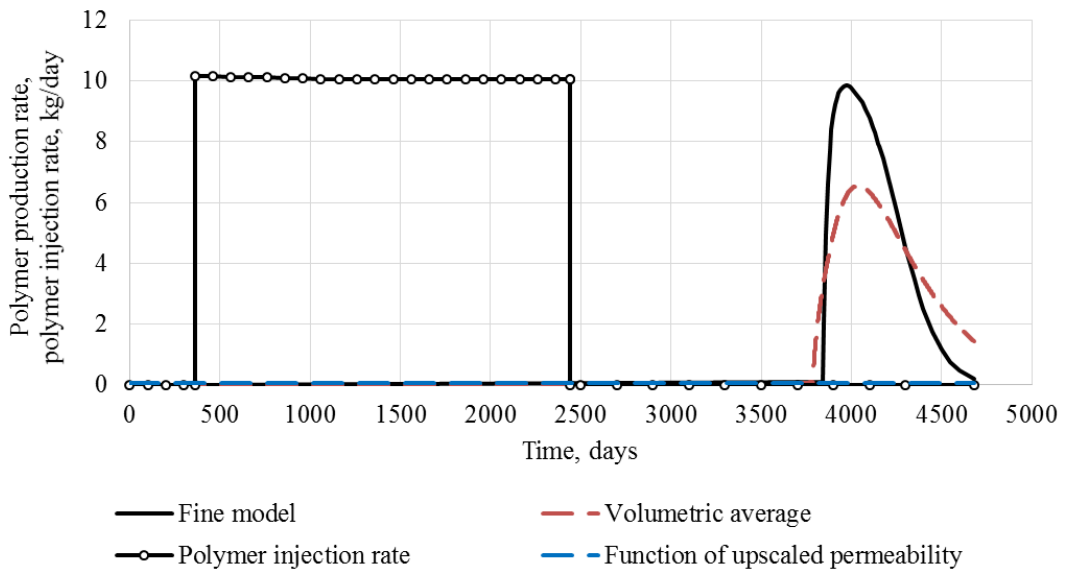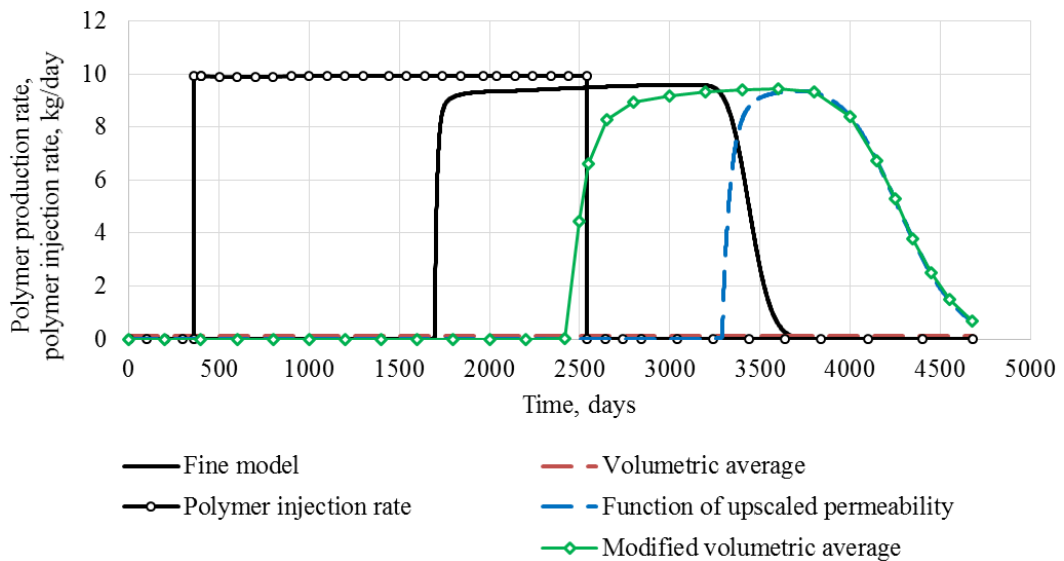

Fig. 5.9 – Comparison of polymer adsorption rates in coarse models with adsorption upscaled using different methods and polymer adsorption rate on fine scale (2D model)

Plots in Figs. 5.8 – 5.9 show that when preferential flow paths are present in the model, meaning that full model saturation with polymer is highly unlikely, it is very important to estimate the level of each zone's contribution to the flow when upscaling polymer adsorption. A simple flow fraction coefficient in Eq. 5.3 does the best job in the 2D case because it represents the main feature of the fluid flow in this model: diversion of the flow streams according to the permeability distribution in the layers. Other methods are less accurate because they miss out either accounting for the pore volume weight of the main flow zone or for the involvement of each zone in the drainage. Nevertheless, in case of infinite polymer injection, when polymer breakthrough time is reached in both layers, volumetric average upscaling gives the best results with respect to fine-scale model (see **Fig. 5.10**).
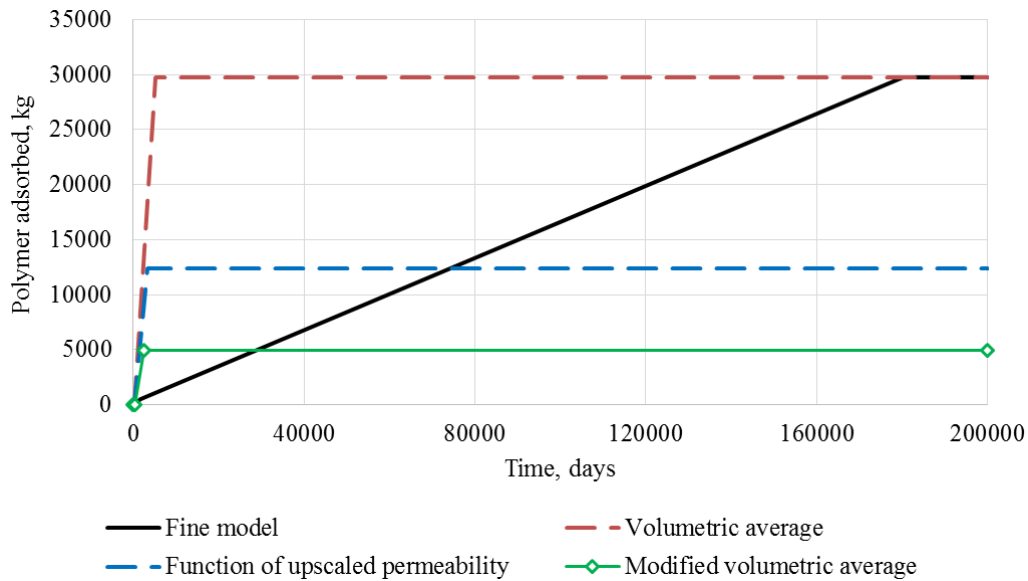
Fig. 5.10 – Comparison of polymer adsorption upscaled using different methods and adsorption on fine scale in case of infinite polymer injection (2D model)

5.2.2. Realistic models

Having illustrated how different methods work in synthetic models, the experiment was performed using realistic models. The realistic models were simply smaller parts of the original SPE10 fine model, and their dimensions were tailored to the degree of coarsening of the upscaled models to avoid surplus computations. Hence, each fine-scale realistic model consisted of five consecutive layers of the original SPE10 model, which corresponded to a single layer of an upscaled model created using one of the methods described in Chapter 3.

Given a total of 85 layers in the original SPE10 model, there were 17 realistic 5-layer models to test polymer adsorption upscaling techniques. It should be noted, however, that in case of using realistic models the two-phase flow parameters (e.g. relative permeabilities, capillary pressure) can be upscaled using different steady-state methods presented earlier in Chapter 3, which may affect the solution. Thus, no plot in this section can represent the pure effect of adsorption upscaling method choice, but only a composite effect of both two-phase flow upscaling and adsorption upscaling.

No changes were made to the 5-layer extracts of SPE10 model except for the injection rate, which was scaled based on the average pore volume in the thin models. Thus, production data in each independent 5-layer model are closer to the production data in the same region when all layers of the model are drained together.

There are 7 models representing Tarbert fm and 10 models representing the underlying Upper Ness fm. In this section, only two realistic models will be discussed: one for each formation. In order to choose realistic models to be presented in this section, fine-scale results were analyzed to determine in which layers polymer breakthrough occurs. Then, two scenarios with different polymer injection periods were tested in such models: one that results in polymer breakthrough (3 years of polymer injection) and one without polymer production (1 year of polymer injection).

For Tarbert fm the area corresponding to layers 11-15 (fine-scale model) or layer 3 (upscaled models) was chosen. The behavior of polymer adsorption on fine and coarse scales at different scenarios is shown in **Figs. 5.11 – 5.12**. Fine-scale results are presented by black curves, and each of steady-state upscaling methods used to perform two-phase upscaling is assigned a specific color too. For the coarse-scale results, the type of line corresponds to the method used to upscale polymer adsorption: solid lines represent the use of adsorption function; dashed lines – simple volumetric average; dotted lines – modified volumetric average (Eq. 5.3) where flow fraction coefficient uses simple volumetric averaged permeability (Eq. 5.4); dash-dotted lines – modified volumetric average (Eq. 5.3) where flow fraction coefficient (Eq. 5.4) uses a permeability upscaled with MRST using a flow-based method instead of volumetric average.
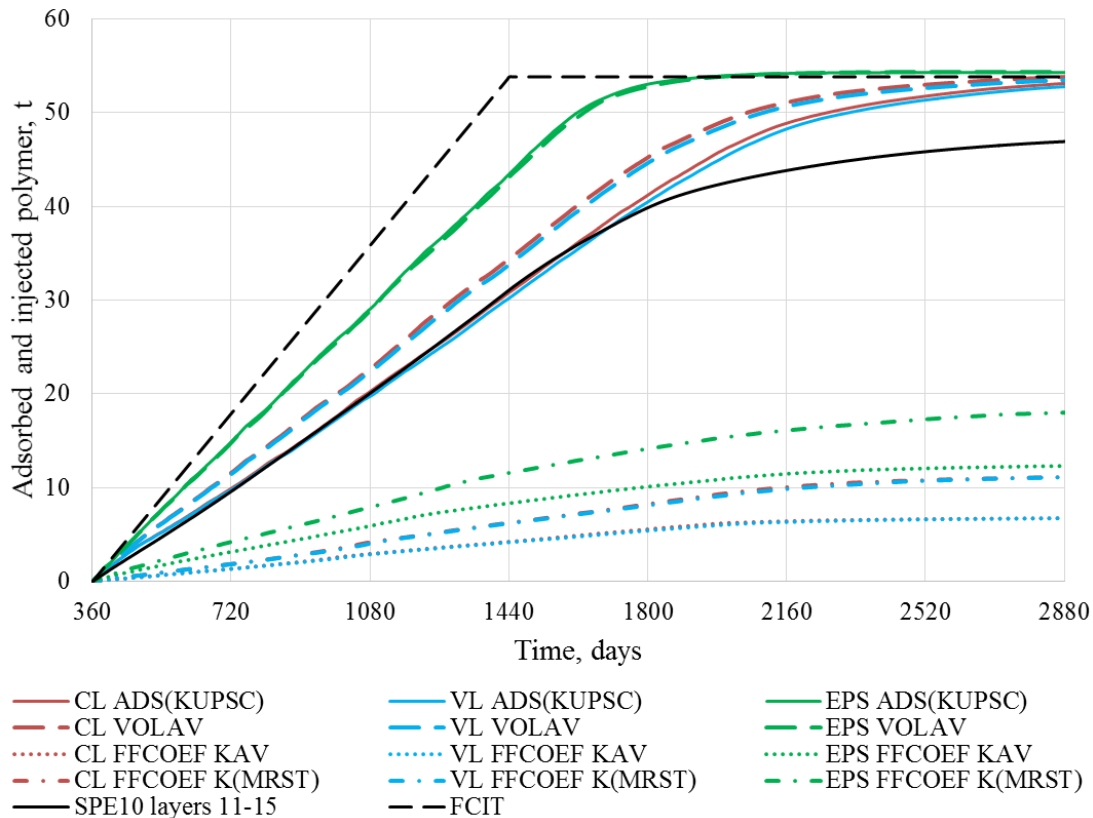
Fig. 5.11 – Comparison of polymer adsorption upscaled using different methods and adsorption on fine scale in Tarbert fm, polymer breakthrough scenario (3D 5-layer model)
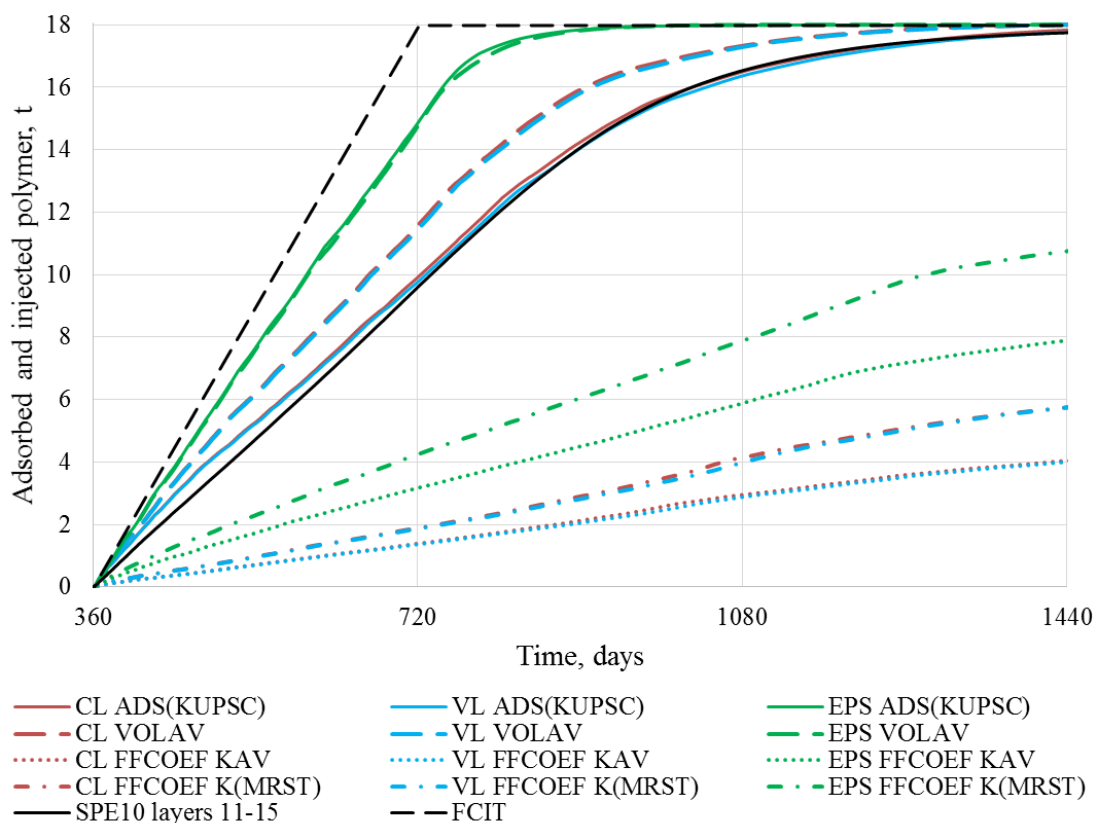
Fig. 5.12 – Comparison of polymer adsorption upscaled using different methods and adsorption on fine scale in Tarbert fm, no polymer breakthrough scenario (3D 5-layer model)

Figs. 5.11 – 5.12 show that the best match of polymer adsorption curve was obtained in the models that used the adsorption function of upscaled permeability, excluding EPS method. Adsorption curves obtained from CL- and VL-upscaled models with upscaled adsorption as a function of upscaled permeability overlap with the fine-scale curve during the whole polymer injection period in case of 3-year injection (Fig. 5.11). At a later stage of production, upscaled curves diverge from fine-scale adsorption in case of 3-year polymer injection, but in case of shorter polymer injection (no polymer breakthrough) they match fine-scale data during the whole simulation period (Fig. 5.12). Previous experiments on simplified models showed that this method was usually overestimating polymer adsorption, and the same was observed in most 3D realistic models in Tarbert fm where polymer breakthrough occurred. As for the models producing with short polymer injection period, no obvious pattern was detected, but the common feature is that models with adsorption upscaled using a function of upscaled permeability give the best match during the period of polymer injection and tend to diverge when the water is injected again.

It can be seen that, at any injection scenario, upscaled adsorption curves obtained using the volumetric averaged adsorption lie above the fine-scale curve. Such behavior is in accordance with what has been seen in the 2D synthetic model with some polymer-undersaturated areas. Volumetric-averaged adsorption tends to expect higher polymer adsorptions in the model due to the influence of low-permeability cells, but the fluids do not enter a large portion of the low permeable region in the fine-scale model; thus, a separation between the fine-scale and coarse-scale curves occurs. This trend was also observed in other 5-layer models extracted from Tarbert fm.

The use of modified volumetric average (Eq. 5.3) gave unexpectedly inaccurate results at all scenarios in Tarbert fm, unlike those seen in 2D simulation. The dotted lines in Figs. 5.11 – 5.12 indicate a large underestimation of the polymer adsorption level in the model. A reason for such performance might be the imperfect flow fraction coefficient estimation due to the use of a simplified average permeability of the coarse cell, which does not take into account which cells are playing bigger role in fluid flow and which are not involved in it. To improve this method's performance, the average permeability in the flow fraction coefficient formula (Eq. 5.4) was replaced by the permeability upscaled in MRST using the method described in Chapter 3. The use of this permeability value as the reference to estimate the degree of each fine-cell involvement to the flow can help to eliminate the shortcomings of the simple averaging formula since the calculations in MRST are flow based. The dash-dotted lines in Figs. 5.11 – 5.12 represent the results of the implementation of the latter formula in polymer adsorption calculations. It can be seen that the use of a more accurate permeability improves the coarse-scale curve performance; however, this improvement is still not enough to consider such method successful.

One may notice that when polymer adsorption plots are concerned, the biggest difference seen between different curves is due to the adsorption upscaling method used. The choice of the steady-state method of two-phase flow parameters upscaling has less influence on the adsorption curves behavior, which is reflected by the CL- and VL-upscaled models results being very close to each other. This behavior along with the fact that CL-curves usually lie above VL-curves were also noticed in other 5-layer models.

The plots obtained from the models upscaled using EPS method deviate from other curves' behavior. In EPS-upscaled models almost no difference is seen between the use of a volumetric averaged adsorption and adsorption function. In addition, polymer adsorption curves in EPS models lie significantly higher compared to curves from other models, and it makes one question the validity of the EPS method for current models.

Another remark is that, even though a sufficiently good match in polymer adsorption was obtained by use of some methods, other production data have not been matched that well. The best methods matching polymer adsorption curve (CL- and VL-upscaled models with adsorption function of upscaled permeability) do not represent oil production profile or water cut behavior as accurately. The models using flow fraction coefficient method that was not very successful in matching polymer adsorption, captured some specific features of the fine scale production data better (e.g. an oil hump in production profile due to an increased drawdown during polymer injection), which creates the effect of similarity between these upscaled curves and fine-scale curves. However, a significant underestimation of polymer adsorption results in an exaggerated oil production because more polymer is left in the reservoir. It is also reflected in an increased polymer production, while the fine-scale model sometimes does not have polymer production at all, depending on the scenario.

The same procedure was repeated for the Upper Ness fm that corresponds to the bottom part of SPE10 model. Results for one of five 5-layer models where polymer breakthrough was observed are shown below in **Figs. 5.13 – 5.14**. The model represents layers 46-50 of the original SPE10 model or layer 10 in the upscaled models. Two different scenarios (with and without polymer production) were analogical to those used in models of Tarbert fm, and the organization of plots in Figs. 5.13 – 5.14 was kept similar.

A poor match of fine-scale polymer adsorption was observed in both scenarios. Coarse models with volumetric averaged adsorption gave a significant overestimation of polymer adsorption in all of the models, which is expected based on the previous results in 2D models. This method of polymer adsorption upscaling together with some methods in EPS-upscaled models (volumetric averaging and use of the adsorption function) estimate full and almost immediate polymer adsorption regardless of the scenario.

Adsorption upscaled as a function of upscaled permeability showed a worse performance in Upper Ness fm. While in models of Tarbert fm adsorption function matches fine-scale data well at least during the polymer injection period (Fig. 5.11), the same polymer adsorption method in Upper Ness models tends to converge to the volumetric averaged adsorption from the very beginning of the polymer injection period. The difference between these two methods may appear at the late stages of simulation period when volumetric averaged adsorption overlaps with the total polymer injection line and adsorption function indicates that there is some amount of polymer being active in the reservoir or being produced (see the gap between polymer adsorption and injection lines in Fig. 5.13). This trend was observed in most 5-layer models of Upper Ness fm.

As regards the modified volumetric average formula to upscale polymer adsorption, or so-called flow fraction coefficient formula, its performance in Upper Ness models differs a lot from what was observed in Tarbert fm models.
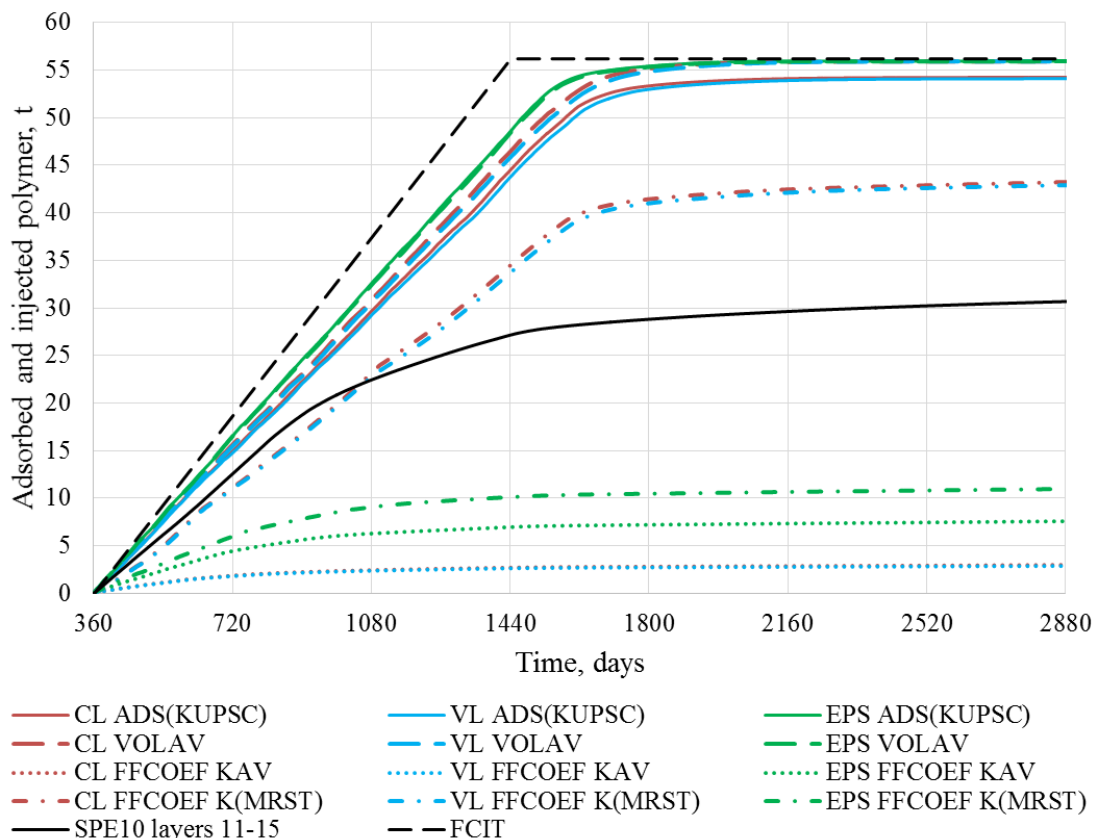
Fig. 5.13 – Comparison of polymer adsorption upscaled using different methods and adsorption on fine scale in Upper Ness fm, polymer breakthrough case (3D 5-layer model)
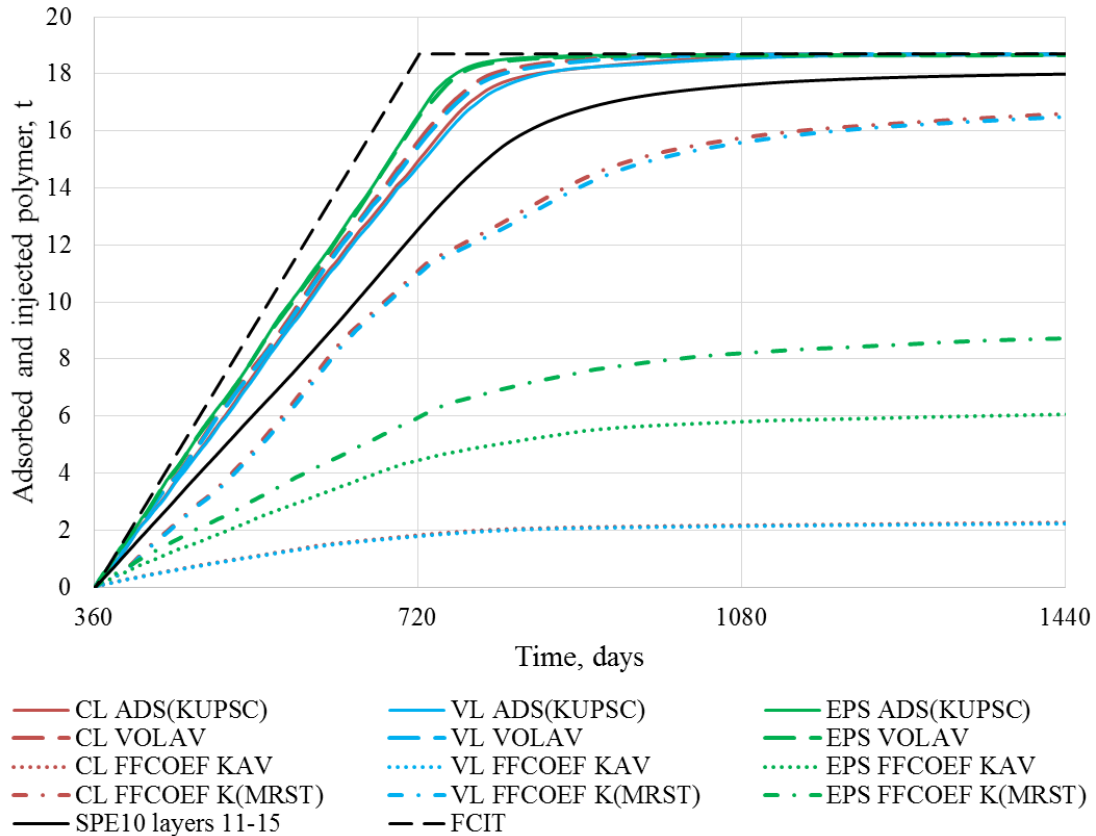
Fig. 5.14 – Comparison of polymer adsorption upscaled using different methods and adsorption on fine scale in Upper Ness fm, no polymer breakthrough case (3D 5-layer model)

As it was mentioned before, the coarse-scale, or average, permeability used in the flow fraction coefficient formula (Eq. 5.4) plays an important role in how close the upscaled data are to the fine-scale data. The use of a flow-based calculated average permeability resulted in a slightly better match, which was, however, insufficient to consider this adsorption upscaling method successful in Tarbert fm models (Fig. 5.12). The effect of the choice of average permeability for the flow fraction coefficient formula is more significant in the Upper Ness fm models. As it is shown in Figs. 5.13 – 5.14, when the flow-based average adsorption is used, the upscaled polymer adsorption curve approaches the fine-scale curve and becomes comparable to other methods. In the 5-layer models of Upper Ness fm where polymer breakthrough occurs, the flow fraction formula estimation is usually significantly better than estimation given by normal volumetric averaging and adsorption function methods. As it can be seen in Figs. 5.13 – 5.14, the flow fraction coefficient line may lie above or below the fine-scale line; however, no particular relation between the polymer injection period length and the position of the upscaled curve was revealed.

Regarding the match in other production data, such as field oil production rate, water cuts, polymer production etc., the same situation as in case of previous set of models was observed. Field oil production curves obtained from the models with flow fraction coefficient formula used to estimate adsorption had more similarities with the fine-scale results, but all upscaled models forecast higher oil rates and later water breakthroughs.

5.2.3. Adsorption maps

This section illustrates how the adsorption values field looks like in the realistic models of Tarbert and Upper Ness fm discussed earlier. The MATLAB scripts written to compute polymer adsorption values presented in **Figs. 5.15 – 5.16** can be found in Appendix 3 (methods using volumetric averaging) and Appendix 4 (method using the adsorption function with upscaled permeability as input).

Figs. 5.15 – 5.16 represent permeability and polymer adsorption maps in 3D realistic models extracted from Tarbert and Upper Ness fm, respectively. Parts (a) and (b) of Figs. 5.15 – 5.16 represent fine scale permeability and adsorption, respectively. One should note that since each upscaled 3D realistic model is an aggregation of five fine layers, the coarse-scale maps might have some features that cannot be observed on the fine-scale representative layer map (Figs. 5.15a – 5.16a) due to the influence of other four layers on the upscaling results. Maps obtained with the flow fraction coefficient formula shown in parts (e) of Figs. 5.15 – 5.16 are using flow-based average permeability; another option (with pore volume averaged permeability) is not shown herein.

It can be observed in Figs. 5.15 – 5.16 that all adsorption maps are in accordance with the permeability distribution. The estimations of adsorption by volumetric average and adsorption function methods look similar, but the difference picture (see Fig. 5.15f and Fig. 5.16f) shows that volumetric averaged adsorption values are greater in the high-permeability areas while in the less permeable zones methods have closer estimations.
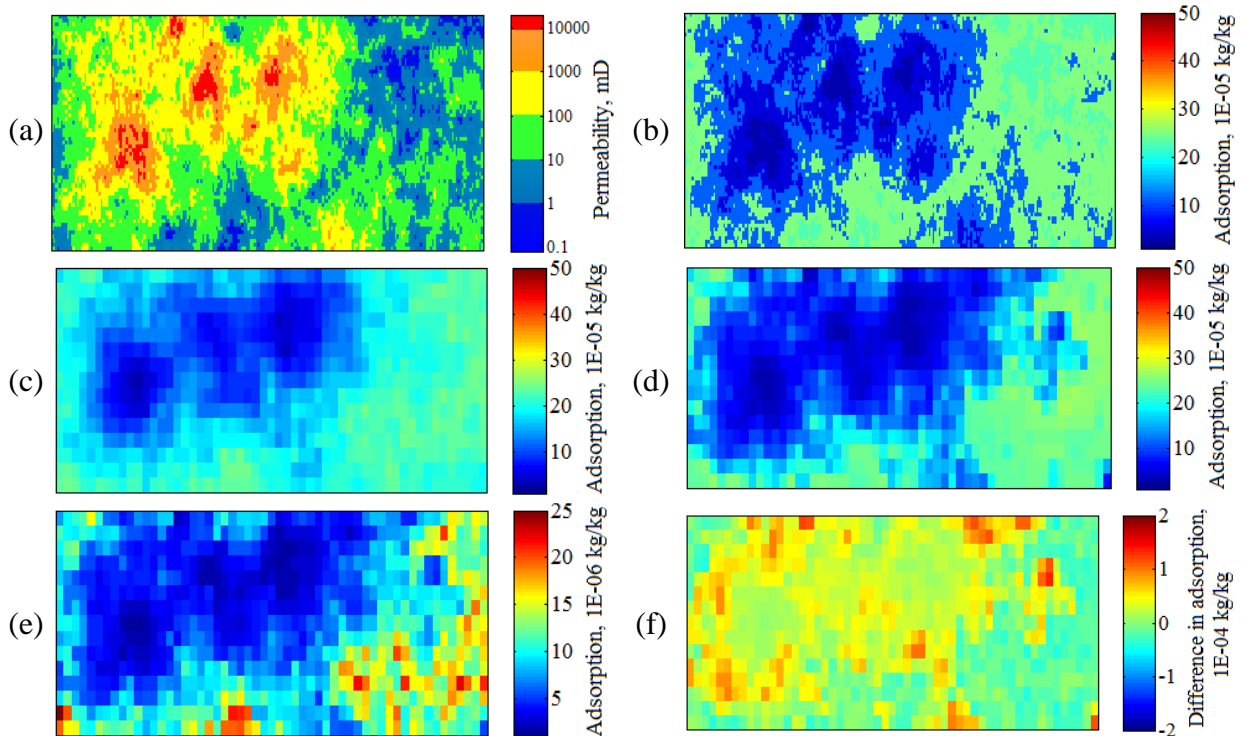
Fig. 5.15 – A sample polymer adsorption map for Tarbert formation : (a) and (b) – permeability and adsorption in layer 14 of the fine model, respectively (corresponds to layer 3 of an upscaled model); (c) – volumetric averaged adsorption; (d) – adsorption as a function of permeability; (e) – adsorption calculated with flow fraction coefficient formula; (f) – difference between (c) and (d)
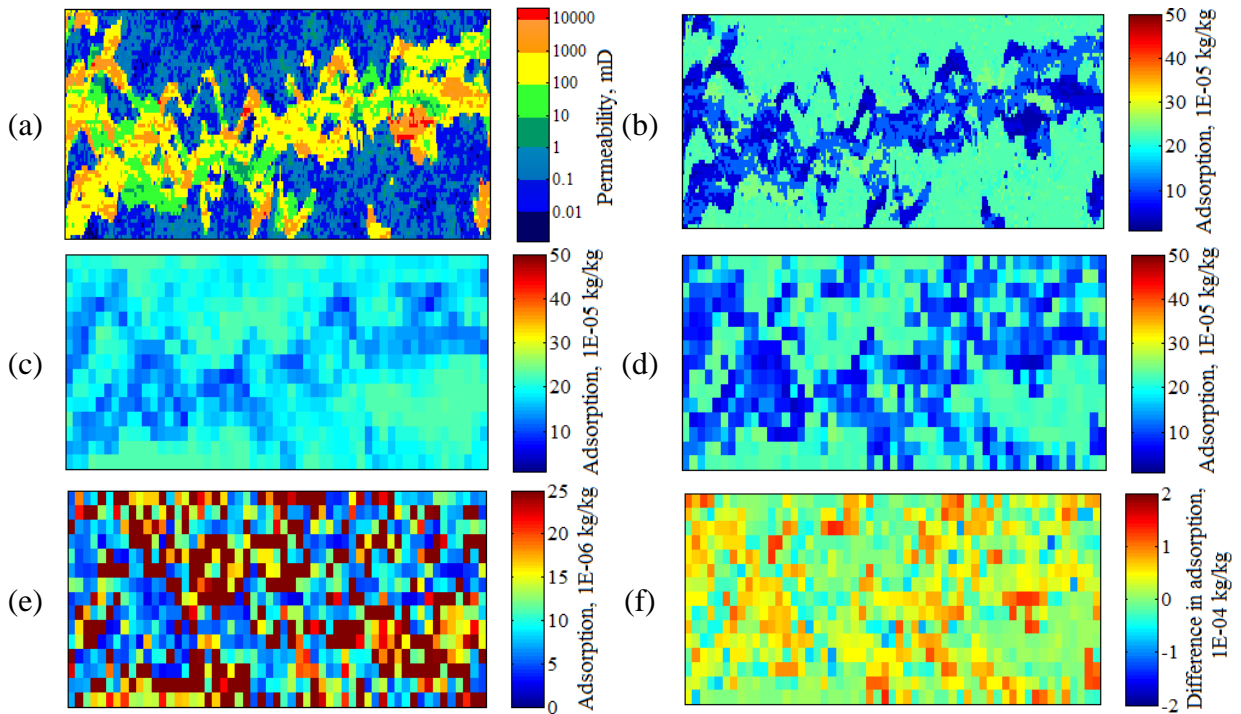
Fig. 5.16 – A sample polymer adsorption map for Upper Ness formation: (a) and (b) – permeability and adsorption in layer 14 of the fine model, respectively (corresponds to layer 3 of an upscaled model); (c) – volumetric averaged adsorption; (d) – adsorption as a function of permeability; (e) – adsorption calculated with flow fraction coefficient formula; (f) – difference between (c) and (d)

The difference between the values computed using these two methods and using the flow fraction coefficient formula are not shown in the plots because the latter method gives adsorption values that are deliberately small.

As it can be seen in colorbar ranges in Figs. 5.15 – 5.16, there is a one-order difference between the values in the modified volumetric averaged adsorption map and values in other maps. Such difference was observed earlier in the 2D model; however, the estimated adsorption in the simplified case was much closer to that estimated by adsorption function.

Adsorption map in Upper Ness fm obtained by using the flow fraction coefficient formula (Fig. 5.16e) seems to differ from other maps; the difference is mainly observed in the low-permeability areas where most maps indicate a uniform distribution of polymer adsorption. Nevertheless, Fig. 5.16e seem to have a lot of noise in the low-permeability areas of the layer, which may be related a different scale of the colorbar, which was kept the same as for corresponding Tarbert fm map, and the impact of dead blocks presence in the layer. The flow fraction coefficient formula has an increased sensitivity to permeability compared to other methods, and the presence of dead blocks that are spread over the layer stimulates the estimated values to rise. The dead blocks mostly occur in the low-permeability areas and are more often encountered in the Upper Ness fm. Inactive blocks appear in Tarbert fm as well, but their number is significantly lower.

51

Chapter 6. Numerical results

6.1. Fine model results analysis

6.1.1. Production data

We first investigated the behavior of the fine-scale model during polymer flooding. Production data obtained for the polymer flooding case were compared to an ordinary waterflooding case. Wells control parameters and injection period length during waterflooding are listed in Table 4.1; wells controls for the polymer injection case were kept the same as for the waterflooding case (except for maximum bottomhole pressure of the injection well, which was increased to a deliberately high value of 5000 bar in order to check the extreme injection pressures that may occur). Injection schedule for the polymer flooding case was as follows:

- 1 year of water injection
- 1 year of polymer injection (at a concentration of 1 kg/Sm^3)
- 2 years of water injection

Fig. 6.1 shows field oil production in case of waterflooding and polymer flooding, and field water production is presented in **Fig. 6.2**.
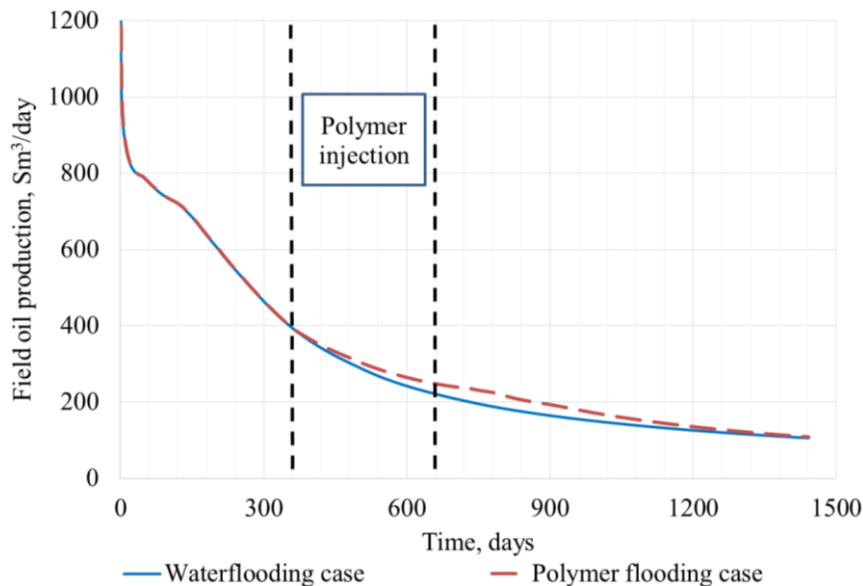
Fig. 6.1 – Field oil production during waterflooding and polymer flooding
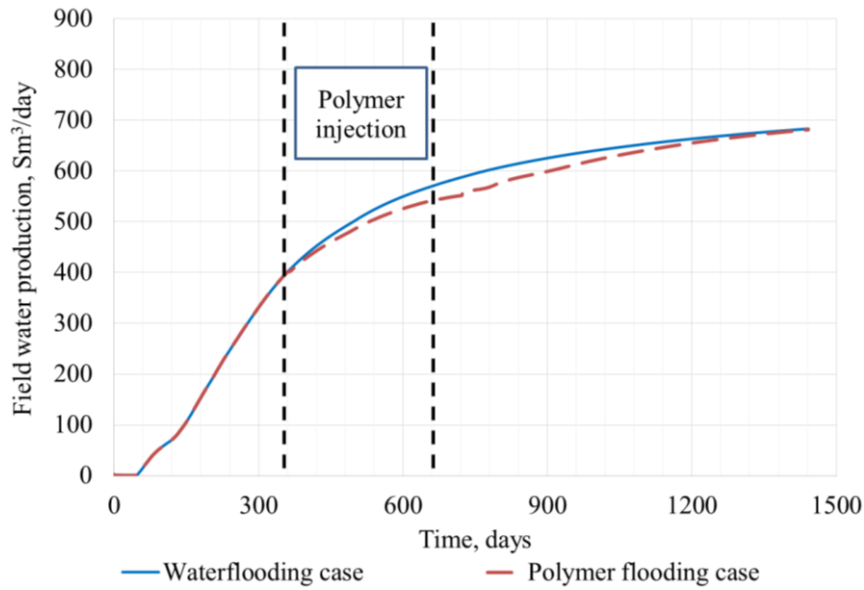
Fig. 6.2 – Field water production during waterflooding and polymer flooding

It can be observed that within 2 months after polymer injection has started polymer flooding effect becomes evident. Field oil production rate increases up to 18% while field water production rate exhibits an equivalent decrease of 5%, so that the total liquid production of the field stays fairly similar in both cases when only water or water with polymer are injected. Among four producing wells in the SPE10 model, wells PROD3 and PROD4 experience the biggest effect of injecting a polymer slug in the reservoir (see **Fig. 6.3**).
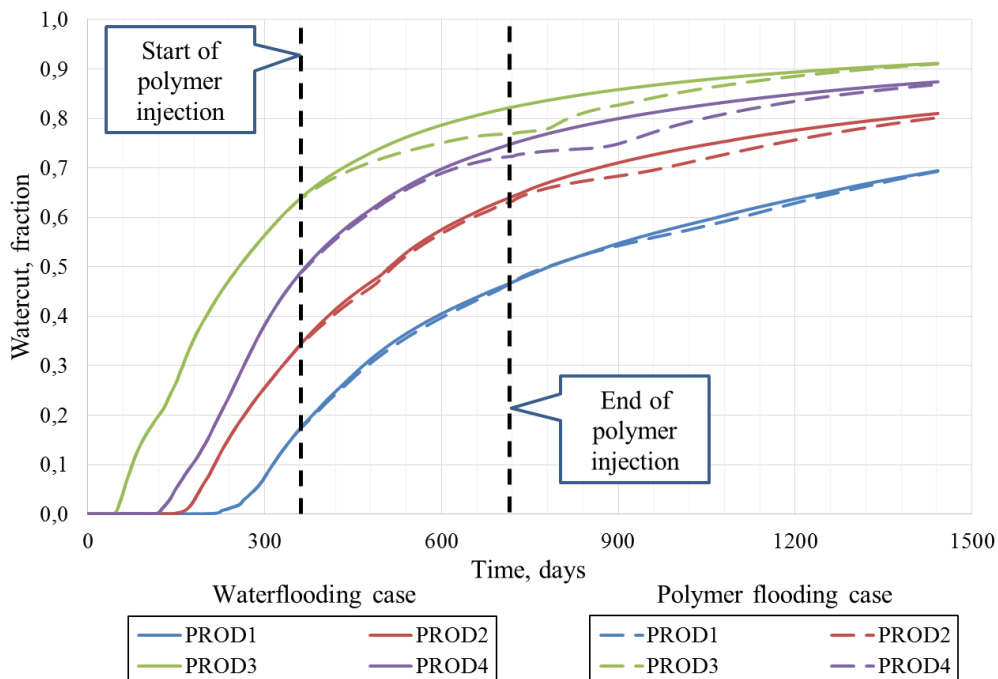
Fig. 6.3 – Well water cuts during waterflooding and polymer flooding

The difference in well PROD3 and PROD4 water cuts between waterflooding and polymer flooding cases can be plotted in a separate figure to highlight the effect of polymer injection (see **Fig. 6.4**).
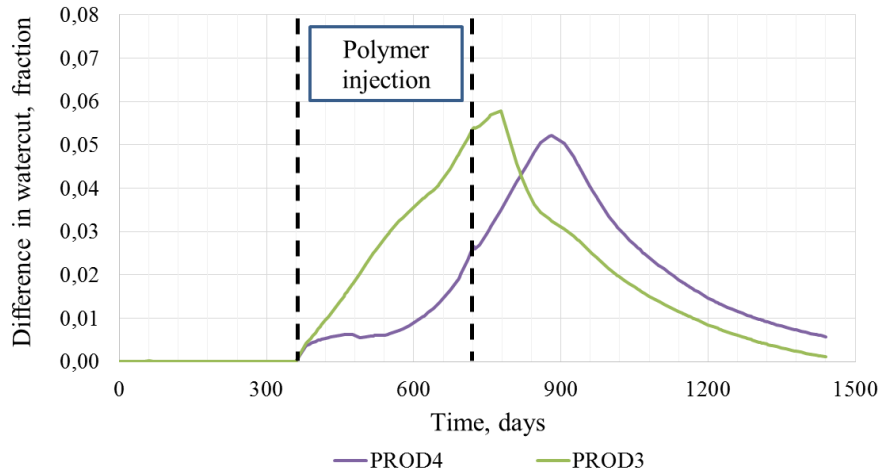
Fig. 6.4 – Difference in water cuts between waterflooding and polymer flooding cases

In well PROD3, the water cut decrease is up to 6%; keeping in mind that liquid production does not change much between cases, the area below the green curve in Fig. 6.4 represents the total effect of adding polymer to the injected water, composed of the impact of different mechanisms of polymer EOR described earlier in Chapter 1.

6.1.2. Sweep efficiency analysis

To investigate where the extra oil production during polymer flooding shown in Fig. 6.1 comes from, an analysis of sweep efficiency of this scenario was made. This analysis focused on the following: identify which regions of the model are involved in the fluid flow process (low-permeability region, high-permeability region etc.), and which of them are more susceptible to the change of injected agent. Permeability based regions will be defined according to the values influencing polymer adsorption function: 20 mD is the upper limit of a low-permeability area, 20-200 mD range corresponds to a medium-permeability area, and high-permeability area is where permeability is above 200 mD.

6.1.2.1. Areal sweep efficiency

At first, the simulation results were analyzed layer-wise to identify the effect of polymer injection on areal sweep efficiency. **Fig. 6.5** represents a relationship between permeability in each grid cell in all layers of Tarbert formation and change in oil saturation in these cells at the end of polymer flooding scenario. The data for plotting were extracted using ResInsight 1.6, an open source 3D visualization and post-processing tool designed to handle ECLIPSE reservoir models. Data points plotted are semitransparent, meaning that the higher color opacity in the plot, the higher the value occurrence. As it can be expected, greatest changes in oil saturation occur in cells with high permeability; however, a number of cells exist where almost all oil has been flushed despite the low permeability (marked with a dashed line in Fig. 6.5). Further analysis of the model revealed that these cells are located in close proximity to the injection well, which explains why saturation changes are so significant. Another feature observed in Fig. 6.5 is that medium to low permeability areas (200 mD and below) tend to have oil saturation changes between 5E-04 and 1E-03, which makes a very small contribution to the oil production but is a very frequent value. Low oil saturation changes in the cells with very low permeability is quite self-explanatory, and medium-permeability areas can exhibit such low changes when

they are located around inactive cells, at the edges of model between production wells where the influence of injector is smaller and even close to production wells in case they penetrate a dead block in the layer.
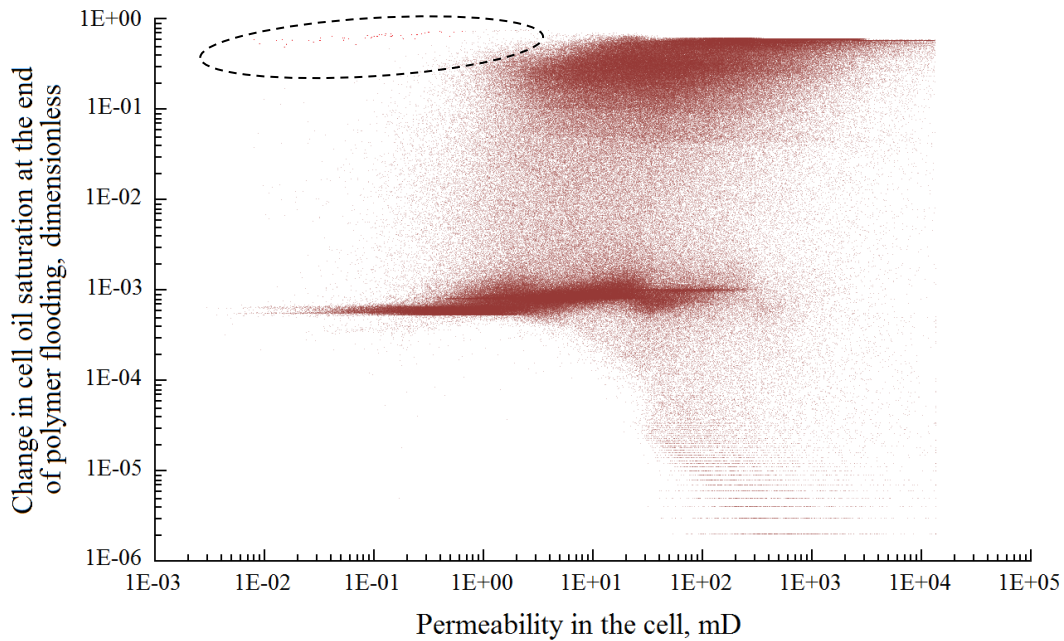
Fig. 6.5 – Change in cell oil saturation at the end of polymer flooding scenario, Tarbert fm. Dashed line marks low-permeability cells where almost all oil was flushed, which corresponds to the area near injection well
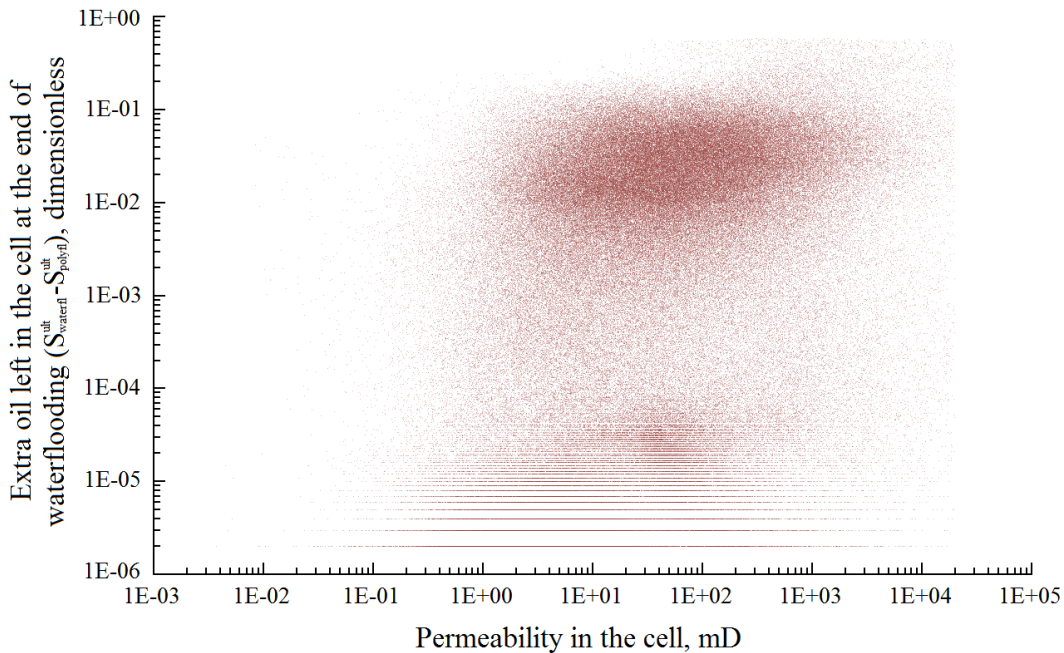
Fig. 6.6 – Difference between oil saturation at the end of waterflooding scenario and oil saturation at the end of polymer flooding scenario, Tarbert fm

Fig. 6.6 represents the effect of polymer flooding in cells with different permeabilities in Tarbert fm when the waterflooding scenario is a reference point. This implies that the vertical axis Y shows the difference in the following oil saturations:

56

$$Y = S_{oil,waterfl}^{ult} - S_{oil,polyfl}^{ult} \quad \dots\dots\dots\dots\dots\dots\dots\dots\dots\dots\dots\dots\dots\dots\dots\dots\dots\dots\dots\dots\dots\dots(6.1)$$

where

$S_{oil,waterfl}^{ult}$ − ultimate oil saturation, waterflooding scenario

$S_{oil,polyfl}^{ult}$ − ultimate oil saturation, polymer flooding scenario

Thus, the scatter plot in Fig. 6.6 presents the effect of the polymer flooding as it shows the extra change in oil saturation in the cells. The first thing that can be observed is that, although both scatters for Tarbert fm (Figs. 6.5 − 6.6) are plotted within the same ranges, the one representing polymer flooding effect with respect to waterflooding is less opaque. That implies that less grid cells have enough extra saturation change to fall within the range on the plot because polymer flooding affected only a part of the cells. Upper part of the scatter corresponds to the areas with greater effect of polymer flooding. Having analyzed Tarbert fm layer by layer, it was observed that this effect appears in cells around injection well and close to production wells perforations, in cells within high-permeability flow paths and cells in vicinity of these high-permeability pathways, in cells corresponding to the edge of swept area (see Appendix 5 for the saturation maps of one of the layers of the formation and Appendix 6 for the MATLAB script used to perform analysis). The latter category of cells, especially if located in the central part of the layer, experiences the greatest effect of polymer flooding (extra change in oil saturation is more than 0.1).

This shows that areal sweep efficiency in shallow marine deposits of Tarbert fm was improved due to the polymer injection; however, the additional effect of polymer injection (or extra oil displaced compared to waterflooding) seen by the most part of the cells is not more than 0.1.

Similar analysis was performed for the underlying Upper Ness fm. **Fig. 6.7** shows change in oil saturation in the cells at the end of polymer flooding scenario. Unlike Tarbert fm where the cells with permeability below 1 mD were almost not involved into the fluid flow, low-permeability cells in Upper Ness fm experience higher oil saturation changes, which can be seen as a wide band on the left side of Fig. 6.7. These cells are located within the fluvial channels or in the close surroundings and in the area near the injection well.

A more interesting feature of the scatter plot in Fig. 6.7 is an area of high occurrence of small oil saturation change in medium to high permeability cells (lower right part of Fig. 6.7). After the data were filtered for each layer, it was observed that this occurs in the cells that are located in those parts of fluvial channels that are poorly connected with the main flow paths and are not perforated by production wells. In some layers where the fluvial channel has more than one branch, these cells belong to the branches that have poor connection with injection well and are therefore insufficiently swept. Other features of the scatter plot in Fig. 6.7 are self-explanatory.

Extra oil displacement during polymer flooding with respect to waterflooding in Upper Ness fm is presented in **Fig. 6.8**. This plot has the same idea as the one in Fig. 6.6 where vertical axis values are obtained using Eq. 6.1. It can be observed that extra oil displacement plot in Fig. 6.8 repeats the main features of the plot in Fig. 6.7, but the values are approximately one order less. Most high-permeability cells where the greatest effect of polymer injection is seen (right

part of Fig. 6.8) are located within fluvial channels that compose pathways between injector and producers.
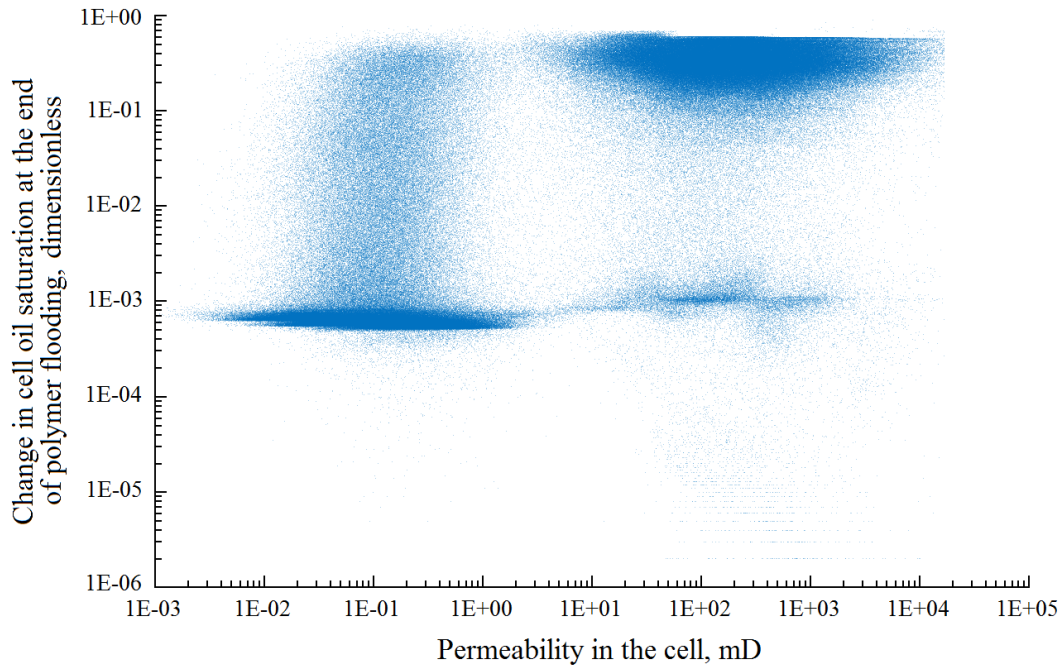
Fig. 6.7 – Change in cell oil saturation at the end of polymer flooding scenario, Upper Ness fm
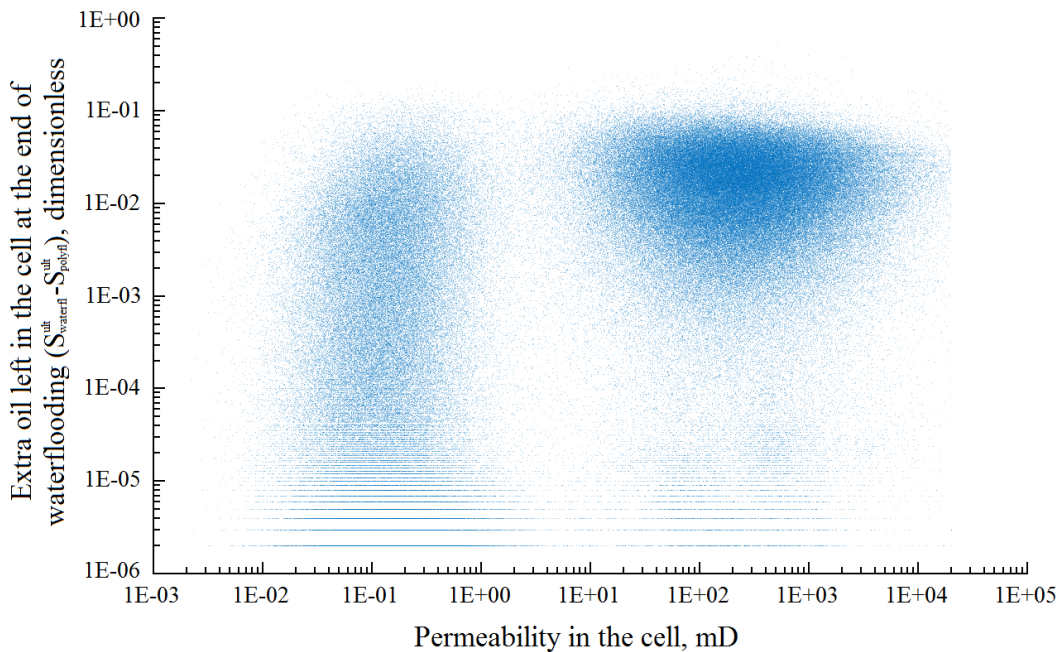
Fig. 6.8 – Difference between oil saturation at the end of waterflooding scenario and oil saturation at the end of polymer flooding scenario, Upper Ness fm

     This big effect is also observed in the laterally isolated parts of the channels that are connected with upper or lower layers. High-permeability points that experience lower extra oil displacement effect correspond to the branches of fluvial channel with insufficient connection to the injector. The left part of the scatter in Fig. 6.8 corresponds to the same group of cells as a similar feature in Fig. 6.7: cells at the edge of fluvial channels and near injection well (see

Appendix 5 for the saturation maps of one of the layers of the formation). Fig. 6.8 shows that fluvial deposits of the Upper Ness fm are swept better when polymer is injected, but additional saturation changes are below 0.1, as for Tarbert fm.

6.1.2.2. Vertical sweep efficiency

Another aspect of sweep efficiency check for polymer flooding is how it acts in presence of vertical heterogeneities. The expected changes in vertical saturation profile are shown in Fig. 1.3. A similar cross-section showing saturations at the end of waterflooding was created for SPE10 model. In **Fig. 6.9**, it is combined with permeability cross-section and a plot showing the difference between oil saturations after waterflooding and after polymer flooding.
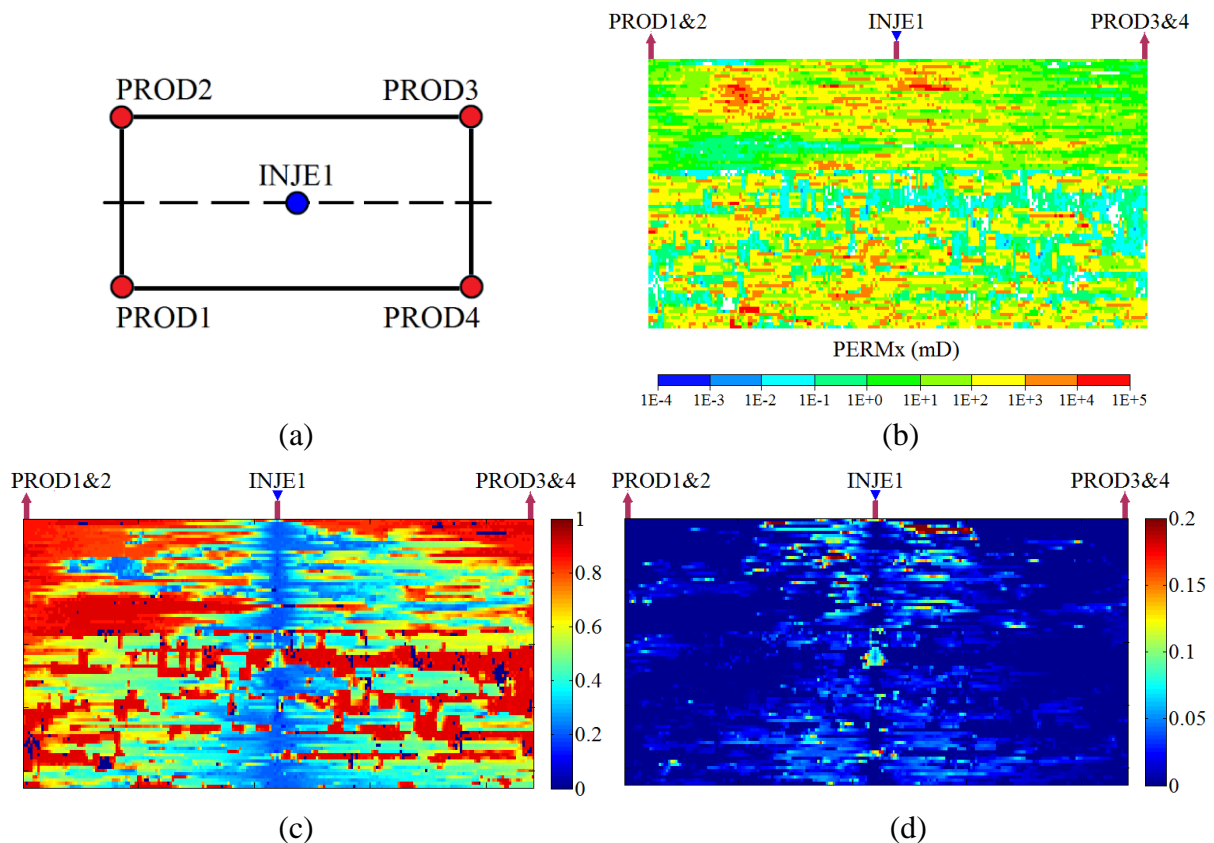
Fig. 6.9 – Vertical sweep in SPE10 fine model: schematic of the top view with the cross-section marked with a dashed line (a), permeability in the cross-section (b), oil saturations in the cross-section at the end of waterflooding (c), sweep efficiency improvement due to polymer injection (d).

Fig. 6.9 shows that the greatest improvement in vertical sweep due to the injection of polymer is noticed in the Tarbert fm, especially in its upper part where the extra change in saturations reaches 0.2. Saturation changes in the Upper Ness fm do not seem that notable in the current cross-section. This is due to the fact that flow paths in Upper Ness fm are very tortuous, and the cross-section cannot follow their shape to highlight polymer flooding effect along these channels, that was discovered during areal sweep analysis. However, one may notice significant changes in the vicinity of injection well where it perforates low-permeability layers. More oil was displaced from this area, and the fluid flow was diverted to the lower layers, as the area of improved sweep efficiency has a triangular shape.

It can be seen in Fig. 6.9 that the flow is more intense in the right-hand side of the model, that is, between the injection well and producers PROD3 and PROD4. As it was shown in Fig. 6.3 earlier, wells PROD3 and PROD4 are more receptive to the change in injection agent. A polyline cross-section of permeability and oil saturation was plotted as denoted in **Fig. 6.10a**.
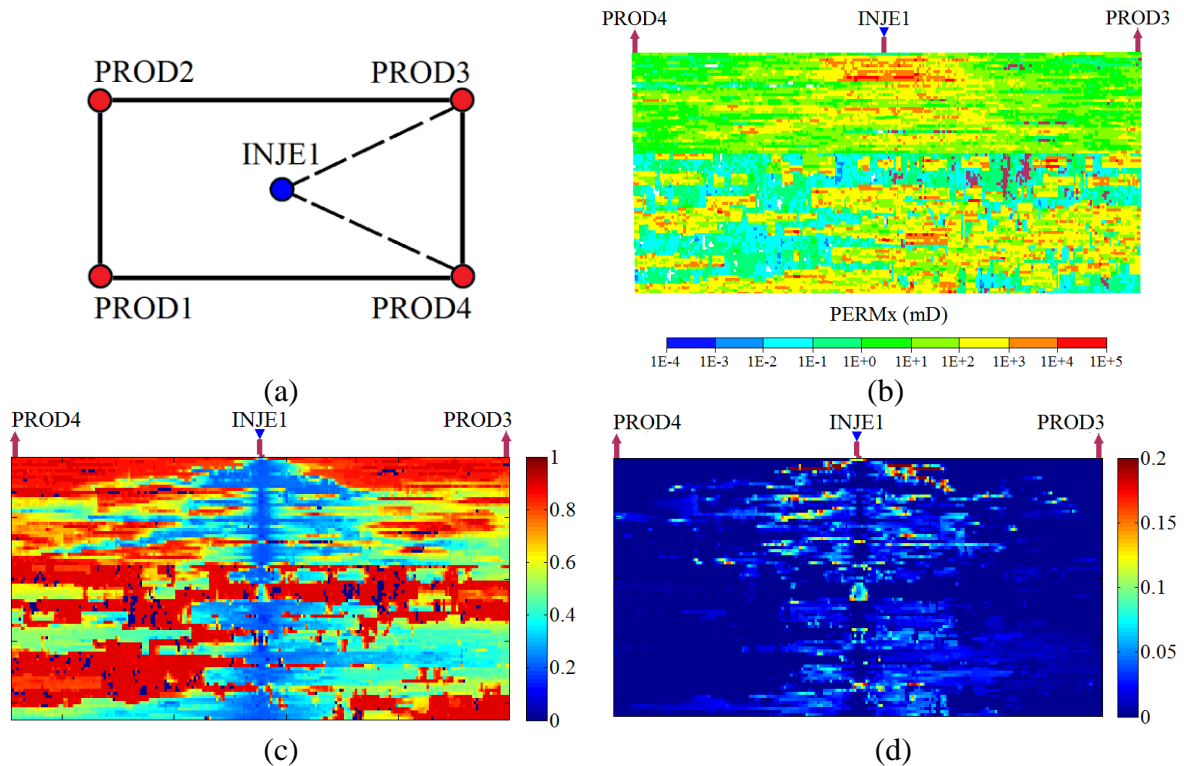
Fig. 6.10 – Vertical sweep in SPE10 fine model: schematic of the top view with the polyline cross-section marked with a dashed line (a), permeability in the cross-section (b), oil saturations in the cross-section at the end of waterflooding (c), sweep efficiency improvement due to polymer injection (d).

As it can be seen in Fig. 6.10, location of wells PROD3 and PROD4 is favorable to establishment of flow paths between injection and producing wells in a large number of layers, which is why production data in these wells respond clearly to a different flooding scenario. Each well perforates all layers, but well PROD3 is actually producing oil from the greatest thickness (around 50-60% of the perforated thickness) which is due to the orientation of fluvial channels in the middle part of Upper Ness formation that positively influences flow conditions. Vertical sweep improvement is mainly notable in the areas around injection well because polymer injection period was too short for such big and heterogeneous model to have polymer slug moved deeper into the formation.

6.1.3. Allocation of fluid flow and polymer adsorption

Allocation in oil and gas industry normally refers to the process of identification of how much each source (field, reservoir, layer, well etc.) contributes to the hydrocarbon extraction. In the context of present thesis, three different permeability areas (high-permeability, medium-permeability and low-permeability area) are considered contributing sources. A MATLAB script (see Appendix 6) was used to estimate the contribution of each source to the oil

production. It was assumed that volume of produced oil could be roughly estimated using the change in oil saturation in each cell as follows:

$$dV_{oil} = \sum_{i=1}^{N} PV_i \left(S_{oil}^{ref} - S_{oil}^{ult} \right)_i \dots\dots\dots\dots\dots\dots\dots\dots\dots\dots\dots\dots\dots\dots\dots\dots (6.2)$$

where

PV_i – pore volume in each ith out of N cells

S_{oil}^{ref} – oil saturation at reference point (e.g. initial state)

S_{oil}^{ult} – oil saturation at the end of the current simulation scenario

Fig. 6.11 is a pie chart showing the results of estimation of oil production from different permeability regions in the model.
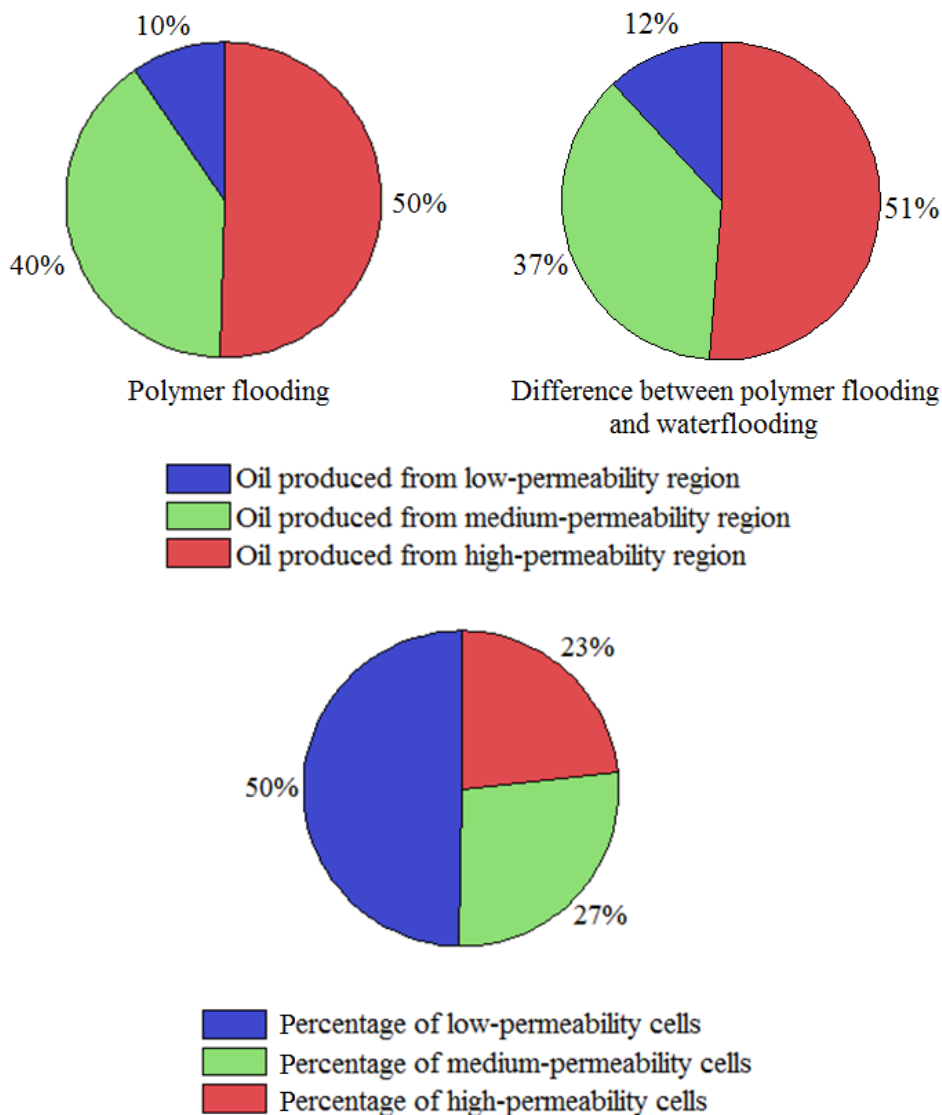
Fig. 6.11 – Percentage of oil produced from different regions of SPE10 model during the polymer flooding scenario and percentage of cells belonging to each region

The biggest part of the model was classified as a low-permeability area, while medium-permeability and high-permeability areas have almost the same bulk volume. As it can be

61

expected, each area contributes to the flow to different degree. It is also obvious that even though the greatest volume is occupied by low-permeability area, its contribution to the oil production is 4 to 5 times lower than the contribution of other sources. At the same time, high-permeability area dominates fluid flow even compared to the medium-permeability area that is assigned a bigger volume in the model. When the extra volumes of oil coming from different sources are being compared, the same trend can be observed in the pie chart: the predominant volume of oil comes from the high-permeability cells, medium-permeability area is the second important contributor, and low-permeability cells supply the smallest extra volume of oil.

To allocate areas that are important contributors to the polymer adsorption in the reservoir, total polymer adsorption data extracted using ResInsight 1.6 were filtered and added up with respect to permeability. In addition, relative pore volume of each permeability region was calculated to evaluate where polymer is more likely to encroach and be adsorbed. The calculations are summarized in **Table 6.1** below.

Table 6.1. Polymer adsorption allocation in SPE10 fine model.

Parameter	Value	Units
Low-permeability area: polymer adsorption	$16.4 \cdot 10^3$	kg
Low-permeability area: PV fraction	29.5	%
Medium-permeability area: polymer adsorption	$13.6 \cdot 10^4$	kg
Medium-permeability area: PV fraction	35.5	%
High-permeability area: polymer adsorption	$12.7 \cdot 10^4$	kg
High-permeability area: PV fraction	35	%

All three permeability areas dispose similar pore space, and low-permeability area is characterized by a greater polymer adsorption values compared to other areas (see Table 4.6). However, only 5.86% of the total adsorption occurs in this area while the greatest amount of polymer is adsorbed in the zones with medium and high permeability: 48.6 and 45.54%, respectively. These numbers are another evidence of poor involvement of low-permeability area to the flow, so that the amount of polymer solution entering this area is too small to influence adsorption allocation significantly.

Nevertheless, one should note that in case of SPE10 model where about 50% of cells are classified as low-permeability area, 64% of these cells have permeability below 1 mD (see Fig. 4.7) and would therefore experience less fluid flow. The rest of low-permeability area with permeabilities between 1 and 20 mD is more suitable for fluid flow and have a high polymer adsorption per kg of rock encountered by polymer solution. In other reservoirs where these cells can be in majority, adsorption distribution between permeability regions may change due to a higher likeliness of fluid flow in low-permeability areas. Thus, while conducting polymer adsorption experiments to produce adsorption data for reservoir simulation models, one should not underestimate the effect of polymer adsorption in low-permeability areas, especially when transitional (low-medium permeability) values are prevailing.

6.2. Upscaling results

6.2.1. Sweep in the upscaled models

Similarly to the analysis performed for SPE10 fine model, a sweep efficiency study in the upscaled models was conducted. However, not all the plots presented in Section 6.1.2 for the fine-scale model were duplicated for the coarse models, but only some selected figures that display the most characteristic trends observed on the fine scale. The workflow and the procedures to obtain analysis results for the coarse model were left the same as in case of fine-scale model analysis.

6.2.1.1. Areal sweep in the upscaled models

Scatter plot of polymer flooding effect with reference to the waterflooding case results was selected to perform coarse models analysis in terms of areal sweep representation. **Fig. 6.12** represents polymer injection effect in coarse models as a correlation between permeability in the grid cell and the amount of extra oil flushed from this cell due to the use of polymer.
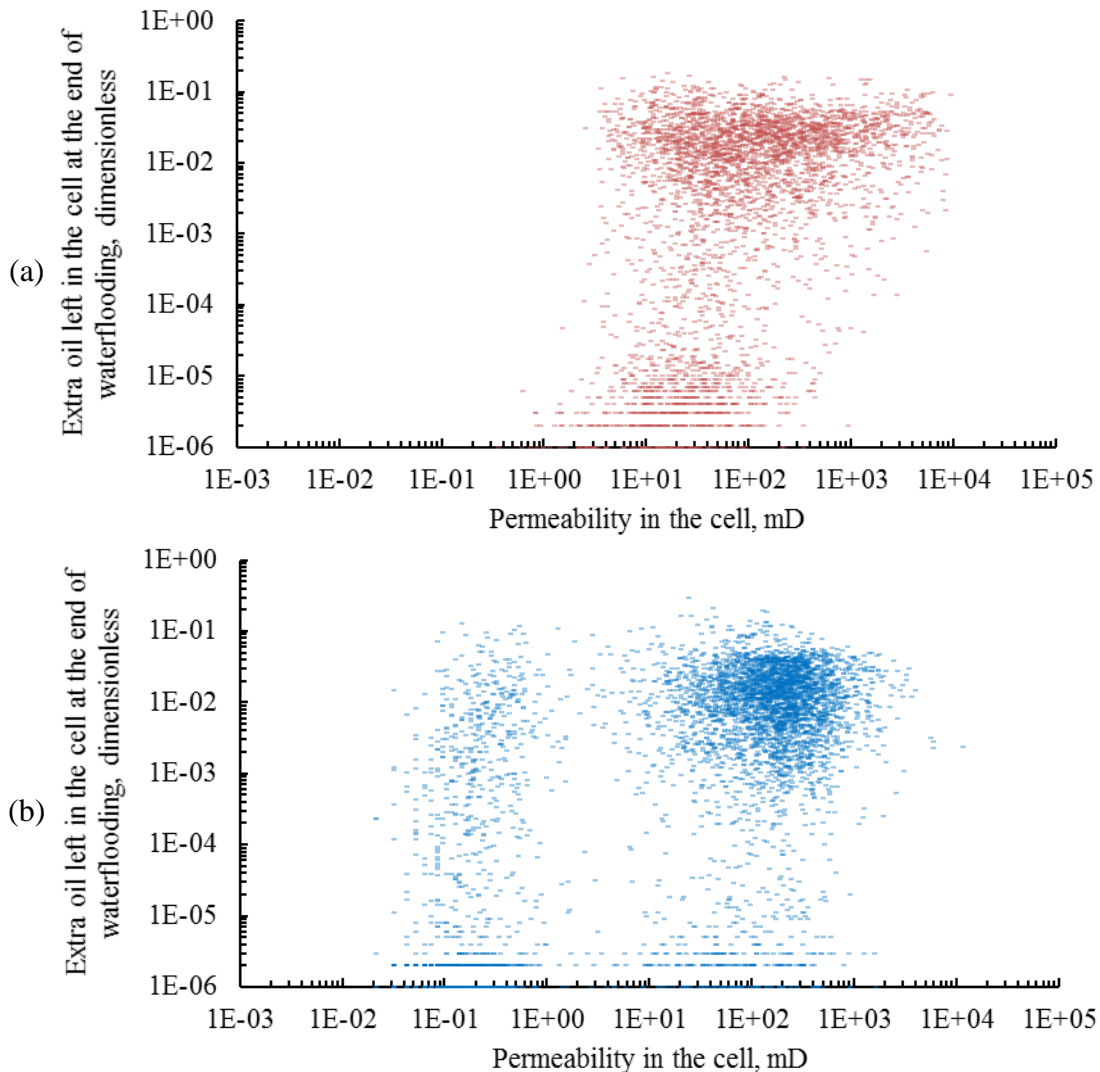
Fig. 6.12 – Difference between oil saturation at the end of waterflooding scenario and oil saturation at the end of polymer flooding scenario, Tarbert (a) and Upper Ness fm (b).

When compared to the data obtained for the fine-scale model (see Fig. 6.6 and Fig. 6.8), it can be seen that the scatter plots of polymer effect in coarse models appears in the same areas as in the fine model: in the preferential flow paths and at the edges of area swept with water in Tarbert formation; near the injection well and within fluvial channels in Upper Ness formation (see Appendix 7).

It should be noted that each upscaling method might have different results because only bulk reservoir properties and absolute permeability were upscaled similarly. Scatter plots in Fig. 6.12 were generated for the model upscaled using CL method, which is assumed a reference coarse-scale solution in this section. Thus, in general, coarse models captured polymer flooding effect fairly well, but due to a decrease in the number of cells, Fig. 6.12 seems to have lower resolution, which is expected.

6.2.1.2. Vertical sweep in the upscaled models

In order to evaluate vertical sweep in coarse models, a polyline cross-section of saturations was generated (see **Fig. 6.13a**). Other possible model slicing options will not be presented herein. In this section, CL-upscaled model results (waterflooding and polymer flooding with upscaled adsorption as a function of upscaled permeability) will be used to generalize the conclusions about vertical sweep in coarse models. One should note, however, that saturation cross-sections might differ from one upscaling method to another, but the rest of upscaled results will be omitted in this section due to their overall similarity.
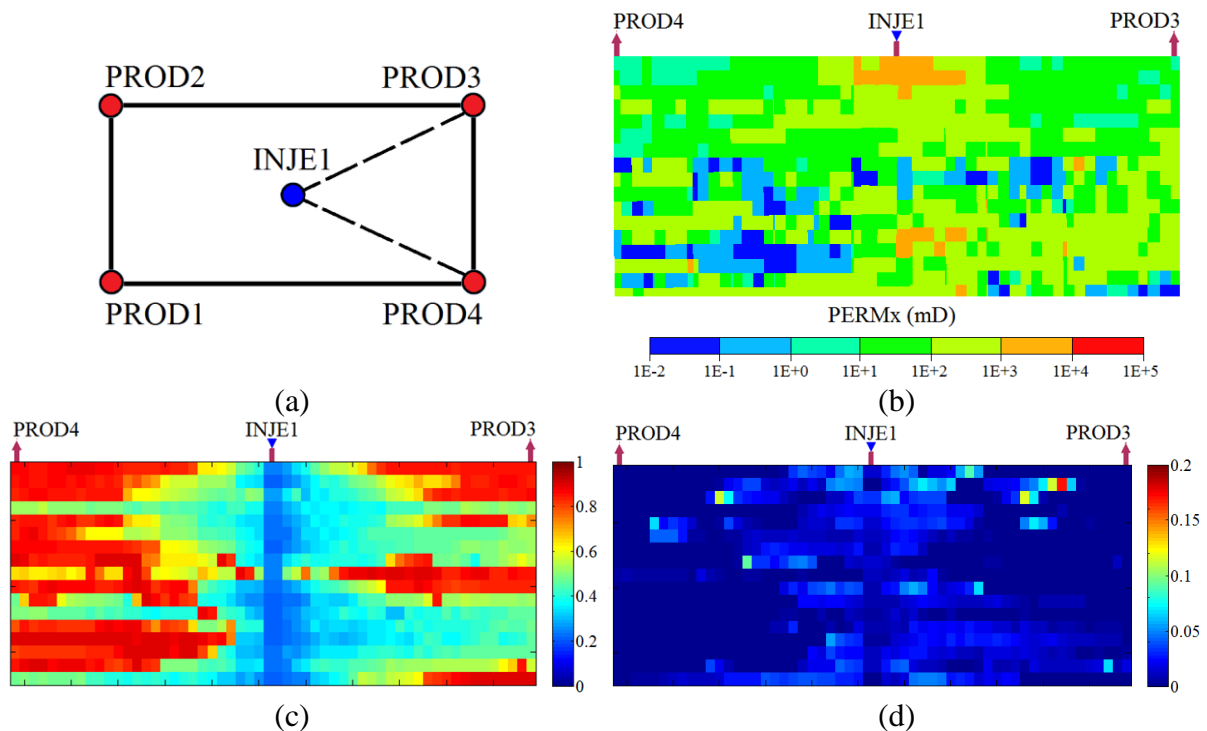
Fig. 6.13 – Vertical sweep in upscaled SPE10 model (CL): schematic of the top view with the polyline cross-section marked with a dashed line (a), permeability in the cross-section (b), oil saturations in the cross-section at the end of waterflooding (c), sweep efficiency improvement due to polymer injection (d).

When compared to the data obtained for the fine-scale model (see Fig. 6.10), it can be noticed that the high coarsening degree affected the resolution of the cross-sections, which is

especially evident in Fig. 6.13b. Having combined 80 fine cells into one coarse cell, the lower permeability values in the model were affected: a two orders of magnitude increase compared to the original permeability scale minimum. However, the ultimate saturation profile in the cross-section captures fine-scale solution quite precisely (compare Fig. 6.10c to Fig. 6.13c), especially in the bottom part of the model corresponding to Upper Ness formation. Nevertheless, the vertical sweep improvement during polymer flooding in the cross-section (see Fig. 6.13d) is not an accurate representation of the fine-scale results, which may be a cumulative effect of errors during two phase flow and polymer flow upscaling.

6.2.2. Allocation of fluid flow and polymer adsorption

The main contributors to extra oil production and polymer adsorption process were defined the same way as for the fine scale model using a code similar to the one presented in Appendix 6. In this section, the results of simulation in CL-upscaled model with adsorption upscaled using a permeability function will represent the performance of coarse models.

Fig. 6.14 shows the results of estimation of oil production from different permeability regions in the model.
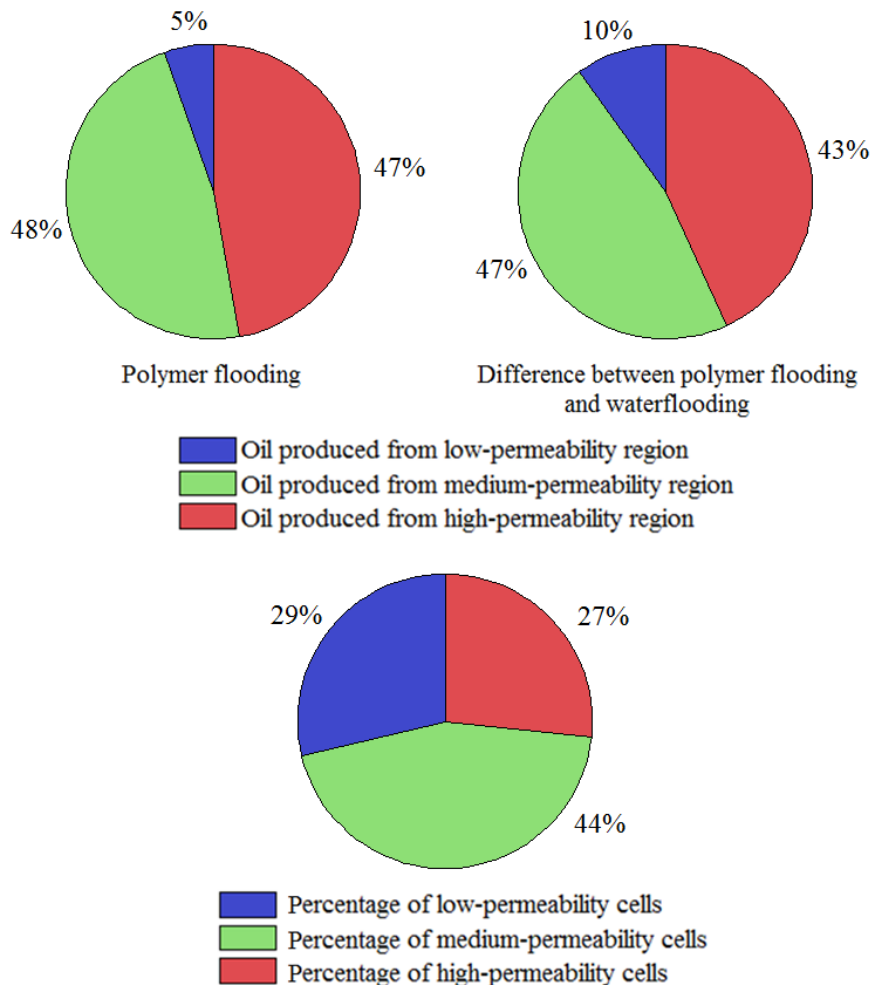
Fig. 6.14 – Percentage of oil produced from different regions of upscaled SPE10 model during the polymer flooding scenario and percentage of cells belonging to each region

The bottommost pie chart in Fig. 6.14 shows the percentage of cells in each permeability group, which ranges were defined earlier in Section 6.1.2. When compared to analogous pie chart in Fig. 6.11, a change in the permeability regions size can be observed. The number of cells considered low permeable decreased after the model has been upscaled (from 50% in the original model to 29% in the coarse models), and slight increase of the high-permeability cells number was observed (from 23% in the fine-scale model to 27% in the upscaled models). This change is an outcome of the upscaling process, and it is more likely to happen in the areas where adjacent cells belong to different permeability groups (e.g. at the edges of fluvial channels or in noisy areas of high-permeability regions).

The upper pie charts in Fig. 6.14 show trends in oil production allocation that are similar to the fine-scale results shown in Fig. 6.11. In the coarse-scale models, the contribution of medium permeability area to oil production is slightly higher than the contribution of high-permeability layers, which is an insignificant deviation from the fine-scale trends. However, this deviation is most likely the result of changes in permeability regions sizes described earlier.

Thus, it can be concluded that coarse-scale models reproduce the main tendencies in oil production and adsorption allocation that have been seen in the original model to a fair degree.

Analogically to Table 6.1, **Table 6.2** presents the amount of polymer adsorbed in each permeability zone and their pore volumes. The changes in zones' pore volumes are in agreement with the changes of zones' sizes mentioned above.

Table 6.2. Polymer adsorption allocation in upscaled SPE10 fine model.

Parameter	Value	Units
Low-permeability area: polymer adsorption	$9.9 \cdot 10^3$	kg
Low-permeability area: PV fraction	19.2	%
Medium-permeability area: polymer adsorption	$14.3 \cdot 10^4$	kg
Medium-permeability area: PV fraction	46.8	%
High-permeability area: polymer adsorption	$12.9 \cdot 10^4$	kg
High-permeability area: PV fraction	34	%

The allocation of polymer adsorption on coarse scale results in the trends similar to those that have been seen on fine scale. Medium- and high-permeability areas correspond to the highest polymer adsorption while only 3.5% of the total adsorption takes place in the low-permeability area. Since the number of cells in the medium-permeability region increased significantly, so did the percentage of adsorbed polymer. This increment of adsorbed polymer mass occurred on account of the low-permeability cells that have been included in the medium-permeability area due to the upscaling process.

6.2.3. Base case upscaling

Base case scenario chosen for SPE10 model was ordinary water flooding during 4 years; the wells controls were identical in fine and coarse models (see Table 4.1). The main purpose of this section is to evaluate the quality of upscaling with fewer parameters that have to be scaled. Any mismatches and errors revealed in this section should be taken into account when

evaluating the performance of polymer flooding upscaling that implies the number of parameters to be scaled is greater.

Fig. 6.15 shows field oil production rate in the fine-scale model and coarse models upscaled using CL, VL and EPS methods. According to Fig. 6.15, an evident difference in the fine-scale and coarse-scale curves occurs during the water injection period (60 – 120 days since the start of simulation). All upscaled models exhibit a production plateau during this period whereas the fine model is characterized by a fall in oil production.
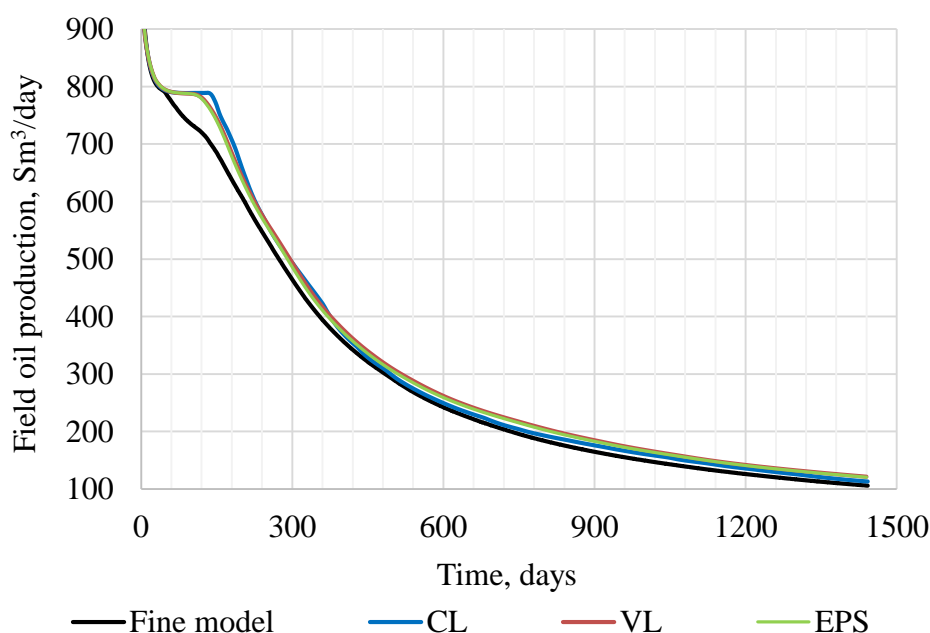
Fig. 6.15 – Base case field oil production comparison

This plateau occurs due to extended waterless oil production observed in all four production wells. In this period, a fairly constant drawdown takes place in the reservoir, and all wells are able to maintain the plateau rate. The upscaled models overestimate water breakthrough time in well PROD3, which is the first one to start water production in the original model (60 days after the start of simulation) that causes a production decrease. Water cuts in wells PROD1-4 can be seen in Appendix 8. A reasonable match in water cuts was obtained for wells PROD2 and PROD4, but in wells PROD1 and PROD3 the water breakthrough is delayed by 60-80 days in average; the discrepancy in water breakthrough time is greater for CL-upscaled model. The effect of bigger delays can be observed in Fig. 6.15 where the curve representing CL-model results has the longest plateau.

The match in oil production improves at the later stages of simulation period, after the water breakthrough appears in all producing wells. Nonetheless, upscaled oil production is higher than the target fine-scale production, which leads to an overestimation of cumulative oil production in the upscaled models (see **Fig. 6.16**).

It is evident that at this early stage some inaccuracy in the upscaled results appears. The coarse models underestimate the speed at which water moves from injector to producers in porous medium, and it results in some discrepancy in oil rates. The CL method gives the least accurate water breakthrough time estimation compared to other methods. The biggest difference is observed in well PROD3, which is dominating the flow on fine scale.
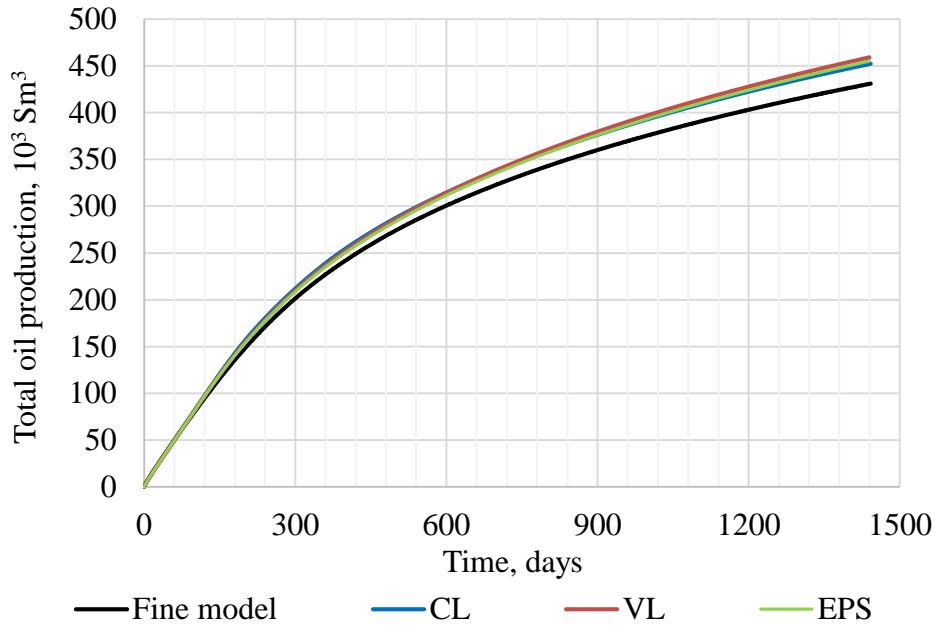
Fig. 6.16 – Base case cumulative oil production comparison

Since the polymer flooding effect is evaluated based on the water cut data herein, the error in water cut forecast in case of waterflooding may be considered the default error appearing in further cases that are using waterflooding as a basis. **Figs. 6.17 – 6.18** show the difference between water cuts on fine scale and on coarse scale as solid lines, and the pie charts included in the pictures serve to compare cumulative errors in water cut estimation, which are areas between the solid lines and the horizontal axis.

According to Figs. 6.17 – 6.18, water cut in well PROD4 are matched better than in well PROD3. The largest errors are observed at the early stage of simulation period, which is caused by delayed water breakthrough in case of well PROD3 and a steeper increase in water cut in the upscaled models compared to fine model in case of well PROD4.
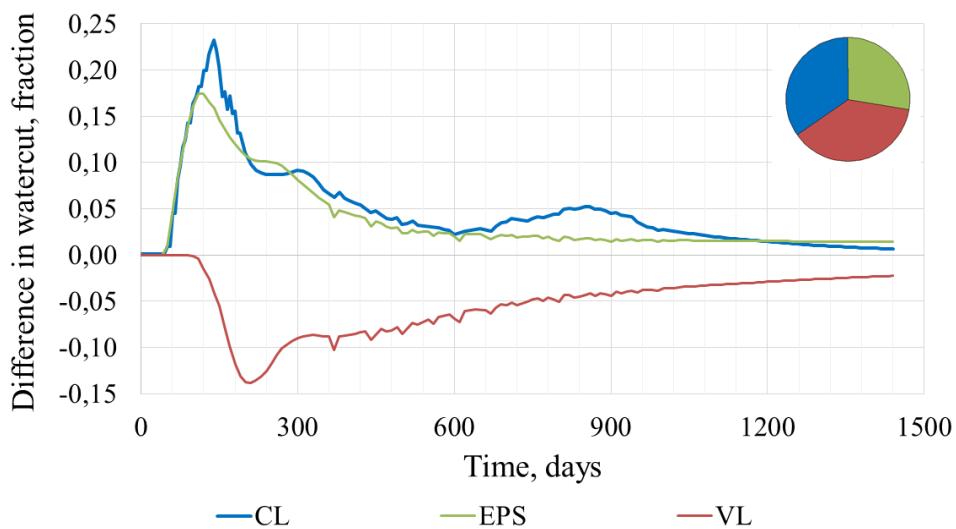
Fig. 6.17 – Error in PROD3 water cut estimation during waterflooding upscaling

CL method appears to give the highest error when estimating water cut in well PROD4, while other methods give almost identical results. All upscaled models show the same trend in water cut estimation for well PROD4, as it can be seen in Fig. 6.18. Hence, it is easier to evaluate the accuracy of each method. In well PROD3, only curves in CL- and EPS-upscaled models correlate, and the water cut in VL-model seems to be a mirror image of the latter curves. Even though VL-curve lies closer to the original water cut in well PROD3 at the beginning of simulation period when the greatest discrepancies are observed, water cuts in CL- and EPS-upscaled models converge to the fine-scale solution faster.
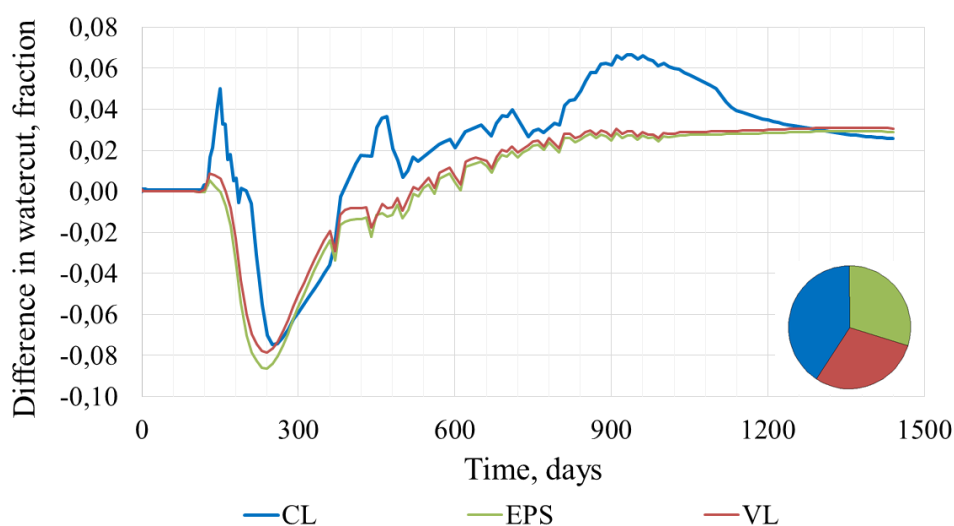
Fig. 6.18 – Error in PROD4 water cut estimation during waterflooding upscaling

6.2.4. Polymer flooding case upscaling

The polymer flooding case on fine scale was introduced in Section 6.1.1. The same scenario was simulated in the CL-, VL- and EPS-upscaled models to evaluate how coarse-scale results match fine-scale data. Each of the models was using polymer adsorption data obtained with the following methods: volumetric averaging, use of the adsorption function, volumetric averaging modified with the flow fraction coefficient. The latter method of adsorption upscaling was using flow-based permeability to calculate the flow fraction coefficient due to the improved results revealed while testing on the 3D realistic models. Thus, a total of 9 different combinations were considered to simulate polymer flooding.

One of the ways to evaluate the effect of polymer slug injection, which is considered herein, is to find the difference between the water cut during normal waterflooding and during the polymer flooding. This difference is expected to appear after the start of polymer injection, and its area is related to the incremental oil produced due to the implementation of this EOR technique.

As it was shown earlier in Chapter 6, wells PROD3 and PROD4 are dominating over other two wells in terms of oil production, and the changes between two scenarios are more significant for these wells. Therefore, polymer flooding effect on fine and coarse scales will be evaluated based on the data in wells PROD3 and PROD4.

Water cut difference in wells PROD3 and PROD4 for 9 different combinations of two-phase flow and adsorption upscaling methods is presented in Appendix 9. **Figs. 6.19 – 6.20** show the polymer flooding effect on fine scale and on coarse scale together for six potentially successful cases. The results for combinations that use flow fraction coefficient formula are not shown in Figs. 6.19 – 6.20 because they highly overestimate the polymer flooding effect, as it can be seen in Appendix 9 (peak values are above 20% for coarse models while fine-scale results' peaks are within 6%).

Both Figs. 6.19 – 6.20 are organized as follows: the left-hand side represents the comparison of the polymer flooding effect on different scales where each color corresponds to one of the two-phase upscaling methods and the type of line corresponds to the adsorption upscaling method. The right-hand side of the figures is a qualitative comparison of the areas below the water cut difference lines on fine scale and on coarse scale, which aims to ease the comparison of the curves that behave differently.

As it can be seen in Figs. 6.19 – 6.20, polymer flooding effect behavior in well PROD3 is captured better than in well PROD4, even though the spreading of area values is less in well PROD4. All the coarse-scale curves tend to have similar type of behavior: a global maximum that occurs with some delay with respect to fine-scale results, and some local maxima and minima corresponding to the start and the end of polymer injection. However, in case of EPS-upscaled models the disturbances due to sharp pressure changes when polymer injection starts or ceases dominate over the maximum that occurs later. Based on Figs. 6.19 – 6.20, the following trend can be noticed: when the model is upscaled using CL method, the use of adsorption function results in a better match of polymer flooding effect in a well than the use of volumetric averaged adsorption; if the VL upscaling is used, the relation is opposite.
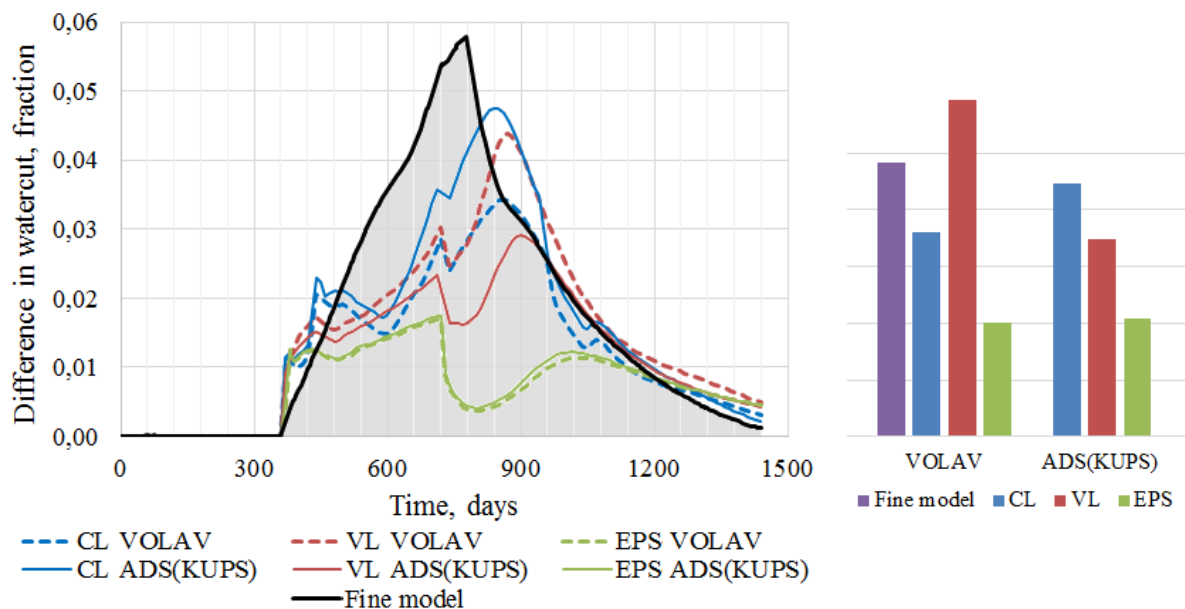
Fig. 6.19 – Difference in water cuts for well PROD3

The following combinations give the best match in both well PROD3 and PROD4: CL-upscaled model with adsorption function and VL-upscaled model with volumetric-averaged adsorption. EPS-upscaled models show poor match, and the choice of polymer adsorption upscaling method does not have a significant impact on polymer flooding effect (excluding the case of flow fraction coefficient formula).

Polymer flooding effect in well PROD4 is more difficult to reproduce, especially due to the considerable instability in water cuts on coarse scale, which results in sharp rise of water cut difference during the polymer injection period. Upscaled models seem to have better connection between the injector and the producers, so any changes in the injection well are reflected on the production data.

Moreover, the default error that occurs at the stage of waterflooding simulation on coarse scale has an effect on the difference in water cuts. For example, the negative default error shown in Fig. 6.18 indicates that the water cut curve during waterflooding simulation in upscaled models lies higher than the corresponding curve in fine model, so the coarse-scale polymer effect curve in Fig. 6.20 will most likely shift upwards with respect to the fine-scale curve. Positive default errors, (see Figs. 6.17 − 6.18) have a reverse effect: they indicate that reference coarse-scale curve is lower than expected, so that the coarse-scale polymer effect is smaller than it should be.
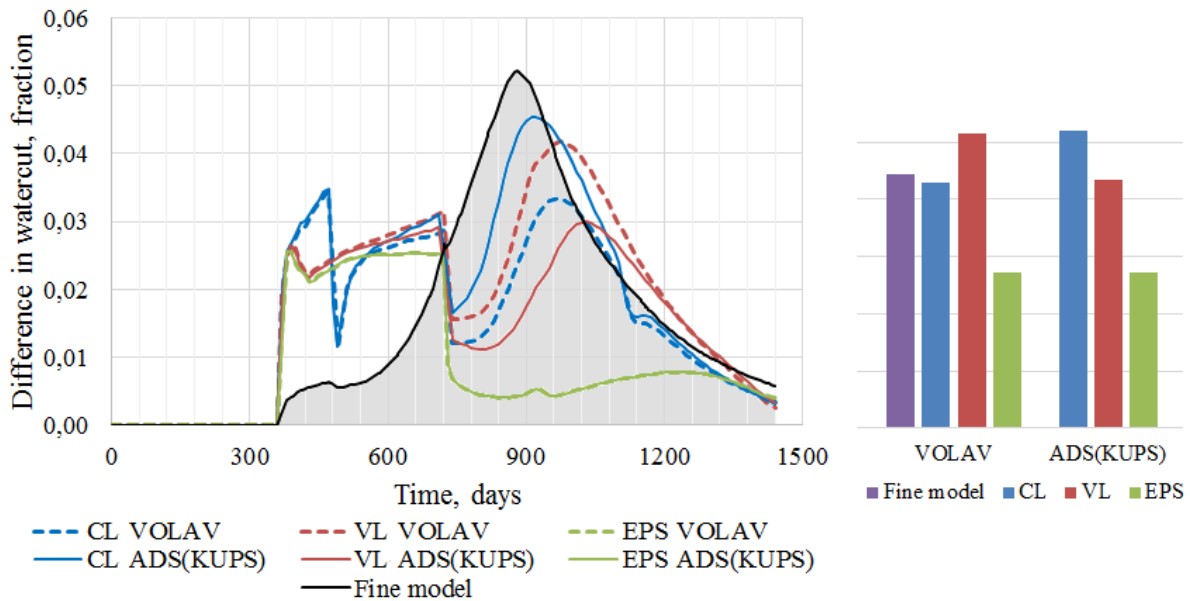
Fig. 6.20 – Difference in water cuts for well PROD4

Chapter 7. Discussions and conclusions

The number of articles concerning the upscaling of single-phase and two-phase flow is high, and these topics have been widely discussed by many authors. However, upscaling of polymer flooding process steps out of the area of well-investigated topics. The number of parameters to be upscaled is greater in polymer flooding upscaling, and the development of the best-fit upscaling techniques is at the first stage for now.

7.1. Discussions

In this thesis, the upscaling of polymer flow in a highly heterogeneous SPE10 model has been considered. This process has been carried out as a two-step procedure: first step consisting of waterflooding parameters upscaling, and second – polymer flooding parameters upscaling. Among all the methods available to perform the first step, or two-phase upscaling, simple and fast steady-state methods were chosen. At the second step, the focus of present thesis has been on polymer adsorption upscaling, whereas other potential upscaling parameters were proven to be constant in space at steady state or were uniformly distributed in the cells by design. Fine-scale polymer adsorption distribution, which is the base in the upscaling procedure, has been estimated as a function of mean permeability of each of ten rock types present in the SPE 10 model and independent on polymer concentration. The amount of adsorbed polymer was upscaled using three approaches: volumetric averaging, adsorption as a function of upscaled permeability, volumetric averaging modified with flow fraction coefficient. In total, three two-phase upscaling methods have been tested to upscale the waterflooding case and nine different combinations of two-phase upscaling and adsorption upscaling methods have been tested to upscale the polymer flooding case.

7.1.1. Polymer adsorption distribution on fine-scale

In the absence of any experimental data on polymer adsorption in Tarbert and Upper Ness fm, the fine-scale polymer adsorption distribution was defined based on the experimental data available in the literature. Obtained polymer adsorption dependency on rock permeability has been adjusted using the Carreau fluid model principle in order to return realistic values even in the low-permeability areas. However, due to the organization of the data file used by ECLIPSE 100, the number of polymer adsorption values accepted by the software was limited by the number of rock types defined in the model. Thus, instead of calculating polymer adsorption value individually for each grid cell, the mean value of permeability for each rock type was used to obtain average polymer adsorption value similar for all the cells within each of these rock types. This can affect the allocation of polymer adsorption on fine scale, which is a reference solution for the upscaled models.

The idea is that if the polymer adsorption values are calculated in a proper way, without averaging the variables used to obtain polymer retention and convert it to adsorption (permeability and porosity, respectively), the contribution of the low-permeability areas to polymer adsorption may increase. Such change would imply that polymer flooding experiments on low-permeability core samples are of importance, even though these cores do not belong to the main facies of interest. Nowadays, most experiments are focused on the core samples from the main targets of field development, which are high-permeability regions.

7.1.2. Polymer adsorption upscaling

The initial concept of the present thesis was, first, to introduce fine-scale adsorption data as a function of permeability and, second, to compare if the application of the same function using coarse-scale permeability is more accurate than volumetric averaging of fine-scale values. Three methods were considered within the introduced concept: simple volumetric averaging, volumetric averaging modified with flow fraction coefficient and adsorption as a function of upscaled permeability. Performance of these different methods was evaluated using simplified and realistic models.

7.1.2.1. Polymer adsorption upscaling using simple volumetric averaging

Volumetric averaging is a simple and straightforward process that needs minimum fine-scale information (no functions or additional calculations needed). In case of polymer adsorption upscaling, it is natural to use rock-volume average because adsorption is a surface phenomenon related to the amount of rock seen by polymer solution. This method proves to be the most accurate in case if polymer concentration is equal in all grid cells. Such situation was obtained in 1D model where the polymer breakthrough occurred; however, when the vertical heterogeneities were introduced into the model, and no polymer breakthrough was observed, this method's accuracy decreased significantly. The main disadvantage of volumetric averaging is that the coarse-scale adsorption value is greatly affected by low-permeability cells that are assigned high polymer adsorption values. However, if some preferential flow paths are present in the model, the influence of low-permeability cells leads to the overestimation of polymer adsorption on coarse scale because the volumetric averaging procedure does not take into account which cells are participating in the fluids flow. In case of the infinite polymer injection into the heterogeneous model the high accuracy of volumetric averaging was observed again, which supports the earlier statement about the favorable conditions for this method.

Nonetheless, the state when all cells are fully saturated with polymer is highly unlikely to be reached in a reservoir, and simple volumetric averaging method overestimated polymer adsorption in 3D models. According to the concept of polymer adsorption distribution on fine scale that has been taken in the present thesis, polymer adsorption should fall close to the flow-based parameters instead of the bulk parameters and, therefore, should be upscaled using a method that takes into account the flow patterns in the model.

7.1.2.2. Polymer adsorption upscaling using modified volumetric averaging

Volumetric averaging modified with the flow fraction coefficient keeps the simplicity of volumetric averaging and improves estimation of flow involvement of the fine cells within the coarse domain. The accuracy enhancement compared to the simple volumetric average was

observed in 2D model with partial polymer invasion into the reservoir; however, this method gave wrong results in three-dimensional models. As it was observed on the simplified 2D model, the flow fraction coefficient works perfectly with the volume averaging formula when only vertical heterogeneities are present in the fine-scale area to be associated in one coarse cell. But this is most likely not the case when it comes to three-dimensional models, and SPE10 model is a good example here. In highly heterogeneous 3D domains, the following situation may happen: a group of high-permeability grid cells is surrounded by low-permeability cells. When using flow fraction coefficient formula, the permeability of the high-permeability cells will influence the upscaled polymer adsorption value. In fact, the presence of such group of cells with low fine-scale adsorption values will make the upscaled polymer adsorption smaller, even though the high permeability cells cannot contribute to the fluid flow. This is most likely the reason for what has been seen in the 5-layer models extracted from the original SPE10 model (fine and upscaled).

Hence, the main disadvantage of the use of the flow fraction coefficient is that it does not take into account how well the cells are connected in the main flow direction and, thus, does not evaluate the real involvement of each pore volume fraction into the fluid flow when the model has lateral heterogeneities. This method also appears to be sensitive to the way the coarse-scale permeability in the flow fraction coefficient formula is computed. Simplified 2D synthetic model case was using the pore-volume average, which could be reduced to the "thickness-average" because of the equal cells dimensions and porosity. This worked perfectly for a simple 2D model, but was insufficient to give an accurate forecast of polymer adsorption in the 3D realistic models because it could not account for the fine-scale flow pattern in presence of many lateral heterogeneities.

When the flow fraction formula was changed, and the flow based upscale permeability estimated during the two phase upscaling in MRST was used to calculate flow contribution of each fine cell within the coarse cell, polymer adsorption estimation improved significantly compared to the solution with volume-averaged upscaled permeability. However, this improvement was not enough to make this method comparable with volumetric averaged adsorption or adsorption as function of upscaled permeability because of a large underestimation. It can be caused by the imperfection of the flow-fraction formula written in MATLAB, which seemed to calculate the adsorption occurring when the flow is through a single fine-scale cross-section within the coarse cell in the direction of fluid flow. This was confirmed when applying the MATLAB version of flow fraction formula to reproduce the calculations in 2D model that have been done in MS Excel.

It was not possible to extend the code to make it calculate polymer adsorption in each fine-scale cross-section during the time that has been allotted for this thesis work. Thus, a simple multiplication factor equal to the number of fine-scale cross-sections, N_{cs}, was used in the formula. However, a proper way to calculate the upscaled adsorption with this formula would be to calculate adsorption for each cross-section and then aggregate these values into a final polymer adsorption value in the coarse cell. This is left as future work.

Other alternatives to improve how flow fraction coefficient formula reflects horizontal connectivity of the fine cells should be tested. For instance, a potential solution might be a multistep flow fraction coefficient calculation: first, calculate average permeability of each fine layer of a coarse cell (that is, homogenize fine layers within each coarse cell) and then use the

technique presented for 2D model, which worked very well for homogeneous layers. This investigation should be considered as a suggestion for further work.

7.1.2.3. Polymer adsorption upscaling using adsorption function on coarse scale

The use of polymer adsorption function on coarse scale is expected to give accurate results because the adsorption distribution would follow the same logic as on fine scale. However, this method showed less accurate results than other methods and a tendency to overestimate adsorption in the synthetic models. This method is more sensitive to permeability on fine scale than volumetric averaging, but the imprecise match in the synthetic models was caused by the predominant influence of low-permeability cells on the coarse-scale adsorption values, especially in 1D model. The performance of this method's forecasting improved when the geometry of the flow became more complicated in 2D model and no uniform polymer concentration was observed in the model. However, the predominance of low-permeability cells could have been observed because the adsorption function solution was between the complete adsorption estimated by the volumetric averaging and the correct solution given by flow fraction coefficient formula. One of the reasons why the use of polymer adsorption function on coarse scale is not showing exceptionally accurate results is related to the different ways of adsorption distribution principles on fine and coarse scales. In the fine-scale model only ten adsorption values calculated based on mean permeability for each rock type are used, whereas in the upscaled models each cell is assigned an individual adsorption value. Thus, the adsorption distribution on fine scale is less detailed, and the cells are forced to take mean adsorption values. In this case it might happen that high-permeability cells where the intense flow occurs are assigned a higher adsorption value because they belong to a rock type, which mean permeability is lower. This may lead to a distortion of the fine-scale adsorption picture and, consequently, to more discrepancies between the simulation results in the original and upscaled models.

7.1.3. Sweep and adsorption allocation in the upscaled models

The upscaling of polymer flooding was first evaluated in terms of how areal and vertical sweeps are reproduced and where most polymer is retained on the coarse scale. The sweep analysis showed that the areal sweep and sweep improvement due to the polymer injection, in particular, are reproduced well and represent the main fine-scale patterns. The similarities between vertical sweep on fine and coarse scale were not so evident, and the principal issue was a higher coarsening degree in the vertical direction, which led to lower resolution of the cross-sections compared to the resolution of horizontal slices. Moreover, the vertical sweep was evaluated based on a diagonal cross-section in the region where the most flow occurs, and the diagonals on different scales could include slightly variant areas due to the size of cells. Lastly, the effect of errors during the two-phase upscaling should not be excluded.

The allocation of polymer adsorption was quite accurate in the upscaled models, and the distinctions between the fine-scale and coarse-scale results were generally caused by the changes in assignments of cells to one or another group based on their permeability. For example, the increase of polymer adsorption in the medium-permeability area occurred owing to a number of low-permeability cells that have been joint to this region. Accordingly, the percentage of adsorbed polymer in the low-permeability area decreased.

7.1.4. Reconstruction of polymer flooding effect in the upscaled models

Some methods have shown quite fair representation of the polymer flooding effect, or the difference between the water cut during waterflooding and polymer flooding, which is considered a mark of this EOR method efficiency. The best match was achieved for well PROD3; however, it should be noted that all the coarse-scale curves have some perturbations during the polymer injection period, which introduces some noise and corrupts the shape of water cuts difference. Methods that were using flow fraction coefficient and were not included into the comparative pictures because of too high water cut differences produced curves with reasonably similar shapes. In general, these curves repeat fine-scale behavior well and do not have the disturbances or noise observed in curves obtained with other methods. If the procedure of volumetric averaging modified with flow fraction coefficient is developed to take into account all the cross-sections through which the fluid flow occurs, this method will potentially be the most precise.

7.1.5. Remarks on the methods performance in 3D realistic models

The results of polymer adsorption upscaling were explicable and quite predictable when tested on synthetic 1D and 2D models, but the attempts to implement it on 5-layer pieces of the real model produced some discrepant output, and it was not possible to define applicable patterns. However, it should be noted that when the analysis of polymer adsorption upscaling was performed for the 3D realistic models, their dimensions corresponded to a single layer of the upscaled models. In fact, this means that the 3D fine-scale results were compared to 2D coarse-scale results in Section 5.2.2 of present thesis. The absence of the third dimension in case of the coarse-scale models might have a negative influence on the comparison since any vertical flow diversion in the upscaled models is then excluded. Thus, it is recommended to modify either the dimensions of the extracts of fine-scale SPE10 model to have more layers in the upscaled models, or to consider more similar flow conditions in fine and coarse models. This can be done by replicating one fine-scale layer in Z-direction and compare the results with those in its upscaled version or by performing grid refinement in the coarse model to include a possibility of flow in vertical direction. These procedures can be carried out as intermediate steps to switch from 2D flow analysis to 3D flow analysis by complicating the model gradually. The aim of such approach may be to identify at which step the biggest mismatch occurs in order to evaluate the impact of vertical heterogeneities on the upscaling quality.

7.1.6. Remarks on the steady-state upscaling methods

The steady-state upscaling methods were used due to their simplicity and relatively low computational costs. Nonetheless, it should be kept in mind that such upscaling methods as viscous limit and capillary limit are asymptotic cases, which assume viscous dominance and dominance of capillary forces, respectively. The rate dependence of two-phase upscaling has been affirmed in the literature, but no investigation has been performed to determine how the rate value used in the current thesis might affect the results because it was out of the scope of this thesis work. Therefore, the validity of the steady-state methods has not been proved or disproved, and one should treat the results carefully. If the steady-state flow assumptions are highly violated in the simulation model, the waterflooding upscaling may result in huge

discrepancies. Thus, other flow rates in fine-scale model should be investigated in order to determine at which rates the solutions converge to either viscous or capillary limit and to find out whether a better match of production data can be achieved.

Some issues arose when using end-point scaling method during polymer flooding upscaling. It was observed that the polymer flooding simulations in EPS-upscaled models resulted in almost identical polymer adsorption curves for volumetric averaging of adsorption and adsorption function use on coarse scale. There is a difference between polymer adsorption estimated with these methods in the EPS-models, but it is indiscernible without zooming into a plot. ECLIPSE input and output files have been studied to detect the reasons for such behavior, but no conclusive explanation has been found. Moreover, in some cases it was observed that estimated polymer adsorption goes above the total amount of injected polymer, which cannot happen in reality. A similar situation has been found in the simplified models results upscaled with the use of adsorption function (1D) and volumetric averaging (2D), but the excess of adsorbed polymer was negligible and was therefore considered a numerical error. No other reasons that would point out to an excessive polymer adsorption in synthetic and realistic models have been detected. Different time steps sizes were tried on the realistic models, but no significant improvements have been obtained; the simulation log files have not revealed any issues in the well production or mass balance. Thus, the main guess is that high excess of polymer adsorption in 3D models is due to the numerical error that was enlarged because of quite big adsorption values used in the models, especially when volumetric averaging was considered.

7.2. Suggestions for the future work

The goal of this thesis has been to investigate different techniques for upscaling of polymer flow, with a focus on polymer adsorption. In order to achieve this goal, nine different combinations of two-phase upscaling and adsorption upscaling methods have been tested. During this study, many questions related to alternative approaches to the procedure and to possible improvements arose. Further studies could be performed in the following directions: trying alternative two-phase upscaling techniques, developing polymer adsorption upscaling techniques, deepen the analysis of the processes during polymer flooding in the fine-scale model and their representation on the coarse scale.

Trying alternative two-phase upscaling methods is necessary to diminish a so-called "default error" occurring at the stage of waterflooding upscaling, which should facilitate the evaluation of polymer upscaling techniques. The validity of steady-state methods at current conditions should be checked, and their performance should be compared to that of other methods available (e.g. dynamic methods or modifications of steady-state methods that treat transient flow better).

Polymer adsorption methods that have been studied herein and the flow fraction coefficient formula in particular require some extra investigation. The flow fraction coefficient formula should be modified in order to take the full flow through each coarse cell into account. Some study should be conducted to compare the fine and coarse models performance in case the polymer adsorption is calculated using the adsorption function for each cell individually.

More synthetic models should be tested to introduce different types of heterogeneities and complicate geology gradually to detect what may cause the behavior without any obvious patterns seen in 3D realistic models.

Sweep analysis and adsorption allocation on different scales showed that upscaled models fairly replicate fine-scale results; however, the differences in polymer adsorption behavior and production data were detected. For a better understanding of the flow patterns on fine and coarse scales, it is suggested to implement tracer tracking option in further simulations. The use of tracers would enhance the analysis of fluid flow allocation on different scales and would help to detect possible inaccuracies in the coarse models cause during the upscaling.

7.3. Conclusions

For steady state flow, when we disregard reduction factor and residual resistance factor in the model and keep inaccessible pore volume constant, the only parameter left to be upscaled in polymer flow is polymer adsorption. Polymer adsorption upscaled with simple volumetric averaging was found to be the most accurate method in case when all grid cells have the same polymer concentration, but this method overestimates the adsorption due to the influence of low-permeability areas in more complex cases when some zones of reservoir are bypassed by polymer. The use of the polymer adsorption function on coarse scale is more sensitive to the influence of fine-scale flow contributors (e.g. highly permeable channels) and gives better results than simple volumetric averaging. The volumetric averaging modified with the flow fraction coefficient formula was found to be the most accurate method implemented in synthetic models, but it needs some improvements to account for the full flow through a coarse cell in the realistic models. The combinations of capillary limit upscaling with polymer adsorption function and viscous limit upscaling with volumetric averaging of adsorption gave better estimations of polymer flooding effect on water cuts in the production wells.

Appendix 1. Derivation of the steady-state flow equation at viscous limit

The derivation presented below is reproducing the procedure presented in the work of Ekrann & Aasen (2000). Assume incompressible two-phase flow through porous media. Such flow is described by continuity equation and Darcy's equation:

$$\begin{cases} -\nabla u_p = \varphi \dfrac{\partial S_p}{\partial t} \\ u_p = -k \dfrac{k_{rp}(S_p)}{\mu_p} \nabla p_p \quad ; \quad p = o, w \\ \sum S_p = 1 \end{cases} \quad\text{...............................(A1)}$$

The pressures of oil and water are related to each other through capillary pressure:

$$p_o - p_w = p_c(S_w)$$

At steady state $\nabla u_p = 0$. Assuming that

$$\lambda_p(x, S_p) = \frac{k_{rp}(S_p)}{\mu_p}$$

and combining the equations for two phases, the following relationship is obtained:

$$\frac{1}{k}\left(\frac{u_w}{\lambda_w(x, S_w)} - \frac{u_o}{\lambda_o(x, S_o)} \right) = \nabla p_c$$

$$u_w \lambda_o(x, S_o) - u_o \lambda_w(x, S_w) = k \nabla p_c \lambda_o(x, S_o) \lambda_w(x, S_w)$$

$$\text{take } f_w = \frac{\lambda_w(x, S_w)}{\lambda_w(x, S_w) + \lambda_o(x, S_o)} = \frac{\lambda_w(x, S_w)}{\lambda_t(x, S)}$$

$$u_w(1 - f_w) - u_o f_w = \frac{k \nabla p_c \lambda_o(x, S_o) \lambda_w(x, S_w)}{\lambda_t(x, S)} \quad |\cdot \nabla$$

$$\nabla u_w - \nabla f_w u_t = \nabla\left(\frac{k \nabla p_c \lambda_o(x, S_o) \lambda_w(x, S_w)}{\lambda_t(x, S)} \right)$$

Remember that at steady state $\nabla u_p = 0$, the saturation equation for steady-state flow becomes:

$$u_t \nabla f_w + \nabla(k G_w \nabla p_c) = 0 \quad\text{..(A2)}$$

where

$$G_w = \frac{\lambda_o(x, S_o) \lambda_w(x, S_w)}{\lambda_t(x, S)}$$

Appendix 2. MATLAB script to define fine-scale adsorption

```matlab
%%%%%%%%%%%%%%%%%%%%%%%%%%%%%%%%%%%%%%%%%%%%%%%%%%%%%%%%%%%%%%%%%%%%%%%%%%%
%                POLYMER FLOODING PARAMETERS UPSCALING                   %
%     Adsorption upscaling using ADS vs PERM relation from lab tests     %
%                        (literature review)                            %
%%%%%%%%%%%%%%%%%%%%%%%%%%%%%%%%%%%%%%%%%%%%%%%%%%%%%%%%%%%%%%%%%%%%%%%%%%%

mrstModule add deckformat

% Extracting data fields used in the fine model
struc=readEclipseDeck('M:\MATLAB\Master thesis\mrst\field-model-
project\code\models\spe10\input\models\spe10\eclipse\fine\vrelperm\SPE10.DA
TA')
permx=struc.GRID.PERMX;
porox=struc.GRID.PORO;
permxmax=max(permx)
permxmin=min(permx)

% Option 2: create a row vector of logarithmically spaced points (bins
% edges)
% Use histc to evaluate how many cells fall into this or that category (two
% humps can be seen - probably because we have two formations in the model)
% + return bin indices for each cell in our model -> so-called ADSNUM.INC
% The Ads vs PERMX formula used is the linear trend line equation obtained
% for experimental data presented in "Enhanced Oil Recovery" (D.W.Green,
% G.P. Willhite), outliers (see Excel file) were excluded

% Creating a historam for logarithmically spaced points:
figure(1)
binsedges=logspace(log10(min(permx)),log10(max(permx)),10)';
[howmanycells, binindices] =
histc(permx,logspace(log10(min(permx)),log10(max(permx)),10));
bar(howmanycells) % Number of cells in SPE10 falling into one of 20 bins
created
title({'Distribution of the cells';'between 10 logarithmically spaced PERMX
bins'},'FontName','TimesNewRoman')
xlabel('Bin #')
ylabel('# of cells in the model withing the bin')
figure(2) % Spacing of PERMX values
semilogy(logspace(log10(min(permx)),log10(max(permx)),10),'LineWidth',1,'Ma
rker','o','MarkerFaceColor','b','MarkerEdgeColor','b','MarkerSize',3)
title({'How bins edges were defined';'(logarithmically spaced bins)'})
xlabel('Bin #')
ylabel('Permeability, mD')

% Introducing trend line equation (outliers excluded), R^2=0,969
% This equation was obtained by using experimental data (retention vs
permeability) presented by Vela
% et al., 1976. The procedure is explained in the .doc file
%retbinnedA=@(x)9561.2308*x.^(-0.97538746);

% Introducing trend line equation / Function D / , R^2=0,9986
% This equation was obtained using experimental data (retention vs
```

```matlab
% permeability) presented in K.S. Sorbie et al., 1982
retbinnedD=@(x)6170.6961*x.^(-0.45374703);

satnum=struc.REGIONS.SATNUM;
[howmanycells1, binindices1] = histc(satnum,[1:10]);
figure(3)
bar(howmanycells1)
title({'Distribution of the cells';'between SATNUM
regions'},'FontName','TimesNewRoman')
xlabel('SATNUM region #')
ylabel('Number of cells in the model within the region')

%Calculating mean PERMX within each SATNUM region
A=zeros(length(permx),10);
B=zeros(length(permx),10);
for i=1:10
    for j=1:length(permx)
        if binindices1(j)==i
            A(j,i)=permx(j);
            B(j,i)=porox(j);
        end
    end
    end

permxsatnum1=nonzeros(A(:,1)); %placing non-zero permeabilities from SATNUM
region 1 to a sepaprate vector to calculate mean value
poroxsatnum1=nonzeros(B(:,1)); %placing non-zero porosities from SATNUM
region 1 to a sepaprate vector to calculate mean value

permxsatnum2=nonzeros(A(:,2)); poroxsatnum2=nonzeros(B(:,2));
permxsatnum3=nonzeros(A(:,3)); poroxsatnum3=nonzeros(B(:,3));
permxsatnum4=nonzeros(A(:,4)); poroxsatnum4=nonzeros(B(:,4));
permxsatnum5=nonzeros(A(:,5)); poroxsatnum5=nonzeros(B(:,5));
permxsatnum6=nonzeros(A(:,6)); poroxsatnum6=nonzeros(B(:,6));
permxsatnum7=nonzeros(A(:,7)); poroxsatnum7=nonzeros(B(:,7));
permxsatnum8=nonzeros(A(:,8)); poroxsatnum8=nonzeros(B(:,8));
permxsatnum9=nonzeros(A(:,9)); poroxsatnum9=nonzeros(B(:,9));
permxsatnum10=nonzeros(A(:,10)); poroxsatnum10=nonzeros(B(:,10));

meanpermx=[mean(permxsatnum1),mean(permxsatnum2),mean(permxsatnum3),mean(pe
rmxsatnum4),mean(permxsatnum5),mean(permxsatnum6),mean(permxsatnum7),mean(p
ermxsatnum8),mean(permxsatnum9),mean(permxsatnum10)];
meanporox=[mean(poroxsatnum1),mean(poroxsatnum2),mean(poroxsatnum3),mean(po
roxsatnum4),mean(poroxsatnum5),mean(poroxsatnum6),mean(poroxsatnum7),mean(p
oroxsatnum8),mean(poroxsatnum9),mean(poroxsatnum10)];

figure(4)
[ax,p1,p2] = plotyy([1:10],meanpermx,[1:10],meanporox,'semilogy','plot');
title('Mean porosity and permeability in SATNUM
regions','FontName','TimesNewRoman')
xlabel(ax(1),'SATNUM region #')
ylabel(ax(1),'Log10 permeability, mD')
ylabel(ax(2),'Porosity, dimensionless')
legend('Mean permeability','Mean porosity','Location','northwest')

% Calculating retention for the mean permeability in each SATNUM region
% units - lbm/acre-ft
retention1=retbinnedD(meanpermx);
%retention1=retbinnedA(meanpermx);
```

```matlab
%In order to convert to adsorption [µg/g], the following
%formula should be used:

rettoads=@(poro)2.717*(1-poro).*2.65
%where poro - mean porosity value for each SATNUM region
%       2.65 - grain density which is assumed to be quartz' density

coef=rettoads(meanporox);
ads1=retention1./coef/1000000; % adsorption in kg/kg

figure(5)
[ax,p1,p2] = plotyy([1:10],meanpermx,[1:10],meanporox,'semilogy','plot');
title('Mean porosity and permeability in SATNUM
regions','FontName','TimesNewRoman')
xlabel(ax(1),'SATNUM region #')
ylabel(ax(1),{'Log10 permeability, mD';'Adsorption, kg/kg'})
ylabel(ax(2),'Porosity, dimensionless') % label right y-axis
hold on
plot(ads1,'LineStyle','-.','Color','r','Marker','o')
legend('Mean permeability','Adsorption','Mean porosity','Location','north')

% Using Carreau fluid model to cut-off too high retention values
% The Carreau model appears as follows:
% µeff(y)=µinf+(µ0-µinf)*( 1+(lambda*y)^2 )^(0,5n-0,5)
% where y      - shear rate
%       µ0     - viscosity at zero shear rate
%       µinf   - viscosity at infinite shear rate
%       lambda - relaxation time
%       n      - power index
% In our case, PERMX is used instead of shear rate and RET is used instead
% of viscosity. Then the Carreau model expression transforms as follows:
% RETeff(PERMX)=RETinf+( RET0-RETinf )*( 1+(lambda*PERMX)^alfa )^(0,5n-0,5)
RETinf=50;
RET0=1500;                      %Carreau model parameters from Excel Solver
results
lambda=0.044691564789017;
n=0.960271737793605;
alfa=24.277887102091;
retcarreau=RETinf+(RET0-RETinf)*(1+(lambda*meanpermx).^alfa).^(0.5*n-0.5);

%Convert to adsorption [µg/g] again:
adscarreau=retcarreau./coef/1000000; % Carreau-modified adsorption in kg/kg

% Writing PLYADS to a separate file
row='PLYADS';
fileID = fopen('M:\MATLAB\Master thesis\mrst\field-model-
project\code\annasincl\finepolymer.inc','w')
fmt='%62s\n%80s\n%6s\n'
%fmt1='%62s\n';
fprintf(fileID,fmt,'--Adsorption as a function of mean permX in each SATNUM
region','--Experimental data set from Sorbie et al., 1982, was used to
generate ADS(PERMX)','PLYADS');
%fmt1='%80s\n';
%fprintf(fileID,fmt1,'--Experimental data set from Sorbie et al., 1982, was
used to generate ADS(PERMX)');
%fmt1='%6s\n';
%fprintf(fileID,fmt1,'PLYADS');
fmt='%4.2f %14.12f\n';
%%
fmt='%4.2f %14.12f\n';
```

```matlab
polyconc=[0.0,0.01,0.5,1.0,2.0]';
adscarreau=adscarreau';
PLYADS(:,1)=polyconc;
PLYADS(:,2)=adscarreau(1);

%%
for j=1:length(polyconc)
    for i=1:10
    PLYADS(:,1)=polyconc;
    PLYADS(:,i+1)=adscarreau(i);
    PLYADS(1,:)=0;
    end
end
```

```matlab
polyconc=[0.0,0.01,0.5,1.0,2.0]';
```

```matlab
for i=1:10
```

Appendix 3. MATLAB script to perform averaging of adsorption values

The following script is the modified MRST-routine to calculate volumetric-averaged adsorption (main principle is shown in Eq. 3.12). This modified function `createCoarseModel` (Hilden, 2016) was used during the upscaling process in MRST to assure correct indexing of the fine cells assigned to each coarse cell.

```matlab
function [ms, part, report, updata] = createCoarseModel(dataFile, varargin)
opt = struct(...
    'debug',        false, ... % debug mode
    'debugblocks',  [], ...
    'coarsefac',    [], ... % carsening factors
    'coarsedims',   [], ...
    'coarselayers', [], ... % Use partitionLayers instead
    'method',       'capillary', ... % relperm upscaling method
    'absmethod',    'pressure', ...
    'periodic',     false, ...
    'globaltrans',  false, ... % global upsc of T
    'relpermdims',  1:3, ... % relperm upscaling dimension(s)
    'waitbar',      false, ...
    'getpartition', false, ...
    'checkblocks',  false, ... % check for idential blocks
    'pcow',         true, ... % upscale pcow or not
    'wellLinSolve', @mldivide, ...
    'savesat',      false, ... % save saturation from upscaling (for debug)
    'endscale',     false ...
    );
opt = merge_options(opt, varargin{:});
require deckformat ad-fi coarsegrid upscaling

%% Read fine model input

fprintf('Reading Eclipse deck...\n');
deck  = readEclipseDeck(dataFile);
deck  = convertDeckUnits(deck);
deck  = fixSpe10DeckForMrstUse(deck); % HACK

%use readSingleEclipseIncludeFile.m to read in krwr
%change swof and SATNUM here
if opt.endscale
    deck = endscaleSwof(deck); %HACK
end

G     = initEclipseGrid(deck);
fprintf('Computing grid geometry...\n');
try
    % Use MEX version if possible
    G = mcomputeGeometry(G);
catch
    fprintf(['MEX version of computeGeometry not available. '...
        'Using Matlab version...\n']);
    G = computeGeometry(G);
end
fprintf('Init Eclipse rock...\n');
```

```matlab
rock  = initEclipseRock(deck);
rock  = compressRock(rock, G.cells.indexMap);
fluid = initDeckADIFluid(deck);

model = TwoPhaseOilWaterModel(G, rock, fluid, 'inputdata', deck);
schedule = convertDeckScheduleToMRST(G, model, rock, deck);


%% Create coarse grid

% Coarse dimensions
if ~isempty(opt.coarsefac)
    cdims = ceil(G.cartDims./opt.coarsefac);
elseif ~isempty(opt.coarsedims)
    cdims = opt.coarsedims;
else
    error('Either ''coarsefac'' or ''coarsedims'' must be given.');
end

fprintf('Will upscale %dx%dx%d grid to a %dx%dx%d grid.\n', ...
    G.cartDims(1), G.cartDims(2), G.cartDims(3), ...
    cdims(1), cdims(2), cdims(3) );

% Partition grid
if isempty(opt.coarselayers)
    part = partitionUI(G, cdims);
else
    part = partitionLayers(G, cdims(1:2), opt.coarselayers);
end
part = compressPartition(part);

% Return if only partition is wanted
if opt.getpartition
    ms = [];
    return
end

% Create coarse grid
CG = generateCoarseGrid(G, part);
CG = coarsenGeometry(CG);

% Adde extra info needed to use gridLogicalIndices
CG.cartDims = cdims;
CG.cells.indexMap = (1:CG.cells.num)';

% To get the logical indecies of the upscaled grid
ijk = gridLogicalIndices(CG);

% Physical dimensions
physdims = max(G.faces.centroids,[],1)-min(G.faces.centroids,[],1);

%% Setup upscaling

% To use capillary upscaling, we need a function pcOWInv
fluid = addPcOWInvADIFluid(fluid, deck);

% To use viscous upscaling, we need a function fracFlowInv
fluid = addFracFlowInvADIFluid(fluid, deck);
```

```matlab
upscaler.blockMap = blockMap;
upscaler.pcow = opt.pcow;
%upscaler.endscale=opt.endscale;


if ~opt.pcow
    fprintf('Capillary pressure will not be included in the upscaling.\n');
end


%% Perform upscaling
% Setup upscaler
switch opt.method
    case 'one-phase'
        upscaler = OnePhaseUpscaler(G, rock, 'periodic', opt.periodic);
    case 'capillary-viscous'
        upscaler = TwoPhaseTwoStepUpscaler(G, rock, fluid, ...
            'OnePhaseMethod', opt.absmethod, ...
            'RelpermAbsMethod1', opt.absmethod, ...
            'RelpermAbsMethod2', opt.absmethod, ...
            'RelpermMethod1', 'capillary', 'dim1', 3, ...
            'RelpermMethod2', 'viscous',   'dim2', 1, ...
            'periodic', opt.periodic);
        if numel(opt.relpermdims)==3
            % Include special upscaling of relperm in z-direction
            upscaler.twostepz = true;
        end
    case 'capillary-viscous_grav'
        upscaler = TwoPhaseTwoStepUpscaler(G, rock, fluid, ...
            'OnePhaseMethod', opt.absmethod, ...
            'RelpermAbsMethod1', opt.absmethod, ...
            'RelpermAbsMethod2', opt.absmethod, ...
            'RelpermMethod1', 'capillary_grav', 'dim1', 3, ...
            'RelpermMethod2', 'viscous',         'dim2', 1, ...
            'periodic', opt.periodic);
        if numel(opt.relpermdims)==3
            % Include special upscaling of relperm in z-direction
            upscaler.twostepz = true;
        end
    otherwise
        upscaler = TwoPhaseUpscaler(G, rock, fluid, ...
            'OnePhaseMethod', opt.absmethod, ...
            'RelpermAbsMethod', opt.absmethod, ...
            'RelpermMethod', opt.method, 'dims', 1:3, ...
            'relpermdims', opt.relpermdims, ...
            'savesat', opt.savesat, 'periodic', opt.periodic);
end
upscaler.partition = part;
upscaler.verbose   = true;
upscaler.timeest   = true;

% Use new block creation method using deck
upscaler.deck = deck;

% Run upscaling
[updata, updataG, report] = upscaler.upscale();

% Line break
fprintf('\n');
```

```
%% Upscale Adsorption values using rock-volume average
% Importing fine-scale ADS for each of SATNUM regions from previous scripts
% results
ADSfine=[1 0.000240215859798884;
        2 0.000234957396152746;
        3 0.000228911752897461;
        4 0.000226954115511936;
        5 0.000250977128199355;
        6 0.000116972438706386;
        7 0.000052624862012409;
        8 0.000026238099755808;
        9 0.000017566857873469;
        10 0.000209339039965287];
%Creating a vector with ADS in each fine cell
for i=1:length(deck.REGIONS.SATNUM)
    ADSarray(i,1)=ADSfine(deck.REGIONS.SATNUM(i),2);
end

ads=ADSarray;
assert(numel(ads)==G.cells.num, 'Unexpected size of ads table');
cads = nan(CG.cells.num, 1);
pv   = poreVolume(G, rock);
poro=deck.GRID.PORO;
cellvol=pv./poro;
IN=isnan(cellvol);
for i=1:length(cellvol)
    if IN(i)==1
        cellvol(i)=0;
    end
end

for i=1:CG.cells.num
    b = blockMap(i);
    inx = part==i; % fine cell indecies in block
    totAdsRockVol = sum(ads(inx).*(1-poro(inx)).*cellvol(inx));
    totCellVol  = sum((1-poro(inx)).*cellvol(inx));
    cads(i)     = totAdsRockVol./totCellVol; % upscaled swat
end
```

Code lines added to the original code version

```
%% Separate upscaling of transmissibility globally if requested

if opt.globaltrans
    % Using Knut-Andreas' code from the MRST book
    fprintf('Starting global upscaling of transmissibility...\n');
    startGT = tic;
    hT = computeTrans(G, rock);
    cf = G.cells.faces(:,1);
    nf = G.faces.num;
    Tf = 1 ./ accumarray(cf, 1 ./ hT, [nf, 1]);
    W  = schedule.control(1).W;
    Wc = coarsenWells(CG, W);
    Wc = addDefaultWellFields(Wc);
    [Tc, cwells] = upscaleTransGlobal(CG, Wc, Tf, ...
        'GlobalFieldCases', 'single', ...
        'handleNegative', 'setToZero', ...
        'fluxThreshold', sqrt(eps), 'LinSolve', @(A,b) agmg(A,b,1), ...
        'pv', G.cells.volumes.*rock.poro);

    % Convert to Eclipse Metric units cP.rm3/day/bars
    Tc = convertTo(Tc, (centi*poise)*(meter^3) / day / barsa);
```

```matlab
    finx = nan(CG.cells.num,3); % Will store as TRANX, TRANY, TRANY
    for c=1:CG.cells.num
        % Faces connected to current cell
        faces = CG.cells.faces(...
            CG.cells.facePos(c) : CG.cells.facePos(c+1)-1, 1);
        % Centroid of each face
        cent  = CG.faces.centroids(faces,:);
        % Face with max value in each direction (we assume Cartesian)
        [~,inx] = max(cent,[],1);
        % Face indecies
        finx(c,:) = faces(inx);
    end
    globtrans = Tc(finx);


    % Write COMPDAT string
    % As each perforation may have a different well index (connection
    % transmissibility factor), we need to add one line in COMPDAT for each
    % perforation (cell).
    s = sprintf([...
        'COMPDAT\n' ...
        '-- WELL   -LOCATION-        OPEN/ SAT   CONN  WELL\n' ...
        '-- NAME    I    J    K1   K2  SHUT  TAB   FACT  DIAM\n']);
    wellsij = cell(1, numel(cwells));
    for w=1:numel(cwells) % Loop over wells
        wellName = cwells(w).name;
        nperf = numel(cwells(w).cells);
        for p=1:nperf % Loop over perforations in well
            c  = cwells(w).cells(p); % Current perforation cell
            I  = ijk{1}(c); J = ijk{2}(c); K = ijk{3}(c);
            if isempty(wellsij{w})
                wellsij{w} = [I,J];
            else
                assert(all(wellsij{w}-[I,J] == 0)); % check
            end
            WI = cwells(w).WI(p); % Upscaled wells index
            % Convert to Eclipse input units
            WI = convertTo(WI, ( centi*poise*(meter^3) / day ) / barsa);
            s  = [s sprintf(['    %s    %d    %d    %d    %d '...
                    '''OPEN''  1*  %8.5f   0 /\n'], ...
                    wellName, I, J, K, K, WI)]; %#ok<AGROW>
        end
    end
    globwellsij = wellsij;
    globcompdat = [s sprintf('/\n')];

    timeGT = toc(startGT);
    timeGTstr = datestr(timeGT, 'MM:SS');
    fprintf('Completed transmissibility upscaling in %s.\n', timeGTstr);
end



%% Create SWOF cell array
% We loop over upscaled blocks and check the saturation limits for each
% block. Then we interpolate the pcOW data to the satraution values used in
% the relperm tables.

swof = [];
updata2p = updata;
endpoint = isfield(updataG, 'relperm');
if endpoint
```

```matlab
    % We have used endpoint scaling, and use the global average upscaling
    % for the SWOF data instead of blockwise upscaled data.
    updata2p = updataG.relperm;
end


if isfield(updata2p, 'krW')
    swof = cell(numel(updata2p),1);
    for i=1:numel(updata2p)

        ndims = numel(updata2p(i).krW);
        swof{i} = cell(1, ndims);

        for d=1:ndims % loop over upscaled dimensions

            sW    = updata2p(i).krW{d}(:,1);
            krW   = updata2p(i).krW{d}(:,2);
            krO   = updata2p(i).krO{d}(:,2);

            if isfield(updata2p(i), 'pcOW')
                pcOW = updata2p(i).pcOW;

              % Check saturation limits before interpolation. Only give
              % warning if the saturation distance of the extrapolation is
              % above some tolerence.
                swWarnTol = 1e-4;
                swDiff = min(pcOW(:,1)) - min(sW);
                if swDiff > swWarnTol
                  warning('Need to extrapolate pcOW. Sat diff=%1.2e\n', ...
                        swDiff)
                end
                swDiff = max(sW) - max(pcOW(:,1));
                if swDiff > swWarnTol
                  warning('Need to extrapolate pcOW. Sat diff=%1.2e\n', ...
                        swDiff)
                end

              % Use linear extrapolation if needed
              % Also convert from psi to barsa, which is the Eclipse input
                pcOW = interp1(pcOW(:,1), pcOW(:,2)./barsa, sW, ...
                        'linear', 'extrap');

            else
                pcOW = zeros(size(sW));
            end
            % SWOF table
            swof{i}{d} = [sW krW krO pcOW];
        end
    end
end

%% Upscale SWAT (initial water saturation) if present

cswat = [];
if isfield(deck.SOLUTION, 'SWAT')
    fprintf('SWAT field found. Will upscale.\n');
    swat = deck.SOLUTION.SWAT;
    assert(numel(swat)==G.cells.num, 'Unexpected size of SWAT');
    cswat = nan(CG.cells.num, 1);
    pv    = poreVolume(G, rock);
```

```matlab
    for i=1:CG.cells.num
        b = blockMap(i);
        inx = part==i; % fine cell indecies in block
        totWaterVol = sum(swat(inx).*pv(inx));
        totCellVol  = CG.cells.volumes(i)*updata(b).poro;
        cswat(i)    = totWaterVol / totCellVol; % upscaled swat

        if ~isempty(swof)
            try
                swofb = swof{b};
                swoftol = 1e-12;
                for d=1:numel(swofb)
                  % Check that upscaled swat is inside the upscaled relperm
                    if cswat(i) < swofb{d}(1,1) - swoftol

warning('createCoarseModel:upscaledValuesOutsideExpected', ...
                      ['SWAT for coarse cell %i, dim %d, is '...
                       'less than swir (%1.4f < %1.4f, diff=%1.2e).'], ...
                            i, d, cswat(i), swofb{d}(1,1), ...
                            abs(cswat(i)-swofb{d}(1,1)) );
                    end
                    if cswat(i) > swofb{d}(end,1) + swoftol

warning('createCoarseModel:upscaledValuesOutsideExpected',...
                      ['SWAT for coarse cell %i, dim %d, is '...
                       'greater than 1-sor '...
                       '(%1.4f > %1.4f, diff=%1.2e).'], i, d, ...
                       cswat(i), swofb{d}(end,1), ...
                       abs(cswat(i)-swofb{d}(end,1)) );
                    end
                end
            catch
                fprintf('Unable to validate upscaled SWAT data!\n');
            end
        end
    end
end

%% Upscale wells
% NOTE: We assume that the wells do not change during the simulation (i.e.
% that wells get shut/opened, perforations change etc.)

fprintf('Will upscale wells...\n');

% Upscale wells
startWells = tic;
wells  = schedule.control(1).W;
cwells = upWells(CG, rock, wells, 'LinSolve', opt.wellLinSolve, ...
    'debug', opt.debug);

% Write COMPDAT string
% As each perforation may have a different well index (connection
% transmissibility factor), we need to add one line in COMPDAT for each
% perforation (cell).
s = sprintf([...
    'COMPDAT\n' ...
    '--  WELL  -LOCATION-        OPEN/ SAT   CONN  WELL\n' ...
    '--  NAME   I   J   K1  K2  SHUT  TAB   FACT  DIAM\n']);
wellsij = cell(1, numel(cwells));
for w=1:numel(cwells) % Loop over wells
```

93

```matlab
        wellName = cwells(w).name;
        nperf = numel(cwells(w).cells);
        for p=1:nperf % Loop over perforations in well
            c   = cwells(w).cells(p); % Current perforation cell
            I   = ijk{1}(c); J = ijk{2}(c); K = ijk{3}(c);
            if isempty(wellsij{w})
                wellsij{w} = [I,J];
            else
                assert(all(wellsij{w}-[I,J] == 0)); % check
            end
            WI = cwells(w).WI(p); % Upscaled wells index
            % Convert to Eclipse input units
            WI = convertTo(WI, ( centi*poise*(meter^3) / day ) / barsa);
            s  = [s sprintf(['   %s    %d    %d    %d    %d '...
                    '''OPEN''  1*  %8.5f   0 /\n'], ...
                    wellName, I, J, K, K, WI)]; %#ok<AGROW>
        end
end
compdat = [s sprintf('/\n')];

timeWells = toc(startWells);
timeStr = upscaler.timingString(timeWells);
fprintf('Completed upscaling of wells in %s.\n', timeStr);

%% Create model property structure

ms.griddims  = cdims;
ms.physdims  = physdims;
csatnum      = blockMap(:);
ms.satnum    = csatnum;
poro         = reshape([updata.poro], [], 1);
perm         = reshape([updata.perm], [], numel(poro))';
ms.poro      = poro(csatnum);
ms.perm      = convertTo(perm(csatnum,:), milli*darcy);
ms.ads       = cads;
if opt.globaltrans
    ms.glob.trans   = globtrans;
    ms.glob.wellsij = globwellsij;
    ms.glob.compdat = globcompdat;
end
ms.swof      = swof;
if isfield(updata, 'swir')
    % Endpoint scaling
    swir        = reshape([updata.swir], [], 1);
    sor         = reshape([updata.sor], [], 1);
    krWmax      = reshape([updata.krWmax], [], 1);

    % Also convert from psi to barsa, which is the Eclipse input
    pcOWmax     = reshape([updata.pcOWmax], [], 1)./barsa;

    ms.swir    = swir(csatnum);
    ms.sor     = sor(csatnum);
    ms.krWmax  = krWmax(csatnum);
    ms.pcOWmax = pcOWmax(csatnum);

    if endpoint
        % NOTE! When using endpoint scaling, we only use A SINGLE SWOF
        % curve
        ms.satnum = ones(size(ms.satnum));
    end
```

```matlab
end
try
    ms.visc  = [convertTo(deck.PROPS.PVCDO(4), centi*poise), ...
                convertTo(deck.PROPS.PVTW(4),  centi*poise) ];
catch
end
ms.wellsij  = wellsij;
ms.compdat  = compdat;
ms.flow     = convertTo(wells(1).val, (meter^3)/day);
% if ~isempty(cswat)
%     ms.swat  = cswat;
% end


%% Some checks of the upscaled model

% Pore volume
pv  = poreVolume(G, rock);
cpv = ms.poro.*CG.cells.volumes;
finePVtot = sum(pv);
coarsePVtot = sum(cpv);
n = norm((finePVtot-coarsePVtot)/finePVtot);
if n > 1e-10
    warning('createCoarseModel:upscaledValuesOutsideExpected',...
        'Total pore volume does not match, reldiff=%1.2e\n', n);
    if opt.debug
        fprintf('The above warning is probably due to debug mode.\n');
    end
end


% Initial water saturation
if isfield(deck.SOLUTION, 'SWAT')
    fineVolTot   = sum(swat.*pv);
    coarseVolTot = sum(cswat.*cpv);
    n = norm((fineVolTot-coarseVolTot)/fineVolTot);
    if n > 1e-10
        warning('createCoarseModel:upscaledValuesOutsideExpected',...
            'Total SWAT do not match, reldiff=%1.2e\n', n)
    end
end



end
```

The following is a script to perform averaging of adsorption using flow fraction coefficient formula (Eq. 5.3). It is independent of the upscaling procedure run because it uses a pre-defined fine cells indexing matrix valid for the coarsening degree investigated in present thesis. If changed a little, the script can use flow-based calculated permeability in the flow fraction coefficient formula (see the comments in the code).

```matlab
mrstModule add deckformat

% Extracting data fields used in the fine model
struc=readEclipseDeck('M:\MATLAB\Master thesis\mrst\field-model-
project\code\models\spe10\input\models\spe10\fine\vrelperm\SPE10.DATA')
struc2=readEclipseDeck('P:\masterthesis\upscaleX15Y55Z17\CAP_MODEL.DATA')
%%
permups=struc2.GRID.PERMX;  % flow-based coarse-scale permeability
permx=struc.GRID.PERMX;     % fine-scale permeability
porox=struc.GRID.PORO;
pv=struc.GRID.DX.*struc.GRID.DY.*struc.GRID.DZ.*porox;
rv=struc.GRID.DX.*struc.GRID.DY.*struc.GRID.DZ.*(1-porox);

% Loading matrix containing correct indices for fine cells assigned to each
% coarse cell
load('part.mat');

% Importing fine-scale ADS for each of SATNUM regions from previous scripts
% results
ADSfine=[1  0.000240215859798884;
         2  0.000234957396152746;
         3  0.000228911752897461;
         4  0.000226954115511936;
         5  0.000250977128199355;
         6  0.000116972438706386;
         7  0.000052624862012409;
         8  0.000026238099755808;
         9  0.000017566857873469;
         10 0.000209339039965287];

% %Creating a vector with ADS in each fine cell
for i=1:length(struc.REGIONS.SATNUM)
    ADSarray(i,1)=ADSfine(struc.REGIONS.SATNUM(i),2);
end
ads=ADSarray;

for i=1:1:14025
    inx = part==i;     % select only the fine cells within coarse cell i
    totCellPV=sum(pv(inx));
    % In case of use of flow-based coarse-scale permeability
    kav(i)=permups(i);
    % In case of use of PV-averaged permeability uncomment 2 rows below
%     kav(i)=sum(pv(inx).*permx(inx))/totCellPV;
%     ADSffcoef1(i,1) =sum(ads(inx).* rv(inx).*pv(inx).* permx(inx)/
      sum(pv(inx).*permx(inx)))/sum(rv(inx));
    ADSffcoef_compl(i,1)=sum(ads(inx).*rv(inx).*pv(inx).*permx(inx)./...
    ...sum(pv(inx))/kav(i))/sum(rv(inx));
end
```

Appendix 4. MATLAB script calculate adsorption as a function of upscaled permeability

```matlab
mrstModule add deckformat

% Extracting data fields used in the fine model
struc=readEclipseDeck('P:\masterthesis\Upscaling\upscaleXYZ\upscaleX15Y55Z1
7\cap_coarse_1d\CAP_MODEL.DATA')
%%
permx=struc.GRID.PERMX;
porox=struc.GRID.PORO;

%%
% Option 2: create a row vector of logarithmically spaced points (bins
% edges)
% Use histc to evaluate how many cells fall into this or that category (two
% humps can be seen - probably because we have two formations in the model)
% + return bin indices for each cell in our model -> so-called ADSNUM.INC
% The Ads vs PERMX formula used is the linear trend line equation obtained
% for experimental data presented in "Enhanced Oil Recovery" (D.W.Green,
% G.P. Willhite), outliers (see Excel file) were excluded

% Creating a historam for logarithmically spaced points:
figure(1)
binsedges=logspace(log10(min(permx)),log10(max(permx)),10)';
[howmanycells, binindices] =
histc(permx,logspace(log10(min(permx)),log10(max(permx)),10));
bar(howmanycells) % Number of cells in SPE10 falling into one of 10 bins
created
title({'Distribution of the cells between 10 logarithmically';'spaced PERMX
bins in CAP-upscaled model'},'FontName','TimesNewRoman')
xlabel('Bin #')
ylabel('# of cells in the model withing the bin')
figure(2) % Spacing of PERMX values
semilogy(logspace(log10(min(permx)),log10(max(permx)),10),'LineWidth',1,'Ma
rker','o','MarkerFaceColor','b','MarkerEdgeColor','b','MarkerSize',3)
title({'How bins edges were defined for CAP-upscaled
model';'(logarithmically spaced bins)'})
xlabel('Bin #')
ylabel('Permeability, mD')

% Introducing trend line equation / Function A / (outliers excluded),
R^2=0.969
% This equation was obtained by using experimental data (retention vs
permeability) presented by Vela
% et al., 1976. The procedure is explained in the .doc file
%retbinned=@(x)9561.2308*x.^(-0.97538746);

% - - - - - - - - - - - - - - - - - - - - - - - - - - - - - - - - - - - - -

% Introducing trend line equation / Function D / , R^2=0.9986
% This equation was obtained using experimental data (retention vs
% permeability) presented in K.S. Sorbie et al., 1982
retbinnedD=@(x)6170.6961*x.^(-0.45374703);
```

```matlab
%%
figure(2)

subplot(2,1,1)
semilogy([1:length(permx)],permx,'r')
title('Permeability of the CAP-upscaled model')
xlabel('Cell #')
ylabel('Log10 permeability, mD')

subplot(2,1,2)
plot([1:length(porox)],porox)
t=title('Porosity of the CAP-upscaled model')
set(t,'FontName','TimesNewRoman')
xlabel('Cell #')
ylabel('Porosity, dimens-s')

%%
% Calculating Retention for each cell directly
% units - lbm/acre-ft
retention1=retbinnedD(permx);

%In order to convert to adsorption [µg/g], the following
%formula should be used:
rettoads=@(poro)2.717*(1-poro).*2.65
%where poro - mean porosity value for each SATNUM region
%      2.65 - grain density which is assumed to be quartz' density
coef=rettoads(porox);
ads1=retention1./coef/1000000; % adsorption in kg/kg

%%
% Using Carreau fluid model to cut-off too high retention values
% The Carreau model appears as follows:
% µeff(y)=µinf+(µ0-µinf)*( 1+(lambda*y)^2 )^(0,5n-0,5)
% where y      - shear rate
%       µ0     - viscosity at zero shear rate
%       µinf   - viscosity at infinite shear rate
%       lambda - relaxation time
%       n      - power index
% In our case, PERMX is used instead of shear rate and RET is used instead
% of viscosity. Then the Carreau model expression transforms as follows:
% RETeff(PERMX)=RETinf+( RET0-RETinf )*( 1+(lambda*PERMX)^alfa )^(0,5n-0,5)
RETinf=50;
RET0=1500;          %Carreau model parameters from Excel Solver results
lambda=0.044691564789017;
n=0.960271737793605;
alfa=24.277887102091;

retcarreau=RETinf+(RET0-RETinf)*(1+(lambda*permx).^alfa).^(0.5*n-0.5);

%Convert to adsorption [µg/g] again:
adscarreau=retcarreau./coef/1000000; % Carreau-modified adsorption in kg/kg

%%
figure(3)

subplot(2,2,1)
semilogy(permx,'r')
title('Permeability of the CAP-upscaled model');
xlabel('Cell #')
ylabel('Log10 permeability, mD')
```

98

```matlab
subplot(2,2,2)
plot(porox)
t=title('Porosity of the CAP-upscaled model');
set(t,'FontName','TimesNewRoman')
xlabel('Cell #')
ylabel('Porosity, dimens-s')

subplot(2,2,[3,4])
semilogy(adscarreau,'g')
t=title('Carreau-modified adsorption in the CAP-upscaled model');
set(t,'FontName','TimesNewRoman')
xlabel('Cell #')
ylabel('Adsorption, kg/kg')

%%
% Creating PLYADS keyword
polyconc=[0.0,0.01,0.5,1.0,2.0]';
% Creating NXxNYxNZ tables (=number of SATNUM regions) tables with
% adsorption vs polymer concentration stored as a multidimensional matrix
for i=1:length(adscarreau)
    for j=1:length(polyconc)
        PLYADS1(:,1,i)=polyconc;
        PLYADS1(:,2,i)=adscarreau(i);
        PLYADS1(1,2,:)=0;
    end
end

%%
% Creating an INCLUDE file for PLYADS keyword with NXxNYxNZ tables with 5
% polymer concentration nodes in each table

testfile = fopen('M:\MATLAB\Master thesis\mrst\field-model-
project\code\annasincl\capcoarsepolymer1.inc','w');
fmt='%62s\n%80s\n%6s\n';
fprintf(testfile,fmt,'--Adsorption as a function of mean permX in each
SATNUM region','--Experimental dataset from Sorbie et al., 1982, was used
to generate ADS(PERMX)','PLYADS');
fmt='%4.2f %14.12f';
for i=1:length(adscarreau)
    for j=1:4
        fprintf(testfile,fmt,PLYADS1(j,1,i),PLYADS1(j,2,i));
        fprintf(testfile,'\n');
    end
    fmt1='%4.2f %14.12f  / \n';
    fprintf(testfile,fmt1,PLYADS1(5,1,i),PLYADS1(5,2,i));
end
fclose(testfile)

% Creating an INCLUDE file for PLYROCK keyword with NXxNYxNZ rows
% Keyword structure:
%  Item1       Item2       Item3       Item4           Item5
%  IPV         RRF         Rock        Adsorption      Max polymer
%                          dens-y      index           adsorp.value
% In this code it is assumed that IPV and RRF are constants

IPV=0.2;
RRF=1.00;
rockden=2650;
adsind=2;
```

```matlab
PLYROCK=zeros(length(adscarreau),5);
PLYROCK(:,1)=IPV;
PLYROCK(:,2)=RRF;
PLYROCK(:,3)=rockden;
PLYROCK(:,4)=adsind;
PLYROCK(:,5)=adscarreau;

%%
testfile = fopen('M:\MATLAB\Master thesis\mrst\field-model-
project\code\annasincl\capcoarsepolymer2.inc','w')
fmt='%54s\n%41s\n%7s\n';
fprintf(testfile,fmt,'-- Rock properties related to polymer flood per
satnum','-- IPV and RRF are assumed to be constant','PLYROCK');
fmt='%3.1f %4.2f %4.0f %1.0f %13.12f / \n';
for i=1:length(adscarreau)

fprintf(testfile,fmt,PLYROCK(i,1),PLYROCK(i,2),PLYROCK(i,3),PLYROCK(i,4),PL
YROCK(i,5));
end
fprintf(testfile,'\n');
%testfile=fopen('M:\MATLAB\Master thesis\mrst\field-model-
project\code\annasincl\capcoarsepolymer3.inc','w');
PLYVISC=[0.00 1.00;0.22 1.48;0.44 2.12;0.67 2.96;0.89 4.01;1.11 5.31;1.33
6.88;1.56 8.77;1.78 11.01;2.00 13.66;4.00 13.66];
fprintf(testfile,'%7s \n','PLYVISC');

for i=1:10
fprintf(testfile,'%4.2f  %4.2f',PLYVISC(i,1),PLYVISC(i,2));
fprintf(testfile,'\n');
end
fprintf(testfile,'%4.2f  %4.2f / \n\n',PLYVISC(11,1),PLYVISC(11,2));
fprintf(testfile,'%34s \n%39s \n%8s \n%3s /','-- Todd-Longstaff mixing
parameter','-- Assume full mixing (full mixing = 1)','PLMIXPAR','1.0');
fprintf(testfile,'\n');
fprintf(testfile,'%62s \n%6s \n%7s','-- Maximum polymer/salt concentrations
for mixing calculations','PLYMAX','2  55 /');
fclose(testfile);
%%
% Plotting Carreau-modified adsorptions for different parts of the upscaled
% model. If the model is 15x55x17, then 1 layer will contain 825 cells
figure(4)

[ax,p1,p2] =
plotyy([1:825],adscarreau(1:825),[1:825],permx(1:825),'semilogy','semilogy'
);
title('Porosity and permeability in the CAP-upscaled
model','FontName','TimesNewRoman');
xlabel(ax(1),'Cell #');
ylabel(ax(1),'Adsorption, kg/kg'); % label left y-axis
ylabel(ax(2),'Log10 permeability, mD'); % label right y-axis
set(p2,'LineWidth',2.5);
set(p1,'LineStyle','-','marker','o','color','red','MarkerSize',2);
set(gca,'ygrid','on');
legend('Adsorption','Permeability','Location','south');
```

Appendix 5. Areal sweep efficiency improvement in the fine scale model
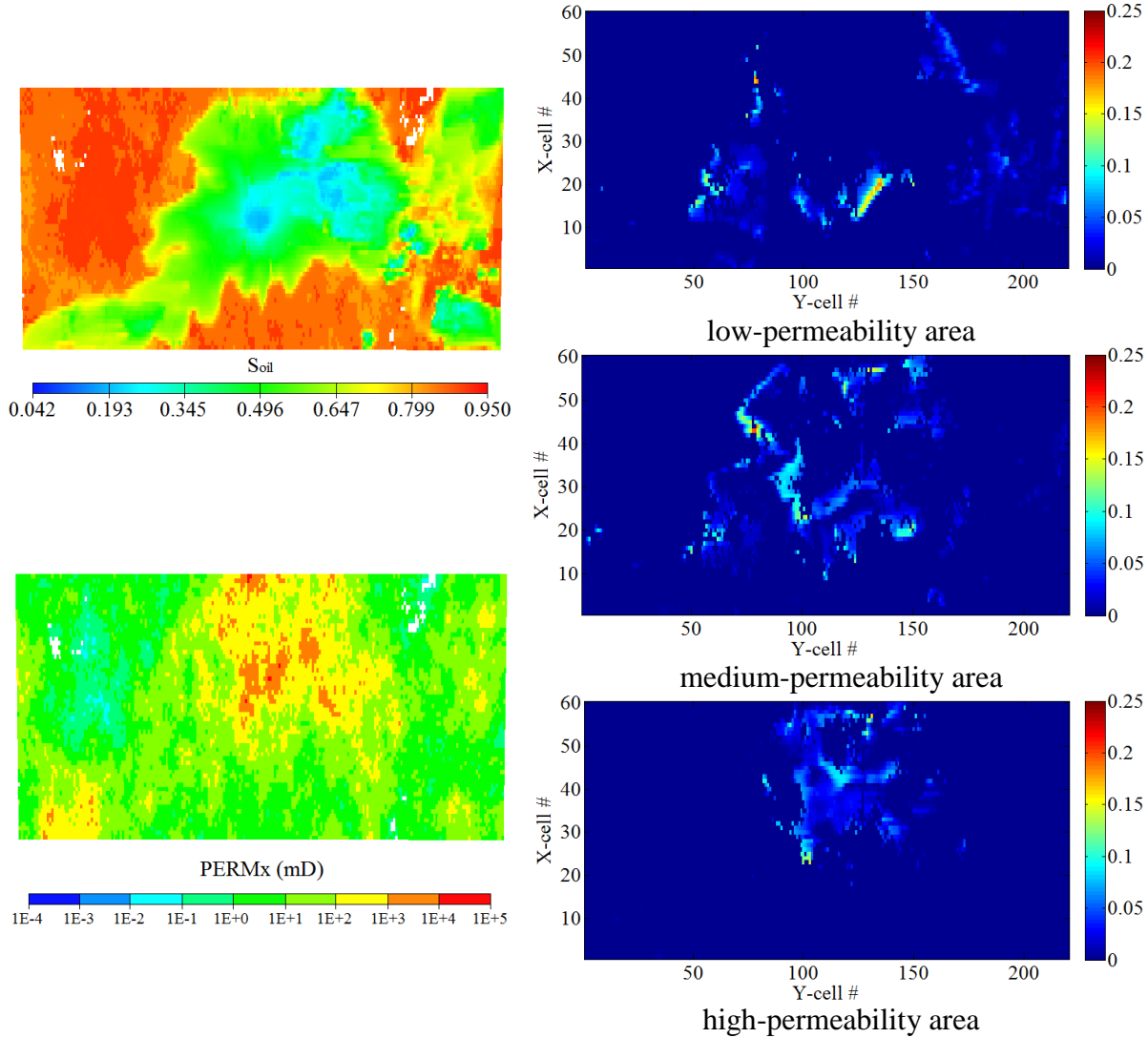

Fig. A5.1 – Tarbert fm (SPE10 fine-scale model, layer 31). Permeability and oil saturations in the layer at the end of waterflooding scenario (left-hand side); areas with extra oil displacement during polymer flooding in different permeability regions of the layer (right-hand side).

One can observe sweep improvement at the edges of the area flooded by water (increase of the swept area during polymer flooding) and sweep improvement within the swept area where there are abrupt changes in permeability.
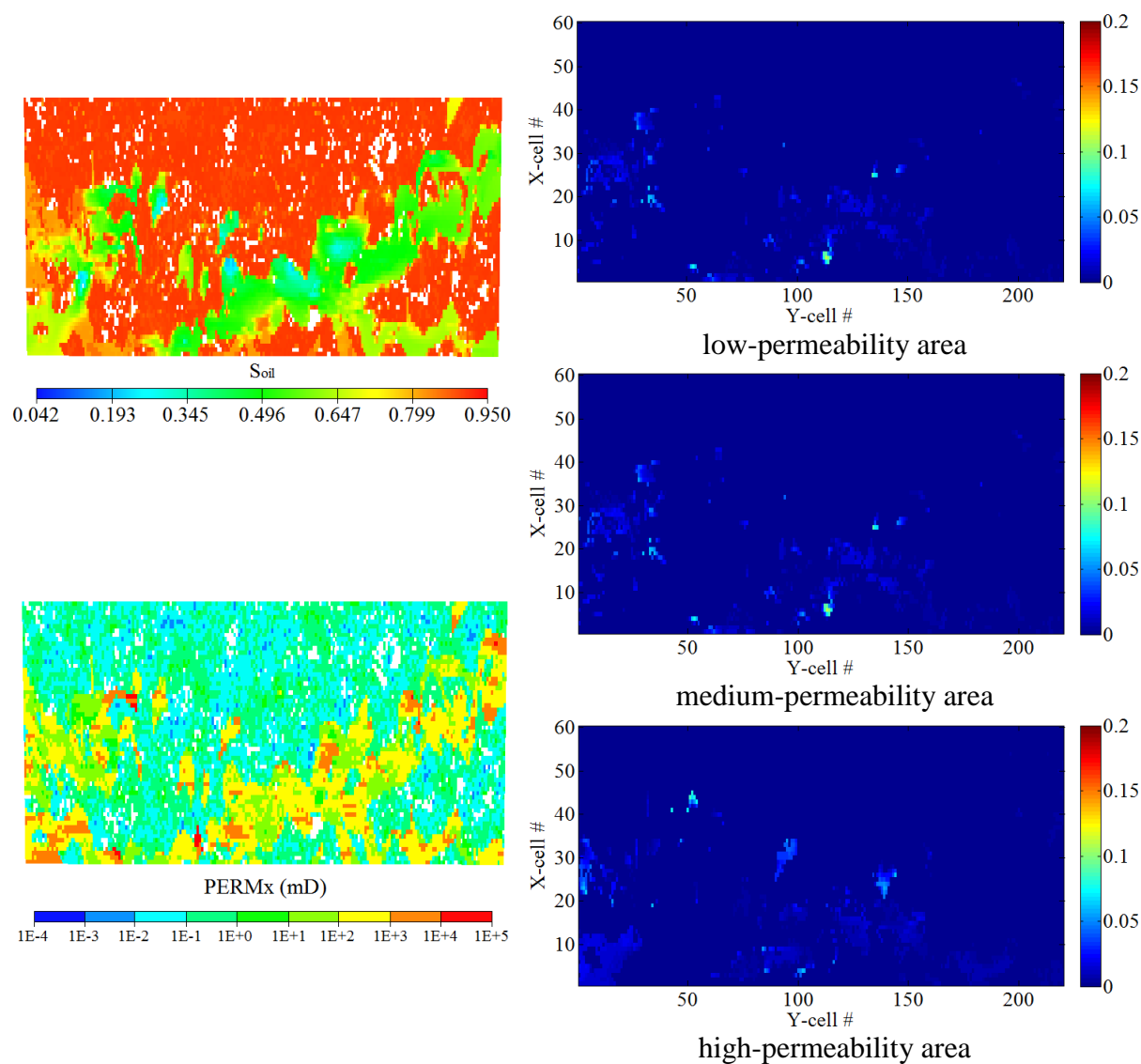
Fig. A5.2 – Upper Ness fm (SPE10 fine-scale model, layer 42). Permeability and oil saturations in the layer at the end of waterflooding scenario (left-hand side); areas with extra oil displacement during polymer flooding in different permeability regions of the layer (right-hand side).

One can observe sweep improvement at the edges of the fluvial channels and in some laterally isolated parts of the channels that are connected to the overlying or underlying layers instead.

Appendix 6. MATLAB script to visualize sweep efficiency improvement in fine scale model

```matlab
%%%%%%%%%%%%%%%%%%%%%%%%%%%%%%%%%%%%%%%%%%%%%%%%%%%%%%%%%%%%%%%%%%%%%%%%%%%%%%
%         DEFINING SWEEP EFFICIENCY OF A POLYMER FLOODING SCENARIO        %
%            AS A DIFFERENCE IN Soil AT THE SAME MOMENT IN TIME           %
%                         Soil(WATERFL)-Soil(POLYFL)                      %
%       POSITIVE DIFFERENCE MEANS MORE OIL LEFT AFTER WATERFLOODING       %
%%%%%%%%%%%%%%%%%%%%%%%%%%%%%%%%%%%%%%%%%%%%%%%%%%%%%%%%%%%%%%%%%%%%%%%%%%%%%%

% Loading matrices with oil saturation data extracted from ResInsight and
% converted to the .mat format
load('SOIL_POLY_23_NOV_2018.mat'); % name in Workspace: SOIL_POLY
load('SOIL_WAT_23_NOV_2018');      % name in Workspace: SOIL_WAT
struc=readEclipseDeck('M:\MATLAB\Master thesis\mrst\field-model-
project\code\models\spe10\input\models\spe10\eclipse\fine\vrelperm\SPE10.DA
TA')

% Since ResInsight puts data in 5 columns and, thus, ordering can be
% complex, it's necessary to rearrange data into a single-column vector
k=1;
for i=1:224400
    for j=1:5
        SOIL_WAT1(k,1)=SOIL_WAT(i,j);   % vector with waterflooding SOIL
        SOIL_POLY1(k,1)=SOIL_POLY(i,j); % vector with polymer flooding SOIL
        k=k+1;
    end
end

% Rearranging data to reproduce SPE10 model dimensions
SOIL_WAT_map=reshape(SOIL_WAT1,60,220,85);
SOIL_POLY_map=reshape(SOIL_POLY1,60,220,85);
% Creating a model containing saturation difference
SOIL_diff_map=SOIL_WAT_map-SOIL_POLY_map;
%%
% Plotting SOIL at the end of waterflooding scenario layer by layer
target_layer=14;

figure(1)
imagesc(SOIL_WAT_map(:,:,target_layer))
colorbar
caxis([0 1]);
title({[sprintf('S_o_i_l in layer %2.0f of the model ', target_layer)];
[('(SPE10 fine waterflooding scenario)')]},'FontName','Times New Roman',
'FontSize',16)
xlabel('Y-cell #');
ylabel('X-cell #');

% Plotting SOIL at the end of polymer flooding scenario layer by layer
figure(2)
imagesc(SOIL_POLY_map(:,:,target_layer))
colorbar
caxis([0 1]);
title({[sprintf('S_o_i_l in layer %2.0f of the model ',target_layer)];
[('(SPE10 fine polymer flooding scenario)')]},'FontName','Times New
Roman','FontSize',16)
```

```matlab
xlabel('Y-cell #');
ylabel('X-cell #');

% Plotting dSOIL between water- and polymer flooding layer by layer
figure(3)
imagesc(SOIL_diff_map(:,:,target_layer))
colorbar
caxis([0 0.5]);
title({[sprintf('S_o_i_l difference (water - polymer) in layer %2.0f of the
model ',target_layer)];[('(SPE10 fine polymer flooding scenario)')]},
'FontName','Times New Roman','FontSize',16)
xlabel('Y-cell #');
ylabel('X-cell #');

%%
figure(4)
%Visualizing results in each layer as an animation
for i=1:85
imagesc(SOIL_diff_map(:,:,i))
% view(90,90)
colorbar
colormap('bone')
caxis([-0.5 0.2]);
title({[sprintf('SPE10 fine, SOIL difference map, layer %2.0f,
',i)];[('(S_o_i_l_,_w_a_t-S_o_i_l_,_p_o_l_y)')]},'FontName','Times New
Roman','FontSize',16)
ylabel('X-cell #','FontName','Times New Roman','FontSize',14)
xlabel('Y-cell #','FontName','Times New Roman','FontSize',14)
M(i)=getframe(gcf);
end
%%
% Creating vertical slices comparison

target_slice=30; % I-slice values can be within the interval (1:60)
for k=1:85
    for j=1:220
        SOIL_WAT_slice(k,j)=SOIL_WAT_map(target_slice,j,k);
        SOIL_POLY_slice(k,j)=SOIL_POLY_map(target_slice,j,k);
    end
end

SOIL_diff_slice=SOIL_WAT_slice-SOIL_POLY_slice;

% Plotting SOIL cross-section of the target slice
% Note: INJE is in the middle of the picture, PROD1 & PROD2 are on the left
% side, PROD3 & PROD4 are on the right side
figure(5)
imagesc(SOIL_WAT_slice)
colorbar
caxis([0 1]);
title({[sprintf('S_o_i_l in I-slice %2.0f of the model ',target_slice)];
[('(SPE10 fine waterflooding scenario)')]},'FontName','Times New
Roman','FontSize',16)
xlabel('Y-cell #');
ylabel('X-cell #');

figure(6)
imagesc(SOIL_POLY_slice)
colorbar
caxis([0 1]);
```

```matlab
title({[sprintf('S_o_i_l in I-slice %2.0f of the model ',target_slice)];
[('(SPE10 fine polymer flooding scenario)')]},'FontName','Times New
Roman','FontSize',16)
xlabel('Y-cell #');
ylabel('X-cell #');


figure(7)
imagesc(SOIL_diff_slice)
colorbar
caxis([0 0.2]);
title({[('S_o_i_l difference (water - polymer) ')];[sprintf('in I-slice
%2.0f of the model ',target_slice)]},'FontName','Times New
Roman','FontSize',16)
xlabel('Y-cell #');
ylabel('X-cell #');


%%
% Creating a diagonal polyline slice
% from PROD3 via INJE to PROD4
% Input coordinates of the left and right points of the diagonal
% For PROD4-INJE part:          For PROD3-INJE part:
Ileft1=30;  Jleft1=110;         Ileft2=30;  Jleft2=110;
Iright1=1;  Jright1=220;        Iright2=60; Jright2=220;


% Defining coefficients of straight line equation for our diagonal
% I=k*J+b + an analogue line for 2nd part of it with subscript 1
k1=(Ileft1-Iright1)/(Jleft1-Jright1);  k2=(Ileft2-Iright2)/(Jleft2-
Jright2);
b1=Ileft1-k1*Jleft1;                    b2=Ileft2-k2*Jleft2;
Jdiag1=[Jleft1:Jright1];                Jdiag2=[Jleft2:Jright2];
Idiag1=floor(k1.*Jdiag1+b1); % Round indices to have only integer values
Idiag2=floor(k2.*Jdiag2+b2);


% Filling the slice with values
for i=1:85
    for j=1:length(Jdiag1)
    SOIL_WAT_diagslice1(i,j)=SOIL_WAT_map(Idiag1(j),Jdiag1(j),i);
    SOIL_POLY_diagslice1(i,j)=SOIL_POLY_map(Idiag1(j),Jdiag1(j),i);
    end
end
for i=1:85
    for j=1:length(Jdiag2)
    SOIL_WAT_diagslice2(i,j)=SOIL_WAT_map(Idiag2(j),Jdiag2(j),i);
    SOIL_POLY_diagslice2(i,j)=SOIL_POLY_map(Idiag2(j),Jdiag2(j),i);
    end
end


% Creating difference map for the slice
SOIL_diff_diagslice1=SOIL_WAT_diagslice1-SOIL_POLY_diagslice1;
SOIL_diff_diagslice2=SOIL_WAT_diagslice2-SOIL_POLY_diagslice2;
%%
% Putting both parts together
% so that PROD3 is on the left, PROD4 is on the right, INJE in the middle
SOIL_WAT_polyline=[fliplr(SOIL_WAT_diagslice2) SOIL_WAT_diagslice1];
SOIL_POLY_polyline=[fliplr(SOIL_POLY_diagslice2) SOIL_POLY_diagslice1];
SOIL_diff_polyline=[fliplr(SOIL_diff_diagslice2) SOIL_diff_diagslice1];


figure(8)
imagesc(SOIL_WAT_polyline(:,:))
colorbar
```

```matlab
caxis([0 1]);
title({['S_o_i_l in the cross-section PROD3-INJE-PROD4 '];['(SPE10 fine
waterflooding scenario)']},'FontName','Times New Roman','FontSize',16)
xlabel('Y-cell #');
ylabel('X-cell #');

figure(9)
imagesc(SOIL_POLY_polyline(:,:))
colorbar
caxis([0 1]);
title({['S_o_i_l in the cross-section PROD3-INJE-PROD4 '];['(SPE10 fine
polymer flooding scenario)']},'FontName','Times New Roman','FontSize',16)
xlabel('Y-cell #');
ylabel('X-cell #');

figure(10)
imagesc(SOIL_diff_polyline(:,:))
colorbar
caxis([0 0.5]);
title({['S_o_i_l in the cross-section PROD3-INJE-PROD4 '];['(SPE10 fine
polymer flooding scenario)']},'FontName','Times New Roman','FontSize',16)
xlabel('Y-cell #');
ylabel('X-cell #');

%%
% Evaluating polymer effect compared to the initial state of the reservoir
% Loading initial oil saturations
load('SOIL_INIT');         % name in Workspace: SOIL_INIT
k=1;
for i=1:224400
    for j=1:5
        SOIL_INIT1(k,1)=SOIL_INIT(i,j);
        k=k+1;
    end
end
SOIL_INIT=reshape(SOIL_INIT1,60,220,85);
SOIL_diff_mapI=SOIL_INIT-SOIL_POLY_map;

target_layer=84;

figure(11)
imagesc(SOIL_WAT_map(:,:,target_layer))
colorbar
caxis([0 1]);
title({sprintf('SPE10 fine, waterflooding, layer %2.0f, ',target_layer)},
'FontName','Times New Roman','FontSize',16);
xlabel('Y-cell #');
ylabel('X-cell #');

figure(12)
imagesc(SOIL_POLY_map(:,:,target_layer))
colorbar
caxis([0 1]);
title({sprintf('SPE10 fine, polymer flooding, layer %2.0f,
',target_layer)},'FontName','Times New Roman','FontSize',16);
xlabel('Y-cell #');
ylabel('X-cell #');

figure(13)
imagesc(SOIL_diff_mapI(:,:,target_layer))
```

```matlab
colorbar
caxis([0 0.8]);
title({sprintf('SPE10 fine, SOIL difference map (init-poly), layer %2.0f,
',target_layer)},'FontName','Times New Roman','FontSize',16);
xlabel('Y-cell #');
ylabel('X-cell #');


%%
%%%%%%%%%%%%%%%%%%%%%%%%%%%%%%%%%%%%%%%%%%%%%%%%%%%%%%%%%%%%%%%%%%%%%%%%%%%%
%                          PERMEABILITY FILTERING                        %
%%%%%%%%%%%%%%%%%%%%%%%%%%%%%%%%%%%%%%%%%%%%%%%%%%%%%%%%%%%%%%%%%%%%%%%%%%%%

%PERM_map=reshape(struc.GRID.PERMX,60,220,85);
% Creating a background for the filtered permeability maps with a negative
% values for the cells outside the target permeability group
PERM_low=-100*ones(length(struc.GRID.PERMX),1);
PERM_mid=-100*ones(length(struc.GRID.PERMX),1);
PERM_high=-100*ones(length(struc.GRID.PERMX),1);

% Filling maps with values
for i=1:length(struc.GRID.PERMX)
    if struc.GRID.PERMX(i)<20
        PERM_low(i)=struc.GRID.PERMX(i);
    elseif struc.GRID.PERMX(i)>200
        PERM_high(i)=struc.GRID.PERMX(i);
    else
        PERM_mid(i)=struc.GRID.PERMX(i);
    end
end
% Rearranging according to the model's dimensions
PERM_map_low=reshape(PERM_low,60,220,85);
PERM_map_mid=reshape(PERM_mid,60,220,85);
PERM_map_high=reshape(PERM_high,60,220,85);
% Counting cells within each permeability group
lowperm_num=numel(find(PERM_low>0));
midperm_num=numel(find(PERM_mid>0));
highperm_num=numel(find(PERM_high>0));


%%
% Creating a contour map of SOIL difference
target_layer=65;

y=[1:60];
x=[1:220];
[X,Y]=meshgrid(x,y);
axes1 = axes('Parent',figure,'YDir','reverse',...
    'Position',[0.13 0.115 0.711969696969697 0.7825],...
    'Layer','top',...
    'FontSize',12,...
    'FontName','Times New Roman',...
    'CLim',[0 0.8]);
contour(X,Y,SOIL_diff_mapI(:,:,target_layer),'LineWidth',2);
xlabel({'Y-cell #'},'FontSize',14,'FontName','Times New Roman');
ylabel({'X-cell #'},'FontSize',14,'FontName','Times New Roman');
title({'Difference in oil saturation: So,poly-So,init (contour map, layer
65)'},...
    'FontSize',16,...
    'FontName','Times New Roman');
colorbar;
caxis([0 0.8]);
```

```matlab
load('Colormap_contour.mat')
colormap(mycmap);

%%
% Filtering SOIL maps with respect to permeability groups
SOIL_diff1=SOIL_WAT1-SOIL_POLY1;        %SOIL_INIT1-SOIL_POLY1;
SOIL_diff_low=-100*ones(length(SOIL_INIT1),1);
SOIL_diff_mid=-100*ones(length(SOIL_INIT1),1);
SOIL_diff_high=-100*ones(length(SOIL_INIT1),1);

for i=1:length(SOIL_INIT1)
    if PERM_low(i)>0
        SOIL_diff_low(i)=SOIL_diff1(i);
    elseif PERM_high(i)>0
        SOIL_diff_high(i)=SOIL_diff1(i);
    else
        SOIL_diff_mid(i)=SOIL_diff1(i);
    end
end
SOIL_diff_low_map=reshape(SOIL_diff_low,60,220,85);
SOIL_diff_mid_map=reshape(SOIL_diff_mid,60,220,85);
SOIL_diff_high_map=reshape(SOIL_diff_high,60,220,85);

%%
% Calculating how much oil (in volume) comes from every permeability group
(low-perm,
% (low-perm, mid-perm, high-perm)
% The main idea is to convert So to volumes (first, at reservoir
% conditions) using Vo=PV*So formula for initial and ultimate time steps
dx=6.0960; dy=3.0480; dz=0.60960;
cellvol=dx*dy*dz;
poro=struc.GRID.PORO;
PV=cellvol*poro;
Voil_diff_low=SOIL_diff_low.*PV;     % There will be some negative values in
Voil_diff_mid=SOIL_diff_mid.*PV;     % the matrix due to the modification
Voil_diff_high=SOIL_diff_high.*PV;   % that has been done for map plotting
                                     % (i.e. when the cell doesn't belong to
                                     % a region, it's SOIL=-100 (deep blue in
                                     % the map)
Voil_diff_low_map=reshape(Voil_diff_low,60,220,85);
Voil_diff_mid_map=reshape(Voil_diff_mid,60,220,85);
Voil_diff_high_map=reshape(Voil_diff_high,60,220,85);

% Calculating total volumes coming from different permeability regions +
% statistics
Voil_low_total=zeros(length(Voil_diff_low),1);
Voil_mid_total=zeros(length(Voil_diff_mid),1);
Voil_high_total=zeros(length(Voil_diff_high),1);

for i=1:length(Voil_diff_low)
    if Voil_diff_low(i)>0
        Voil_low_total(i)=Voil_diff_low(i);
    end
    if Voil_diff_mid(i)>0
        Voil_mid_total(i)=Voil_diff_mid(i);
    end
    if Voil_diff_high(i)>0
        Voil_high_total(i)=Voil_diff_high(i);
    end
end
```

```matlab
Total_low=sum(Voil_low_total)
Total_mid=sum(Voil_mid_total)
Total_high=sum(Voil_high_total)
%%
% Pie chart
Figure(14)
pie([Total_low,Total_mid,Total_high]);
labels = {'Oil produced from low perm','Oil produced from mid perm','Oil
produced from high perm'};
legend(labels,'Location','southoutside','Orientation','horizontal')
figure
pie([lowperm_num,midperm_num,highperm_num]);
labels = {'# of low perm cells','# of mid perm cells','# of high perm
cells'};
legend(labels,'Location','southoutside','Orientation','horizontal')


%%
% Plotting changes in SOIL compared to waterflooding within each
permeability group
target_layer=42;

figure(15)
subplot(3,1,1)
imagesc(SOIL_diff_low_map(:,:,target_layer))
colorbar
caxis([0 0.2]);
t=title({[sprintf('SPE10 fine, SOIL-diff-low-map, layer %2.0f,
',target_layer)];[('(S_o_i_l_,_i_n_i_t-
S_o_i_l_,_p_o_l_y)')]},'FontName','Times New Roman','FontSize',16)
xlabel('Y-cell #');
ylabel('X-cell #');

subplot(3,1,2)
imagesc(SOIL_diff_mid_map(:,:,target_layer))
colorbar
caxis([0 0.2]);
t=title({[sprintf('SPE10 fine, SOIL-diff-mid-map, layer %2.0f,
',target_layer)];[('(S_o_i_l_,_i_n_i_t-
S_o_i_l_,_p_o_l_y)')]},'FontName','Times New Roman','FontSize',16)
xlabel('Y-cell #');
ylabel('X-cell #');

subplot(3,1,3)
imagesc(SOIL_diff_high_map(:,:,target_layer))
colorbar
caxis([0 0.2]);
t=title({[sprintf('SPE10 fine, SOIL-diff-high-map, layer %2.0f,
',target_layer)];[('(S_o_i_l_,_i_n_i_t-
S_o_i_l_,_p_o_l_y)')]},'FontName','Times New Roman','FontSize',16)
xlabel('Y-cell #');
ylabel('X-cell #');
```

Appendix 7. Areal sweep efficiency improvement in the coarse models
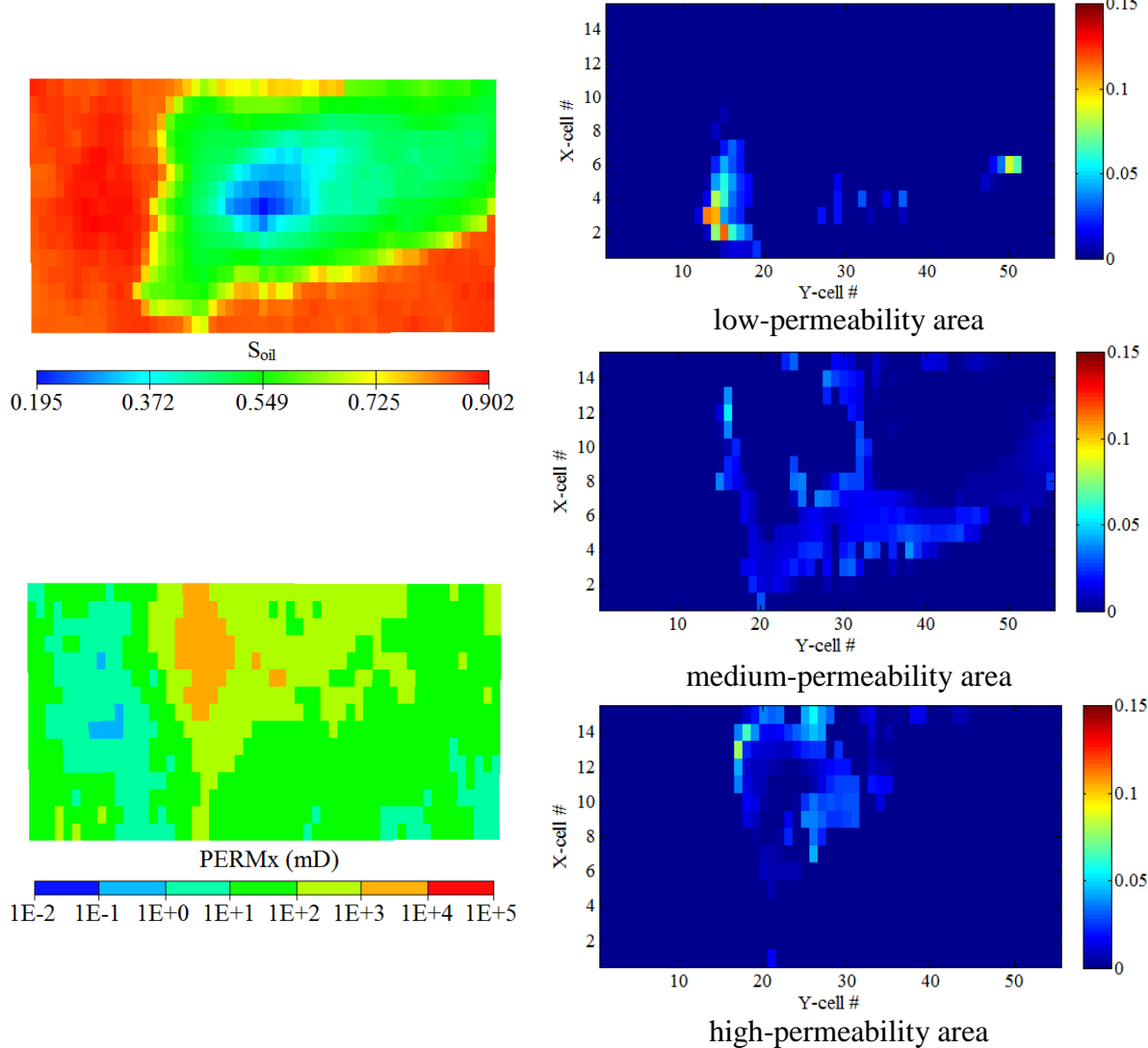

low-permeability area

medium-permeability area

high-permeability area

S_{oil}

0.195   0.372   0.549   0.725   0.902

PERMx (mD)
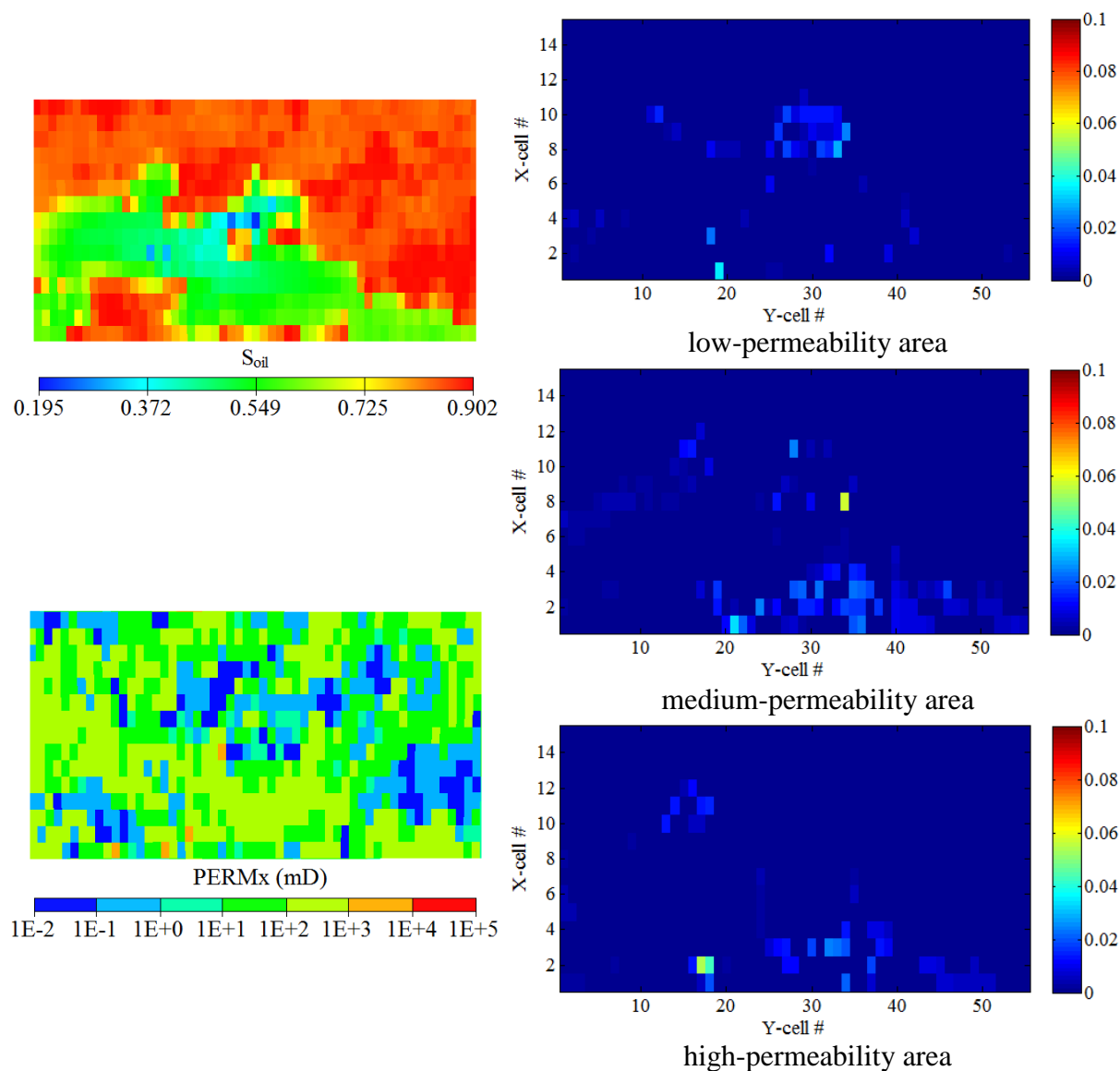
1E-2   1E-1   1E+0   1E+1   1E+2   1E+3   1E+4   1E+5

Fig. A7.1 – Tarbert fm (SPE10 upscaled model, layer 7). Permeability and oil saturations in the layer at the end of waterflooding scenario (left-hand side); areas with extra oil displacement during polymer flooding in different permeability regions of the layer (right-hand side).

One can observe sweep improvement at the edges of the area flooded by water (increase of the swept area during polymer flooding) and sweep improvement within the swept area.

Fig. A7.2 – Upper Ness fm (SPE10 upscaled model, layer 9). Permeability and oil saturations in the layer at the end of waterflooding scenario (left-hand side); areas with extra oil displacement during polymer flooding in different permeability regions of the layer (right-hand side).

One can observe sweep improvement at the edges of the fluvial channels and in near the injection well.

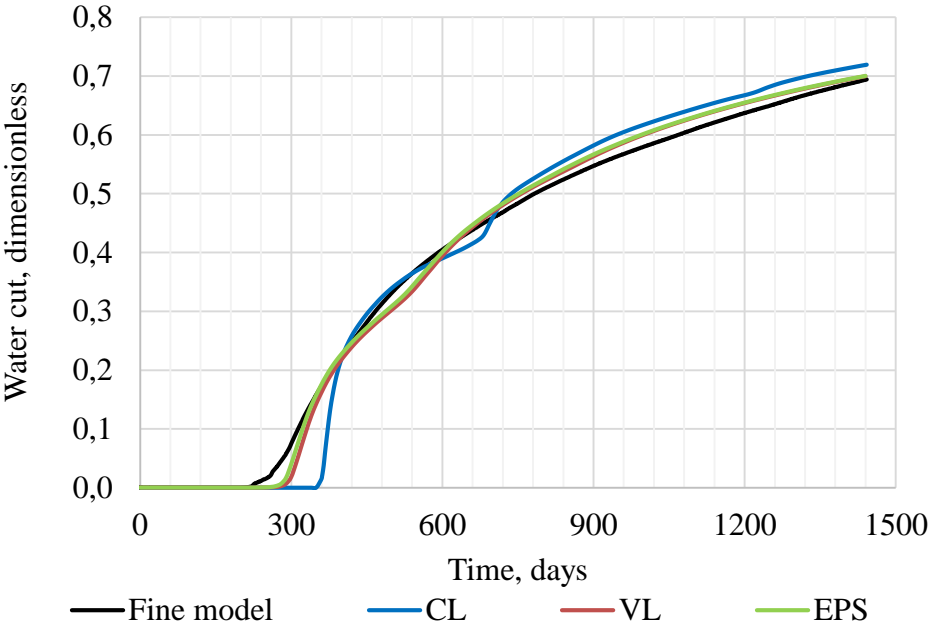# Appendix 8. Base case upscaling results
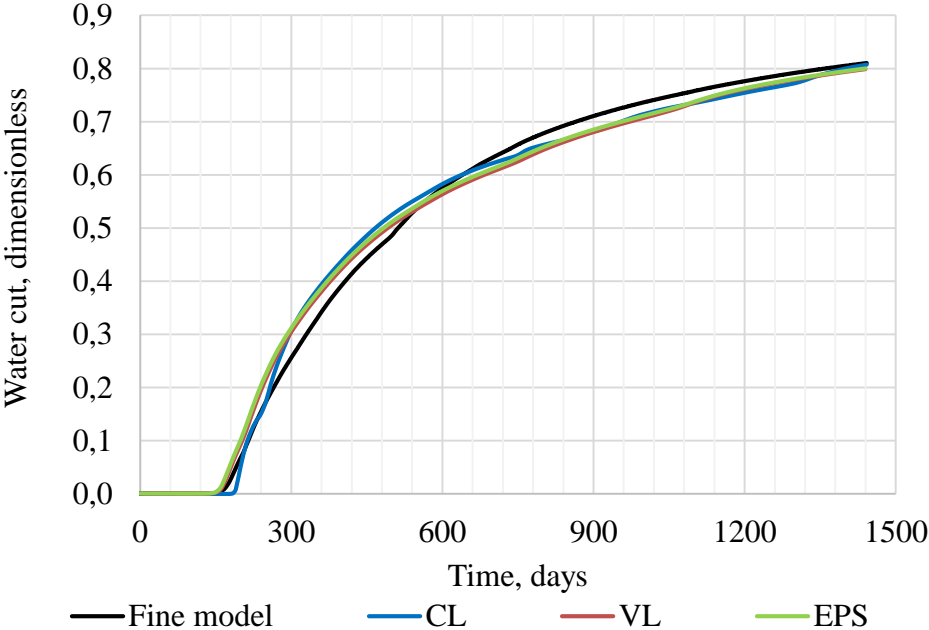

Fig. A8.1 – Base case water cut in well PROD1 comparison

Fig. A8.2 – Base case water cut in well PROD2 comparison
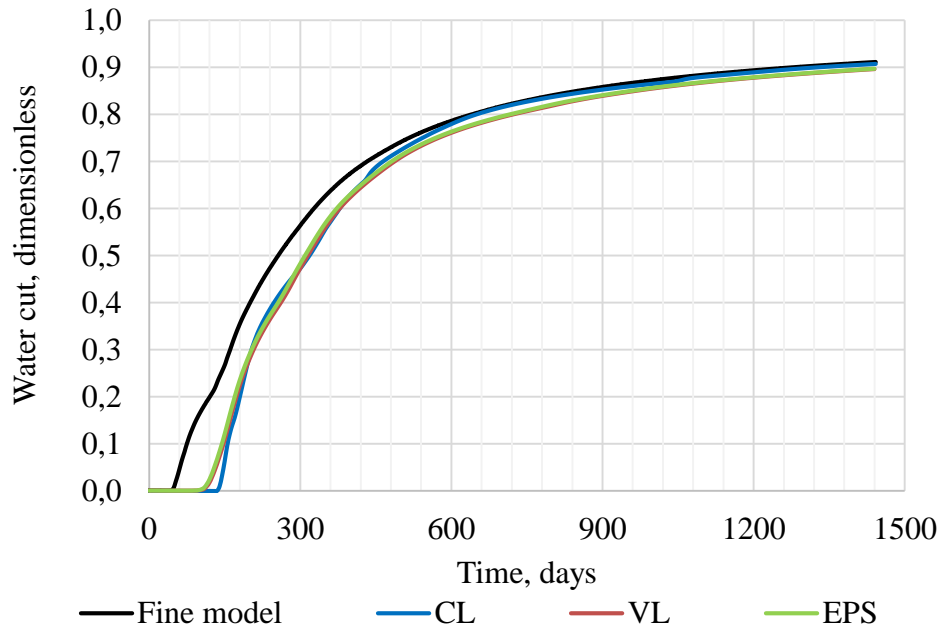
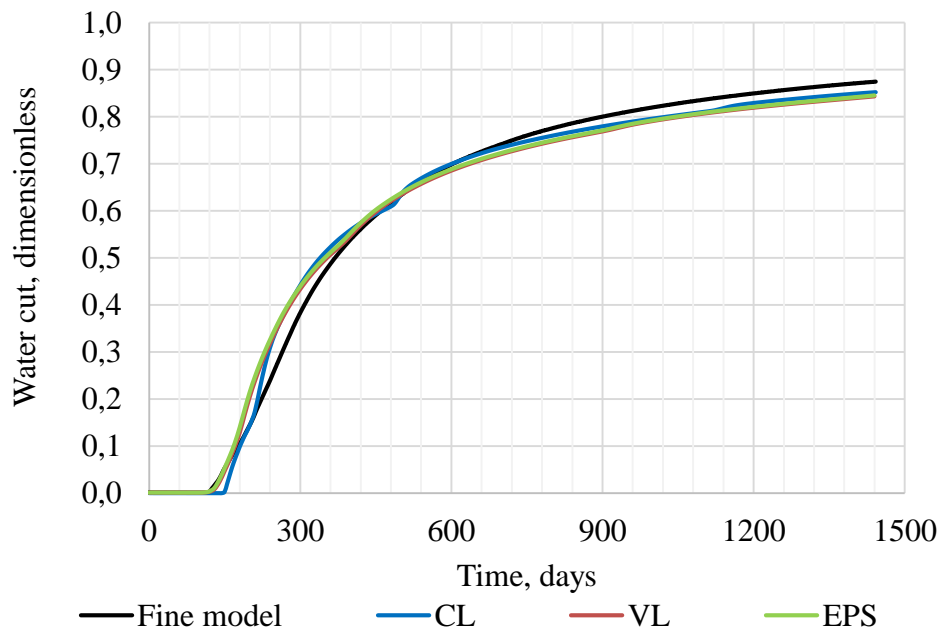**Fig. A8.3 –** Base case water cut in well PROD3 comparison

Fig. A8.4 – Base case water cut in well PROD4 comparison
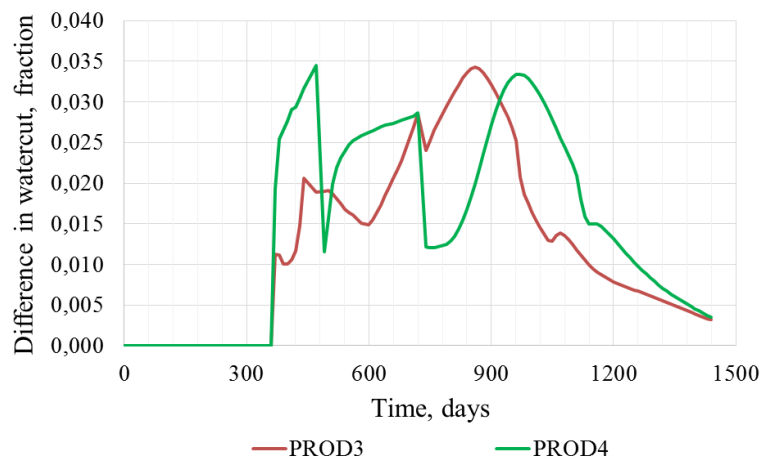
Appendix 9. Polymer flooding upscaling results

Fig. A9.1 – Difference between water cut in base case and polymer flooding case for CL-upscaled model, volumetric-averaged adsorption
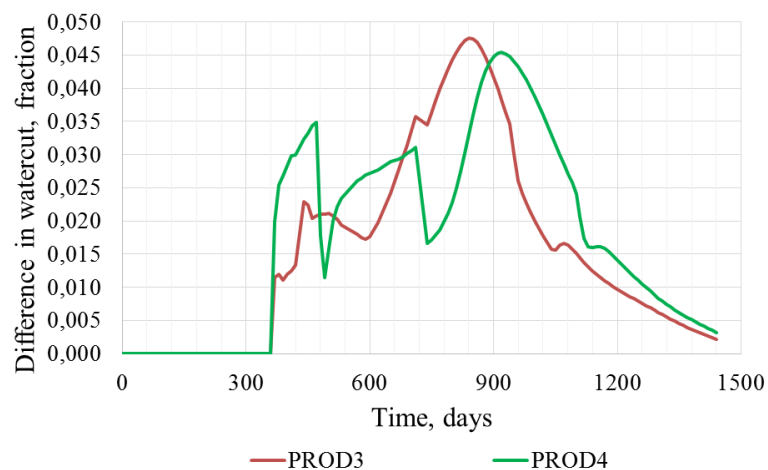

Fig. A9.2 – Difference between water cut in base case and polymer flooding case for CL-upscaled model, adsorption as a function of upscaled permeability
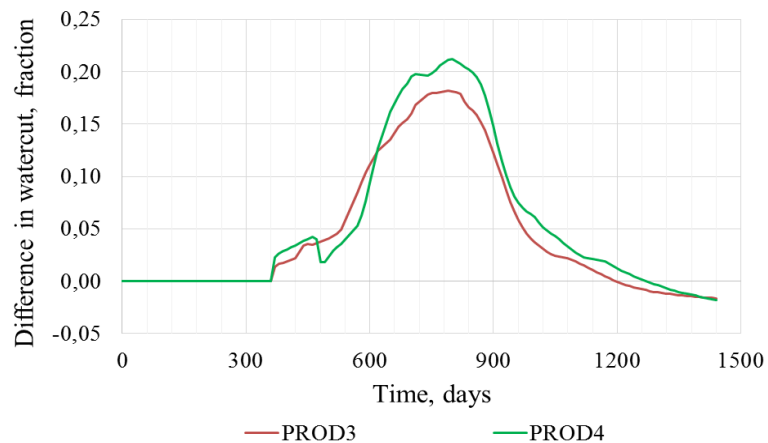

Fig. A9.3 – Difference between water cut in base case and polymer flooding case for CL-upscaled model, modified volumetric average of adsorption (flow fraction coefficient formula)

Fig. A9.4 – Difference between water cut in base case and polymer flooding case for VL-upscaled model, volumetric-averaged adsorption

Fig. A9.5 – Difference between water cut in base case and polymer flooding case for VL-upscaled model, adsorption as a function of upscaled permeability

Fig. A9.6 – Difference between water cut in base case and polymer flooding case for VL-upscaled model, modified volumetric average of adsorption (flow fraction coefficient formula)
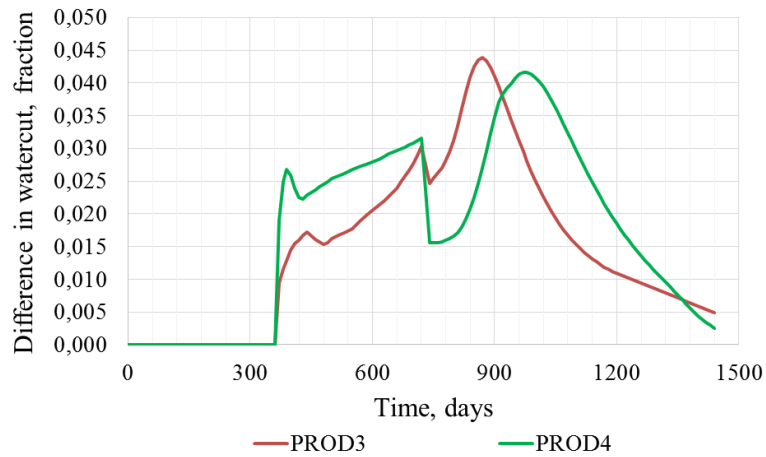
Fig. A9.7 – Difference between water cut in base case and polymer flooding case for EPS-upscaled model, volumetric-averaged adsorption
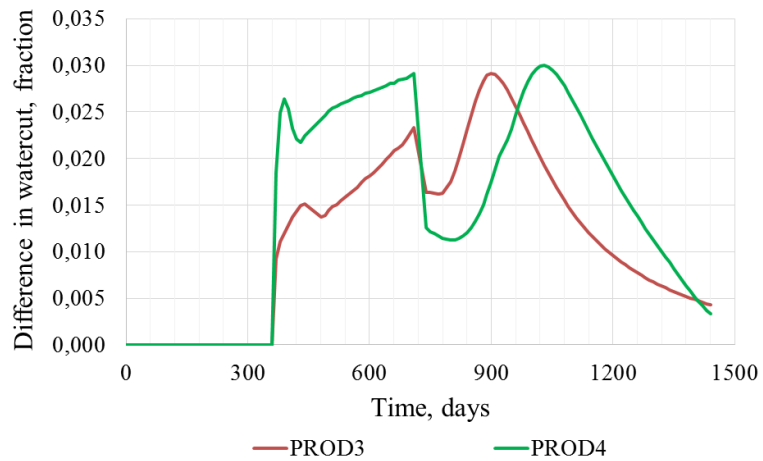

Fig. A9.8 – Difference between water cut in base case and polymer flooding case for EPS-upscaled model, adsorption as a function of upscaled permeability
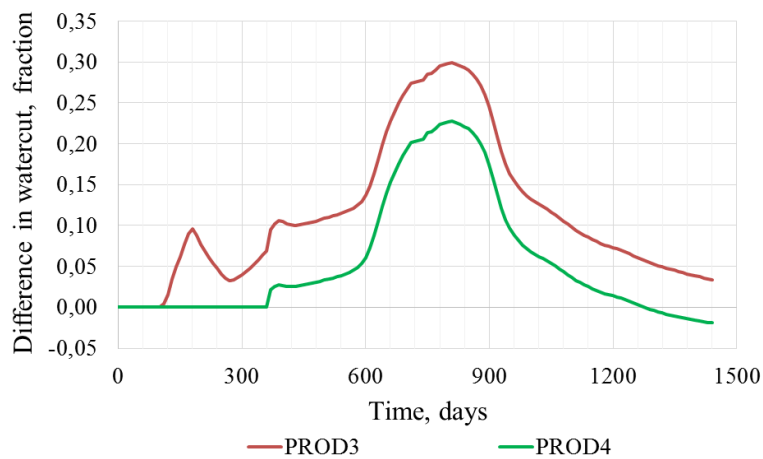

Fig. A9.9 – Difference between water cut in base case and polymer flooding case for EPS-upscaled model, modified volumetric average of adsorption (flow fraction coefficient formula)
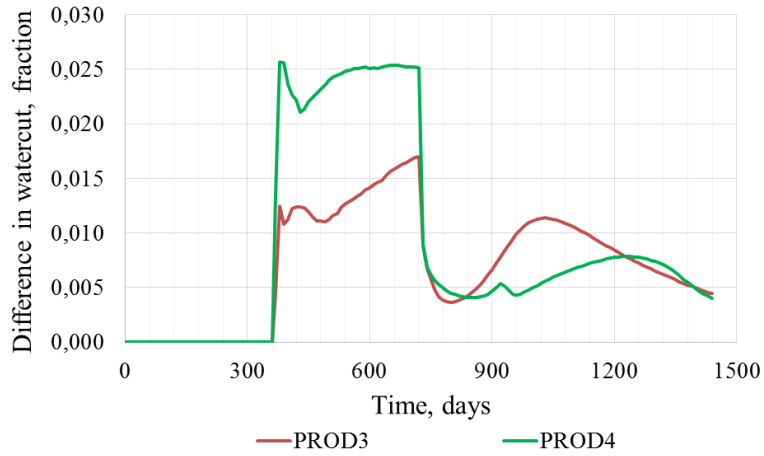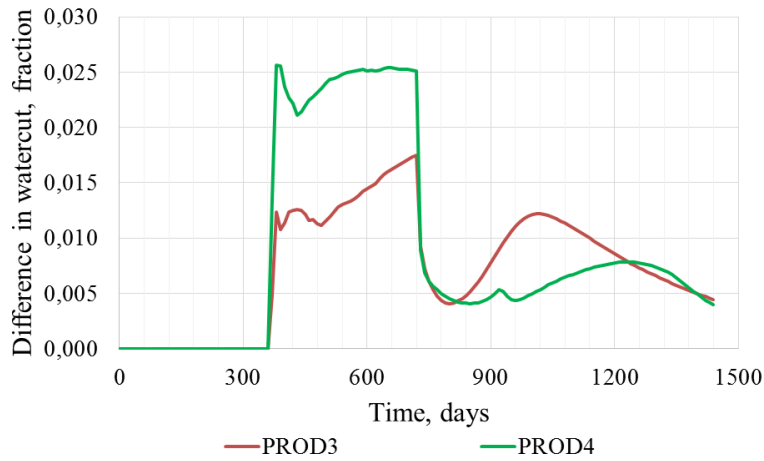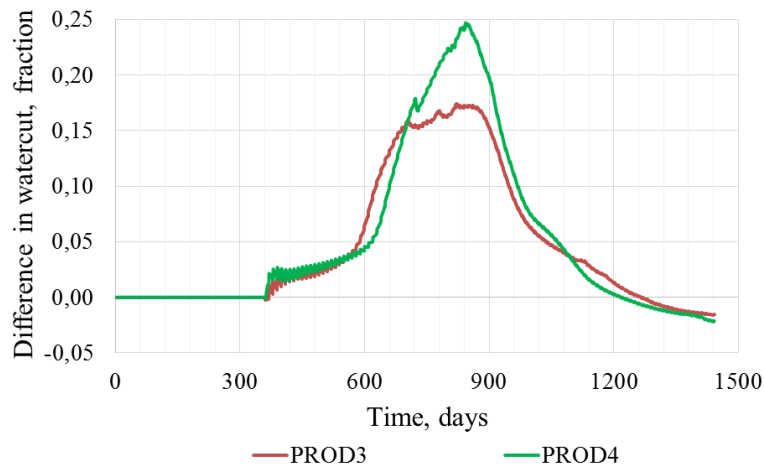
References

Al-Shammari, B., Al-Fariss, T., Al-Sewailm, F., & Elleithy, R. (2011). The Effect of Polymer Concentration and Temperature on the Rheological Behavior of Metallocene Linear Low Density Polyethylene (mLLDPE) Solutions. *Journal of King Saud University - Engineering Sciences, 23*, 9-14.

Aronofsky, J. (1952). Mobility Ratio - Its Influence on Flood Patterns During Water Encroachment. *SPE 132-G presented at the Fall Meeting of the Petroleum Branch in Oklahoma City, Okla., October 3-5, 1951. Vol. 195*, pp. 15-24. AIME.

Barker, J., & Dupouy, P. (1999, November). An Analysis of Dynamic Pseudo-Relative Permeability Methods for Oil-Water Flows. *Petroleum Geoscience, 5*, 385-394.

Barker, J., & Thibeau, S. (1997, May). A Critical Review of the Use of Pseudorelative Permeabilities for Upscaling. *SPE Reservoir Engineering, 12*(2), 138-143.

Bingham, E. (1962). *Fluidity and Plasticity.* New York: McGraw-Hill.

Bird, R., Armstrong, R., & Hassager, O. (1987). *Dynamics of Polymeric Liquids, Volume 1: Fluid Mechanicsa* (2nd ed.). New York: Wiley.

Bird, R., Stewart, W., & Lightfoot, E. (1960). *Transport Phenomena.* New York: Wiley.

Blackwell, R., Rayne, J., & Terry, W. (1959). Factors Influencing the Efficiency of Miscible Displacement. *SPE 1131-G presented at 33rd Annual Fall Meeting of Society of Petroleum Engineers in Houston, October 5-8* (pp. 1-8). SPE.

Bradley, H., Heller, J., & Odeh, A. (1960). A Potentiometric Study of the Effects of Mobility Ratio on Reservoir Flow Patterns. *SPE 1585-G presented at 35th Annual Fall Meeting of SPE, October 2-5, 1960, in Denver* (pp. 125-129). SPE.

Burcik, E. (1965). Note on the Behavior of Polyacrylamide Solutions in Porous Media. *Producers Monthly (United States), 29*(6).

Bøe, Ø. (1994, January). Analysis of an Upscaling Method Based on Conservation of Dissipation. *Transport in Porous Media, 17*(1), 77-86.

Carreau, P. (1972). Rheological Equations From Molecular Network Theories [PhD Thesis, University of Wisconsin, Maddison, USA, 1968]. *Transactions of the Society of Rheology, 16*(1), 99-127.

Chain, S. (1965). *The Study of the Flow Behavior of Partially Hydrolized Polyacrylamide Solutions in Porous Media.*

Chang, H. (1978, August). Polymer Flooding Technology - Yesterday, Today, and Tomorrow. *Journal of Petroleum Technology*, 1113-1128.

Chaveteau, G., & Kohler, N. (1974). Polymer Flooding: The Essential Elements for Laboratory Evaluation. *SPE 4745 presented at the Improved Oil Recovery Symposium of the Society of Petroleum Engineers of AIME in Tulsa, April 22-24.* SPE.

Cheek, R., & Menzie, D. (1955). Fluid Mapper Model Studies of Mobility Ratio. *SPE-432-G. Vol.204*, pp. 278-281. AIME.

Christie, M. (1996, November). Upscaling for Reservoir Simulation. *Journal of Petroleum Technology, 48*(11), 1004-1010.

Christie, M., & Blunt, M. (2000, May 9). *SPE Comparative Solution Project*. Retrieved January 20, 2016, from Society of Petroleum Engineers: http://www.spe.org/web/csp/

Craig, F. (1971). *The Reservoir Engineering Aspects of Waterflooding*. Dallas: AIME.

Dawson, R., & Lantz, R. (1972). Inaccessible Pore Volume in Polymer Flooding. *SPE 3522 presented at SPE Annual Fall Meeting in New Orleans, October 3-6* (pp. 448-452). SPE.

De Waele, A. (1923). Viscometry and Plastometry. *Journal of the Oil & Colour Chemists' Association, 6*, 33-88.

Dominguez, J., & Willhite, G. (1977, April). Retention and Flow Characteristics of Polymer Solutions in Porous Media. *Society of Petroleum Engineers Journal, 17*(2), 111-121.

Donaldson, E., Chilingarian, G., & Yen, T. (1989). *Enhanced Oil Recovery, II: Processes and Operations* (Vol. 17). Elsevier.

Dougherty, E. (1963, June). Mathematical Model of an Unstable Miscible Displacement. *Society of Petroleum Engineers Journal*, 155-163.

Dr. Wamser, C. (2000). *Organic Chemistry III*. Retrieved February 20, 2016, from Portland State University: http://web.pdx.edu/~wamserc/C336S00/23notes.htm

Durlofsky, L. (1991, May). Numerical Calculation of Equivalent Grid Block Permeability Tensors for Heterogeneous Porous Media. *Water Resources Research, 27*(5), 699-708.

Durlofsky, L. (2005). Upscaling and Gridding of Fine Scale Geological Models for Flow Simulation. *Paper presented at the 8th International Forum on Reservoir Simulation in Stresa, June 20-24.*

Dyes, A., Caudle, B., & Erikson, R. (1953). Oil Production After Breakthrough - As Influenced by Mobility Ratio. *SPE 309-G presented at the Petroleum Branch Fall Meeting at Dallas, Tex., Oct. 19-21* (pp. 27-32). AIME.

Ekrann, S., & Aasen, J. (2000, December). Steady-State Upscaling. *Transport in Porous Media, 41*(3), 245-262.

Ekrann, S., Dale, M., Langaas, K., & Mykkeltveit, J. (1996). Capillary Limit Effective Two-Phase Properties for 3D Media. *SPE 35493 presented at the European 3-D Reservoir Modelling Conference in Stavanger, April 16-17.* SPE.

Evans, H., & Young, D. (1942, April). Solubility of Polybutene in Pure Solvents. *Industrial and Engineering Chemistry, 34*(4), 461-466.

Farmer, C. (2002). Upscaling: a Review. *International Journal for Numerical Methods in Fluids, 40*, 63-78.

Filak, J.-M., Van Lint, J., & Le Guerroue, E. (2012, August 31). *3-D Geological Modeling of the Wprld's Largest Siliciclastic Reservoirs: Greater Burgan Field, Kuwait.* Retrieved February 25, 2016, from AAPGDatapages/Search and Discovery: http://www.searchanddiscovery.com/documents/2012/20169filak/ndx_filak.pdf

Flory, P. (1953). *Principles of Polymer Chemistry.* Cornell University Press.

Gogarty, W. (1967). Mobility Control With Polymer Solution. *SPE 1566B presented at SPE 41st Annual Fall Meeting in Dallas, October 2-5* (pp. 161-173). SPE.

Green, D., & Willhite, G. (1998). *Enhanced Oil Recovery.* Richardson, Texas: Society of Petroleum Engineers.

Habermann, B. (1960). The Efficiency of Miscible Displacement as a Function of Mobility Ratio. *SPE 1540-G presented at 35th Annual Fall Meeting of SPE in Denver, October 2-5* (pp. 264-272). SPE.

Hackley, V., & Ferraris, C. (2001, January). *Expressions for Describing Steady Shear Non-Newtonian Flow*. Retrieved February 24, 2016, from Guide to Rheological Nomenclature for Liquid-Based Particle Systems: http://ciks.cbt.nist.gov/~garbocz/SP946/node8.htm

Hilden, S. (2016). *Upscaling of Water-Flooding Scenarios and Modeling of Polymer Flow.* NTNU, Department of Mathematical Sciences. Trondheim: Skipnes Kommunikasjon AS.

Hilden, S., & Berg, C. (2016, March). Comparison of Two-Phase Upscaling Methods on Field Models. *Advances in Water Resources (in press; posted 29 March 2016).*

Hilden, S., Lie, K., & Raynaud, X. (2014). Steady-State Upscaling of Polymer Flooding. *Poster presentation at ECMOR XIV - 14th European Conference on the Mathematics of Oil Recovery in Catania, September 8-11.*

Jennings, R., Rogers, J., & West, T. (1971, March). Factors Influencing Mobility Control by Polymer Solutions. *SPE 2867 presented at SPE 9th Biennal Production Symposium in Wichita Falls, May 14-15. 23*, pp. 391-401. SPE.

Kincaid, J., Eyring, H., & Stearn, A. (1941). The Theory of Absolute Reaction Rates and Its Application to Viscosity and Diffusion in the Liquid State. *Chemical Reviews, 28*(2), 301-365.

Kleppe, J. (2015). *Buckley-Leverett Analysis.* Retrieved March 15, 2016, from TPG4150 Reservoir Recovery Techniques: http://www.ipt.ntnu.no/~kleppe/TPG4150/BL.pdf

Koval, E. (1963, June). A Method for Predicting the Performance of Unstable Miscible Displacement in Heterogeneous Media. *Society of Petroleum Engineers Journal*, 145-154.

Kumar, A., Farmer, C., Jerauld, G., & Li, D. (1997). Efficient Upscaling From Cores to Simulation Models. *SPE 38744 presented at the 1997 SPE Annual Tevhnical Conference and Exhibition in San Antonio, October 5-8.* SPE.

Lake, L. (1989). *Enhanced Oil Recovery.* Prentice Hall.

Larssen, K. (2013, June 3). Steady-State Upscaling of Polymer Flow (Thesis for the Degree Master of Science). Oslo, Norway.

Mansoori, J. (1994). A Review of Basic Upscaling Procedures: Advantages and Disadvantages. In J. Yarus, & R. Chambers, *Stochastic Modelling and Geostatistics: Principles, Methods, and Case Studies* (pp. 65-74). AAPG.

Marker, J. (1973, November). Dependence of Polymer Retention on Flow Rate. *Journal of Petroleum Technology, 25*(11), 1307-1308.

Martin, F., & Sherwood, N. (1975). The Effect of Hydrolysis of Polyacrylamide on Solution Viscosity, Polymer Retention and Flow Resistance Properties. *SPE 5339 presented for the Rocky Mountain Regional Meeting of the Society of Petroleum Engineers og AIME in Denver, April 7-9.* SPE.

Metzner, A., & Otto, R. (1957, March). Agitation of Non-Newtonian Fluids. *The American Institute of Chemical Engineers Journal, 3*(1), 3-10.

Mungan, N. (1969). Rheology and Adsorption of Aqueous Polymer Solutions. *PETSOC-69-02-01 presented at the 20th Annual Technical Meeting of The Petroleum Society of CIM in Edmonton* (pp. 45-50). Petroleum Society of Canada.

Mungan, N., Smith, F., & Thompson, J. (1966, September). Some Aspects of Polymer Floods. *Journal of Petroleum Technology, 18*(9), 1143-1150.

Needham, R., & Doe, P. (1987, December). Polymer Flooding Review. *Journal of Petroleum Technology, Vol.39*(12), 1503-1507.

Norwegian Petroleum Directorate. (2016). *Facts 2014. The Norwegian Petroleum Sector.* (Y. Tormodsgard, Ed.) Retrieved February 18, 2016, from Norwegian Petroleum Directorate: http://www.npd.no/Global/Engelsk/3-Publications/Facts/Facts%202014/Facts_2014_nett_.pdf

Odsæter, L., Berg, C., & Rustad, A. (2015, December). Rate Dependency in Steady-State Upscaling. *Transport in Porous Media, 110*(3), 565-589.

Ostwald, W. (1925, February). Ueber Die Geschwindigkeitsfunktion Der Viskositat Disperser Systeme. I. *Kolloid-Zeitschrift, 36*(2), 99-117. doi:10.1007/BF01431449

Philips, J., Miller, J., Wernau, W., Tate, B., & Auerbach, M. (1985, August). A High-Pyruvate Xanthan for EOR. *Society of Petroleum Engineers Journal, 25*(4), 594-602.

Pickup, G., Ringrose, P., Jensen, J., & Sorbie, K. (1994, February). Permeability Tensors for Sedimentary Structures. *Mathematical Geology, 26*(2), 227-250.

Pye, D. (1964). Improved Secondary Recovery by Control of Water Mobility. *SPE 845 presented at SPE Secondary Recovery Symposium in Wichita Falls, May 4-5* (pp. 911-916). SPE.

Resource Management in Mature Areas. (2016, February 18). Retrieved 2016, from Norwegian Petroleum: http://www.norskpetroleum.no/en/developments-and-operations/resource-management-in-mature-areas/

Sandiford, B. (1964). Laboratory and Field Studies of Water Floods Using Polymer Solutions to Increase Oil Recoveries. *SPE-844-PA presented at SPE Secondary Recovery Symposium in Wichita Falls, May 4-5* (pp. 917-922). SPE.

Schlumberger. (2015). ECLIPSE Industry-Reference Reservoir Simulator. Retrieved from https://www.software.slb.com/products/eclipse

Sheng, J. (2010). *Modern Chemical Enhanced Oil Recovery: Theory and Practice.* Gulf Professional Publishing.

SINTEF ICT. (2015). MRST - MATLAB Reservoir Simulation Toolbox. Retrieved from http://www.sintef.no/projectweb/mrst/

Sorbie, K. (1991). *Polymer-Improved Oil Recovery.* New York: Springer Science + Business Media.

Sorbie, K., Roberts, L., & Foulser, R. (1982). Polymer Flooding Calculations for Highly Stratified Brent Sands in the North Sea. *Presented at 2nd European Symposium Enhanced Oil Recovery in Paris, November 8-10* (pp. 175-190). Edition TECHNIP.

SPE International. (2015, June 12). *Upscaling of Grid Properties in Reservoir Simulation.* Retrieved March 22, 2016, from PetroWiki: http://petrowiki.org/Upscaling_of_grid_properties_in_reservoir_simulation

Su, H., Ali, F., Orjuela, J., & Al Gheorghiu, S. (2011). Advanced Reservoir Management of Greater Burgan Field. *SPE 148198 presented at the SPE Reservoir Characterisation and Simulation Conference and Exhibition in Abu-Dhabi, October 9-11.* SPE.

Szabo, M. (1975). Some Aspects of Polymer Retention in Porous Media Using a C14-Tagged Hydrolized Polyacrylamide. *SPE 4668 presented at the SPE-AIME 48th Annual Meeting in Las Vegas, September 30 - October 3* (pp. 323-337). SPE.

The MathWorks, Inc. (2014). MATLAB R2014a. Retrieved from http://www.mathworks.com/products/matlab/

Thomas, S. (2008). Enhanced Oil Recovery - An Overview. *Oil and Gas Science and Technology, Vol. 63*(No.1), 9-19.

Todd, M., & Longstaff, W. (1972, July). The Development, Testing, and Application of a Numerical Simulator for Predicting Miscible Flood Performance. *Journal of Petroleum Technology*, 874-882.

Vela, S., Peaceman, D., & Sandvik, E. (1976, April). Evaluation of Polymer Flooding in a Layered Reservoir With Crossflow, Retention, and Degradation. *Society of Petroleum Engineers Journal, 16*(2), 82-96.

Virnovsky, G., Friis, H., & Lohne, A. (2004, February). A Steady-State Upscaling Approach for Immiscible Two-Phase Flow. *Transport in Porous Media, 54*(2), 167-192.

Wang, J., Porter, R., & Knox, J. (1970, October). Temperature Coefficients for the Viscosity of Poly-1-Olefins. *Journal of Polymer Science Part B: Ploymer Letters, 8*(10), 671-675.

Willhite, G., & Seright, R. (2011). *Polymer Flooding (Digital Edition).* Richardson, Texas: SPE.

Yasuda, K., Armstrong, R., & Cohen, R. (1981, March). Shear Flow Properties of Concentrated Solutions of Linear and Star Branched Polystyrenes. *Rheologica Acta, 20*(2), 163-178.